PoCoLoCo, Positioning through Cooperating Loquacious Communications

Jorge Ramirez

Advisers:
Cristina Barrado Muxi
Pablo Royo Chic

Escola d'Enginyeria de Telecomunicació i Aerospacial de Castelldefels
Technical University of Catalonia, Barcelona Tech

A thesis submitted for the degree of
PhilosophiæDoctor (PhD) in Aerospace Science and Technology

September 2013

Abstract

Aerial Transportation system is based in a legacy infrastructure that supports its different functionality separately. There is a tendency to simplify the infrastructure, increasing its efficiency, technical and monetary.

UAS are perceived by the general public as simplified versions of the conventional aviation because they have not any human flight crew on board. In fact, they have a flight crew, but this flight crew is placed on ground adding some complications to the system (e.g: Command & Control link).

Conventional aviation perceives UAS as a source of problems, mainly because they have no human flight crew on board capable of creating the situational awareness of the UAS. This lack of situational awareness compromises as well the rest of airspace users safety.

This PhD explores the capability of UAS to contribute to the situational awareness of both the own aircraft (generating navigation data) as to the situational awareness of the rest of airspace users (generating surveillance data).

The contribution to the situational awareness of both the own aircraft (navigation data) as well as the rest of airspace users (surveillance) is simulated assuming UAS communications based on TDMA and at the communication rates described in the literature.

The simulation scenario has been kept simple with a low communication rate and a low number of UAS flying in the simulated area.

The results of navigation are in line with the RNP1. The results in surveillance are in line with the 3NM separation but with a refresh rate much higher. Then, with this proposal, UAS could be considered as contributors to the situational awareness instead as the problem that destroys the situational awareness

To my beloved daughters Iria and Eireen, you suffered my dedication to this PhD instead building your's dolls house. It has been only a small delay for improving the blue prints.

To Eli my wife. You're the only one who understands how hard it has been to continue with this PhD. Fortunately for me you hit your head on something that keeps you from being demanding with me. I love you so much.

To my PhD advisor, Cristina Barrado who had to withstand changes in orientation of the thesis and the dispersion generated by the many activities in which I have been involved.

To Dagoberto Salazar, more than a teacher, a master. He has been the man who makes bread grow.

Contents

List of Figures

LIST OF FIGURES

LIST OF FIGURES

List of Tables

LIST OF TABLES

List of Publications

The list of publications resulting from this PhD dissertation is given in inverse chronological order as follows:

Journal Papers

- C. Barrado, J. Ramírez, M. Pérez-Batlle, E. Santamaria, X. Prats, E. Pastor. 2011. Remote Flight Inspection using Unmanned Aircraft. *AIAA Journal of Aircraft.*

- Jorge Ramírez, Dagoberto Salazar, Xavier Prats, Cristina Barrado. 2012. C3 in UAS as a means for secondary navigation. *Royal Institute of Navigation Journal of Navigation.*

- Xavier Prats, Luis Delgado, Jorge Ramírez, Pablo Royo, Enric Pastor. 2012. Requirements, Issues, and Challenges for Sense and Avoid in Unmanned Aircraft. *AIAA Journal of Aircraft.*

Book Chapters

- Xavier Prats, Jorge Ramírez, Luis Delgado & Pablo Royo. 2011. Regulations and requirements, human factors aspects and situational awareness. *Wiley STM / P. Angelov: Sense and avoid in UAV. Research and applications, Book Chapter.*

Conference Proceedings

- Torras, Oscar; Ramírez, Jorge; Barrado, Cristina, & Tristancho, Joshua. 2011 (October). Synthetic vision for remotely piloted aircraft in non-

segregated airspace. *In: Proceedings of the 30th Digital Avionics Systems Conference.* IEEE, Seattle, WA (USA).

- Santamaria, Eduard, Pérez, Marc, Ramírez, Jorge, Barrado, Cristina, & Pastor, Enric. 2009 (September). Mission formalism for UAS based navaid flight inspections. *In: Proceedings of the 9th AIAA Aviation Technology, Integration, and Operations (ATIO) conference.* AIAA, Hilton Head, South Carolina (USA).

- Ramírez, Jorge, Barrado, Cristina, Pastor, Enric, & J.C. Garcia. 2009 (January). A proposal for using UAS in radio navigation aids flight inspection. *In: 47th AIAA Aerospace Sciences Meeting and Exhibit with New Horizons Forum (2009).* AIAA, Orlando World Center Marriott, Orlando, Florida (USA).

- Ramírez, Jorge, Barrado, Cristina, Pastor, Enric. 2008 (October). Navaid flight inspection optimization with UAS technology. *In: Proceedings of the Remote Sensing Conference.* German Institute of Navigation Deutsche Gesellschaft für Ortung und Navigation e.V. (DGON),Bonn (Germany).

- Pastor, Enric, Barrado, Cristina, Peña, Marco, Lopez, Juan, Prats, Xavier, Ramirez, Jorge, Royo, Pablo,& Santamaria, Eduard. 2008 (April). An Architecture for Seamless Integration of UAS-based Wildfire Monitoring Missions. *In: Proceedings of the Remote Sensing Conference.* Salt Lake City (USA).

- Pastor, Enric, Barrado, Cristina, Lopez, Juan, Prats, Xavier, Ramirez, Jorge, Royo, Pablo, & Santamaria, Eduard. 2007. Advances in UAS for forest fire fighting. *In: Proceedings of the Innovation in Unmanned Air Vehicles Systems. pp. 1 - 46.* INTA, Madrid (Spain).

Glossary

χ^2	Chi-square distribution; Statistical distribution of the sum of the squares of k independent variables
Δt_{est}	time elapsed since the last estimation of a pseudorange
Δt_{meas}	time elapsed since the last measurement of a pseudorange
$\hat{X}$	EKF State vector estimation
$\hat{X}^-$	EKF prediction of the state
ρ_{i_0}	pseudorange estimation between target and user i.
$\rho^*_{i_0}$	pseudorange estimation between track and user i improved thanks to the use of both $\vec{Sp}$ and $\vec{Sp}_i$
$\rho^+_{i_0}$	Pseudorange estimation between track and user i improved thanks to the use of $\vec{Sp}$
ρ_i	Pseudorange measurement between target and user i
σ_i^2	variance of random variable i
σ_{A_i}	Allan deviation of the clock of user i
$\sigma^2_{dmt_i}$	variance of the error generated by the different measurement times of the pseudoranges.
$\sigma^2_{synch_i}$	variance of the error generated by the synchronism.
$\vec{r}$	unitary vector following indicating the own trajectory direction and sense.
$\vec{Sp}_i$	speed vector as reported through the network (2 dimensional vector).
$\vec{Sp}$	own speed of the user expressed as 2 dimensional vector.
A	EKF transition matrix
d_i	Actual distance between target and user i
d_{proj}	distance between the receiver of a message and the projection of the emitter over the plane containing the receiver
e_{at}	Along track error as defined by ICAO
e_{ct}	Cross track error as defined by ICAO
e_{dmt}	different measurement time error; error in the distance measurement due to the use of measures taken at different instants of time between network users which have relative positions evolving in the time.
e_{M^i}	Multipath component; Range measurement error caused by the different trajectories that the signal could take between target an user i
e_{proj}	error of projection; error in the distance measurement due to the use of 3D measures in a 2D model
e_{synch}	Range measurement error caused by the synchronism of emitter and receivers clocks
e_{T^i}	Range measurement error caused by the Troposphere between target an user i
H	EKF Geometry matrix; contains the unitary vector of the lines relying the stations with the track
H^*	EKF Geometry matrix (H) optimized using both $\vec{Sp}$ and $\vec{Sp}_i$
H^+	EKF Geometry matrix (H) optimized using $\vec{Sp}$
K	EKF Kalman Gain

GLOSSARY

N_i Noise added to the actual ranges to simulate realistic conditions

N_e Component of N_{synch_i} simulating the noise generated by the emitter in the synchronism with the network

N_{M_i} Component of N_i simulating the noise generated by the multiple path in the signal propagation

N_{proj_i} Component of N_i simulating the noise generated by the projection of the 3D position of the aircraft over the surface

N_{Rx} Component of N_{synch_i} simulating the noise generated by the receiver in the synchronism with the network

N_{synch_i} Component of N_i simulating the noise generated by the synchronism with the network

N_{T_i} Component of N_i simulating the noise generated by the content of water vapour in the troposphere

$P_{\hat{X}}$ EKF Covariance matrix of the states estimation

P_Y EKF measure covariance

Q EKF Process Noise

x_0^+ x component of the track position estimation improved by the use of $\vec{Sp}$

x_i^* x component of the user i position estimation improved by the use of $\vec{Sp_i}$

Y EKF set of observations, consists in differences between observed and predicted distances

Y^+ Y improved by using the $\vec{Sp}$ to obtain more accurate estimations of pseudorange ($\rho_{i_0}^+$)

y_0^+ y component of the track position estimation improved by the use of $\vec{Sp}$

y_i^* y component of the user i position estimation improved by the use of $\vec{Sp_i}$

Spd_{Max}^0 maximum speed achievable by the aircraft

A-NPA Advanced notice of Proposed Amendment

ACAS Automatic Collision Avoidance System

ACM Airworthiness Certification Matrix

ADF Automatic Direction Finder

ADS Automatic Dependent Surveillance

ADS-B Automatic Dependent Surveillance Broadcast

ADS-C Automatic Dependent Surveillance Contract

AGL Above Ground Level

AIAA American Institute of Aeronautics and Astronautics

aka Also Known As

AMC Acceptable Means of Compliance; Set of recognized means to obtain a certification

AMSL Above Mean Sea Level

ANSP Air Navigation Service Provider

AOC Aeronautical Operational Control

ARINC Aeronautical Radio Incorporated

AS Aerospace Standard (SAE)

ASE Altimetry System Error

ASL Above Sea Level

ASTERIX All Purpose STructured Eurocontrol SuRveillance Information EXchange

ASTM Currently known as ASTM International, known until 2001 as American Society for Testing and Materials

ATC Air Traffic Control

ATCO Air Traffic Controller

ATIO Aviation Technology, Integration and Operations conference

ATM Air Traffic Management

BLOS Beyond Line Of Sight

C3SS Command Control Communication Security and Spectrum

C&C Command & Control

CASA Civil Aviation Safety Authority of Australia

CASR Civil Aviation Safety Regulation

CDF Cumulative Distribution Function

CDMA Code Division Multiple Access

CDTI Cockpit Display Traffic Information

CDTI Cockpit Display Traffic Information

CNS Communication Navigation Surveillance

COA Certificate of Approval

CONOPS CONcept of OPerationS

COTS Common Off The Shelf

CSAC Chip Scale Atomic Clock

CTR ConTRol zone

DGAC Dirección General de la Aviación Civil

DGON Deutsche Gesellschaft für Ortung und Navigation

DME Distance Measuring Equipment

DOP Dilution Of Precision

EASA European Aviation Safety Agency

EATMN European Air Traffic Management Network

EGNOS European Geostationary Navigation Overlay System

EHS EnHanced Surveillance (capacitats del Transponder Mode S)

EKF Extended Kalman Filter

ELOS Equivalent Level Of Safety

ELS ELementary Surveillance (capacitats del Transponder Mode S)

ETSO European Technical Standard Order

EUROCAE European Organisation for Civil Aviation Equipment

FAA Federal Aviation Administration

FAR Federal Aviation Regulations, Rules prescribed by the FAA governing all aviation activities in USA

ft feet; imperial unit of measure

GAL/GBAS Ground Based Augmentation System using Galileo as space segment

GAT General Air Traffic

GLONASS Globalnaya navigatsionnaya sputnikovaya sistema; Russian Global Navigation Satellite System

GNSS Global Navigation Satellite System

GPS Global Positioning System

GPS/GBAS Ground Based Augmentation System using GPS as space segment

GS Ground Station; The Control Station of the UAS, usually placed at ground.

GSN Goal Structured Notation

HF High Frequency

ICAO International Civil Aviation Organization

ICC Institut Cartogràfic de Catalunya

ICNS Integrated Communications Navigations and Surveillance

IFR Insltrumental Flight Rules

ILS Instrument Landing System

INS Inertial Navigation System

INTA Instituto Nacional de Tecnica Aerospacial; Spanish Institute of Aerospace Techniques

ITU International Telecommunication Unit

JAA Joint Aviation Authorities

JTIDS Joint Tactical Information Distribution System

LDACS L-band Digital Aeronautical Communication System (LDACS)

LoS Line of Sight; Communications performed in straight Line

MASPS Minimum Aviation System Performance Standard

METAR METeorological Aerodrome Report

MIDS Multifunctional Information Distribution System

MOPS Minimum Operational Performance Standard

MSL Mean Sea Level

MSR Multistatic Secondary Radar

NDB Non Directional Beacon

NEXTGEN NEXT GENeration of ATM system proposed by FAA

NLR Nationaal Lucht- en Ruimtevaartlaboratorium

NM Nautical Mile

NOTAM NOtice To AirMen

NPA Notice of Proposed Amendment

OAT Operational Air Traffic

OFDMA Orthogonal Frequency Division Multiple Access

OSI Open System Interconnection

PANS Procedures for Air Navigation Services from ICAO

PBN Performance Based Navigation; ICAO concept of Navigation

PCA Principal Component Analysis

PCI Peripheral Component Interconnect; Computer bus for interconnection of hardware devices

PDE Portable Device Equipment

PDF Portable Document Format

PDF Probability Density Function

PhD Philosophiae Doctor

PiC Pilot in Command

PoCoLoCo Positioning through Cooperating Loquacious Communications

PSR Primary Surveillance Radar

PT Paquet de Treball

RAF Royal Air Force

RCP Required Communication Performance

RelNav Relative Navigation; Navigation techniques based on the positioning information retrieved from the communications

RF Radio Frequency

RNAV aRea NAVigation

RNP Required Communication Performance

RNP Required Navigation Performance

RNP Required Navigation Performance

RNP Required Surveillance Performance

ROA Remotely Piloted Aircraft

RPAS Remotely Piloted Air Systems

RSP Required Surveillance Performance

RTCA Radio Technical Commission for Aeronautics

RTSP Required Total System Performance

RVSM Reduced Vertical Separation Minimum

SAE Society of Automotive Engineers

SARP Standards And Recommended Practices of ICAO

SBAS Satellite Based Augmentation System

SC Special Committee; working group of the RTCA

SESAR Single European Sky ATM Research

SID Standard Instrumental Departure

SNR Signal to Noise Ratio

SoL Safety of Lyfe

SPI Surveillance Performance and Interoperability

SSR Secondary Surveillance Radar

STAR Standard Terminal Arrival Route

SWIM System Wide Information Management

TCAS Traffic Collision Avoidance System

TDMA Time Division Multiple Access

TGL Temporary Guidance Leaflet

TIS Traffic Information System

TLS Target Level of Safety

TMA Terminal Manoeuvring Area

TOA Time Of Arrival

ToF Time of Flight of a signal between emission and reception

U.S. United States

UAPO Unmanned Aircraft Program Office of the FAA

UAS Unmanned Aerial System

UASSG UAS Study Group of ICAO

UAV Unmanned Air Vehicle

UERE User Equivalent Range Error

UPS Uninterruptible Power Supply

USA United States of America

UTC Coordinated Universal Time

VDOP Vertical Dilution of Precision

VFR Visual Flight Rules

VHF Very High Frequency

VLJ Very Light Jet

VLOS Visual Line Of Sight

VME Computer bus for interconnection of hardware devices

VOR VHF Omnidirectional Range

VPL Vertical Protection Level

vs versus

WA Washington State, USA

WAM Wide Area Multilateration

WLAN Wireless Local Area Network

Study the past
if you would define the future.
Confucius (551 BC - 478 BC)

1 Civil Aviation Concerns

1.1 Certificated activity

Regulation currently applicable to civil aviation does not contemplate the absence of the pilot in command on board, reason why UAS could not be operated as conventional aviation in non restricted airspace. Figure 1.1 shows how the operational use of an aircraft depends on some certificates that ensure the compliance with some regulation:

- Type certificate who certifies that the aircraft design is safe,
- Airworthiness certificate who certifies that a specific unit of a type of aircraft is safe for its current operation,

Figure 1.1 shows how these certifications are granted by a certification authority (e.g: EASA, FAA) following their regulations (see (3), (4), (5), (6)). These regulations have the objective of guarantee the safety of the aircraft (see (7)) or aeronautical parts based on the fulfilment of some standards or methods equivalents to those standards.

These recognised standards are, usually, object of an agreement among the different actors related with the subject of the standard (see (8), (9) and (10)) e.g: the design of

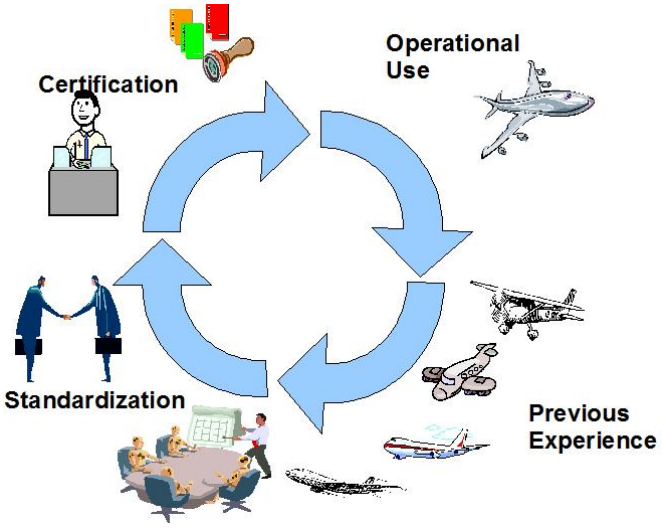

Figure 1.1: Aeronautical Standard lyfe cycle

an aircraft, a part, a safety analysis, etc. The aviation authorities (e.g: EASA, FAA...) recognise some of those standards as acceptable means of compliance (AMC) , enabling the acquisition of a certificate by the fulfilment of the standard. In fact, this recognition transform the standard in the only mean for certificate viable in the industry because the alternative way recognised by the authorities is to show equivalence to the standard (equivalence that could be hard to demonstrate).

The implication of standards on future developments makes the creation of a standard an arduous negotiation (see (11), (10)) among the involved actors, often with conflicting interests. The agreed standards usually reflects previous experiences of the involved actors that has satisfactory results; they reflect the more usual way of solving the common problems.

The application of safety to the a generic product development life cycle is analysed in (12). It is specially interesting how in the initial phase describes the documentation of risks and the requirement of a safety policy when in final phases it is described the collection of safety data from the safety test as well as from the user experience.

In aeronautical systems, safety is paramount in design. The requirement of safety based design is regulated and compliance with this regulation is recognised through the type certificate. EASA states in (13) the requirement for considering the risks associated to systems and proposes (1) as an acceptable mean of compliance. (1) describes the development life cycle for highly integrated systems, describing also the

processes that survey the integrity of the development (a.k.a. integral processes) and citing the relation with a safety process which is defined in (14).

This logical relation between certification, standards, previous experience and operational use creates a virtuous circle that takes advantage of the experience available. Nevertheless this circle becomes a vicious circle when the lack of previous experience flying UAS in civil environments impedes the creation of the standards required for the certification that shall obtain each aircraft before its operational use. Currently there are big efforts in achieving some interim standards (see (15)) that will constitute the essential regulatory toolbox that permits the achievement of operational experience required for publishing definitive standards.

Figure 1.2 from (1, p. 32) summarizes the relation between the development processes described in (1, p. 32) and the safety assessments described in (14).It could be appreciated how the aircraft level requirement are refined into more detailed requirement up to arrive to the system implementation in a five steps process. The second step ("Allocation Aircraft Functions to Systems") divides the responsibility of an aircraft function between the human flight crew and the system supporting the functionality. The fact of having the human displaced from the cabin could difficult the assignment to the humans of some responsibility. E.g: See & Avoid, which is usually performed by human crew in conventional aviation

The design of a certifiable part or component of an aircraft starts at a high level of abstraction with the definition of the aircraft functions. These functions must describe the intended operations of the aircraft, the type of aircraft and the basic functionalities offered by the aircraft(16).

Fig. 1.3 shows some functions implemented by any aircraft capable to operate in civil airspace: The capacity of see other aircraft, detect collision trajectory, avoid collision...

Once the criticality of the aircraft functions are established those are divided into flight procedures to be performed by the flight crew (and must be detailed in the flight manual), and requirements for the systems (both functional and Safety related).

Fig. 1.4 shows how this separation could simplify the aircraft systems by increasing the complexity of the flight procedures on the airplane of the left or simplify the flight procedures of the flight crew by increasing the responsibility assumed by the systems onboard on the UAS on the right. This is a key point in the development of systems

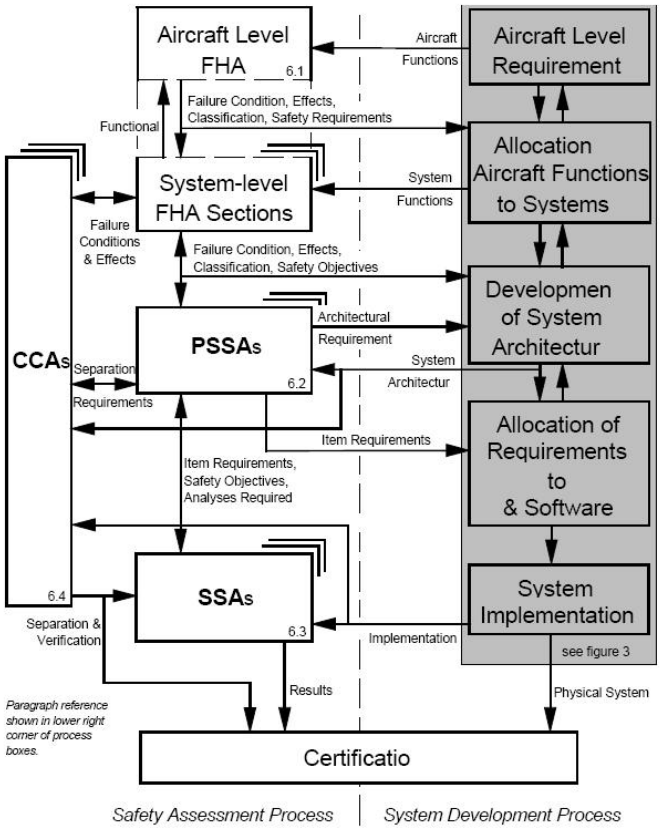

Figure 1.2: Safety Considerations in aeronautical design from ref. (1)

for UAS because there are some aircraft functions historically performed by the flight crew on board that could not be performed by flight crew on a UAS, just because flight crew are not longer on board e.g: Sense & Avoid, Command & control (C&C) and telemetry datalinks.

With the requirements allocated to the systems, those are developed following the recommendations (usually including several standards that have been agreed) of the certification authorities.

Fig. 1.5 shows how the adequacy of the design to the recommendations is recognized by the authorities with a Type certificate. An aircraft produced accordingly to this certificate could obtain its airworthiness certificate that serves to grant the access to the airspace. Here appears the problem of the lack of standards to certify the new systems appeared in the separation between system requirements and flight procedures (e.g: sense & avoid, Command & control and telemetry datalinks).

Figure 1.3: Some Aircraft Functions

ATM functions are currently evolving to a more integrated scenario with the examples of the European SESAR program (17), (18) and the American NextGen (19). In the European case, the different countries in Europe are also in a process of integration of the different airspaces (until now depending on each country) named European Single Sky based on the following regulation:

- The framework Regulation (20),
- service provision (21),
- Airspace regulation(22),
- Interoperability (23)

Some aspects of the aviation have been already unified (e.g: type certificates for aircraft, thanks to EASA (4)) but some other still remains under the responsibility of different states (e.g: Radionavigation aids certification)

In November 2007 (24), EASA published a NPA in which stated its aim to assume at medium or long term the certification of Air Traffic Management Services, including in this consideration the CNS systems.

1.2 Current CNS

The Air Navigation Service Providers (ANSPs) allows the airspace integration providing its air Traffic Management Services (ATM). Air Traffic Controllers (ATCOs) has three main functionalities to perform its duty:

Figure 1.4: Aircraft Functions assignment

- Communication
- Navigation
- Surveillance

The use of radio signals for navigation or surveillance has been a constant along the history of aviation; (25) offers a historical overview of the beginnings of the radio navigation.

Those radio signals must comply with a set of standards in order to provide an accurate navigation and surveillance. As the radio signals are used to provide positioning services for the aircraft and for the ANSPs, before authorising its use, their performance shall be verified with a flight inspection. The performance to be achieved by the signal is described in the country flight inspection manual: Spanish ANSP AENA Radio Navigation aids flight inspection manual (26), USA flight inspection manual (27). These performances are coordinated at international level by the ICAO which periodically evolutes its flight inspection manual (28).

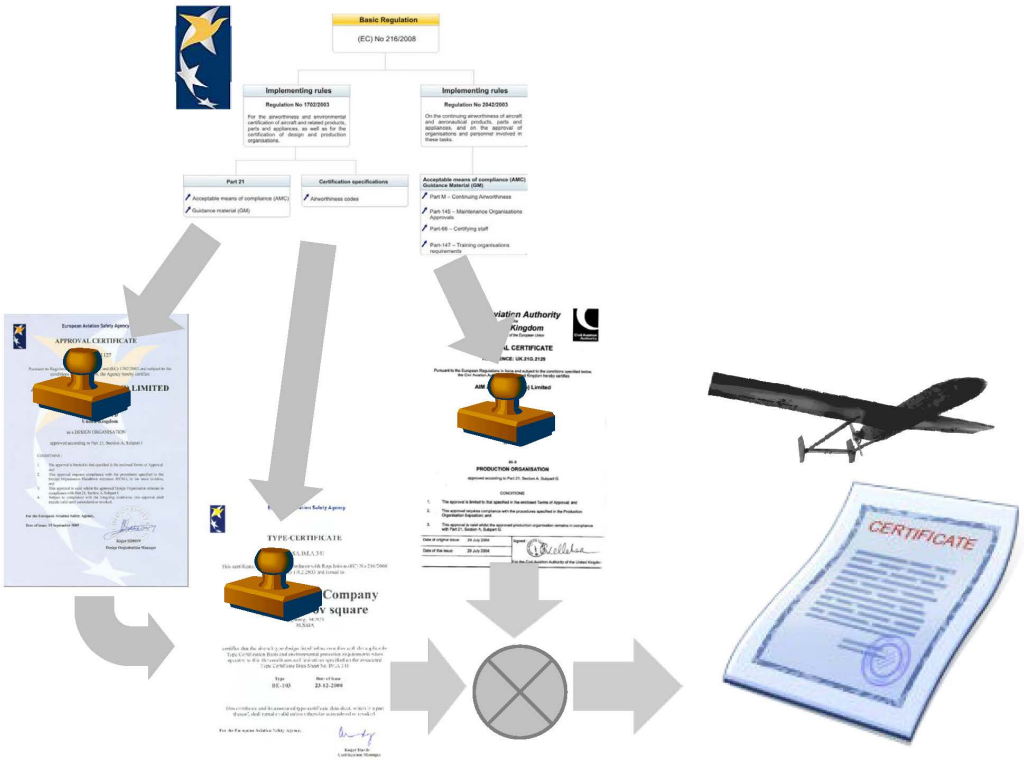

Figure 1.5: Aircraft Airworthiness obtention

Flight inspection is performed with conventional aircraft conveniently equipped with instruments that captures the radio signals and analyses its performance. Nevertheless, there is some interest in the flight inspection community to use UAS as platforms for flight inspection as a method to decrease the cost of the flight inspections. (29) describes the use of a remotely controlled flight inspection system for the calibration of enroute facilities. (30) cites UAS as one of the trends that could affect the flight inspection in the future.

These functionalities are implemented in system whose technology was developed decades ago, before the deployment of digital telecommunications. The use of the radiofrequency spectrum made by these systems is mainly analogical and each system supports exclusively one functionality. E.g:

- Radar provides surveillance.
- VOR and DME provides navigation.

- VHF provides communication.

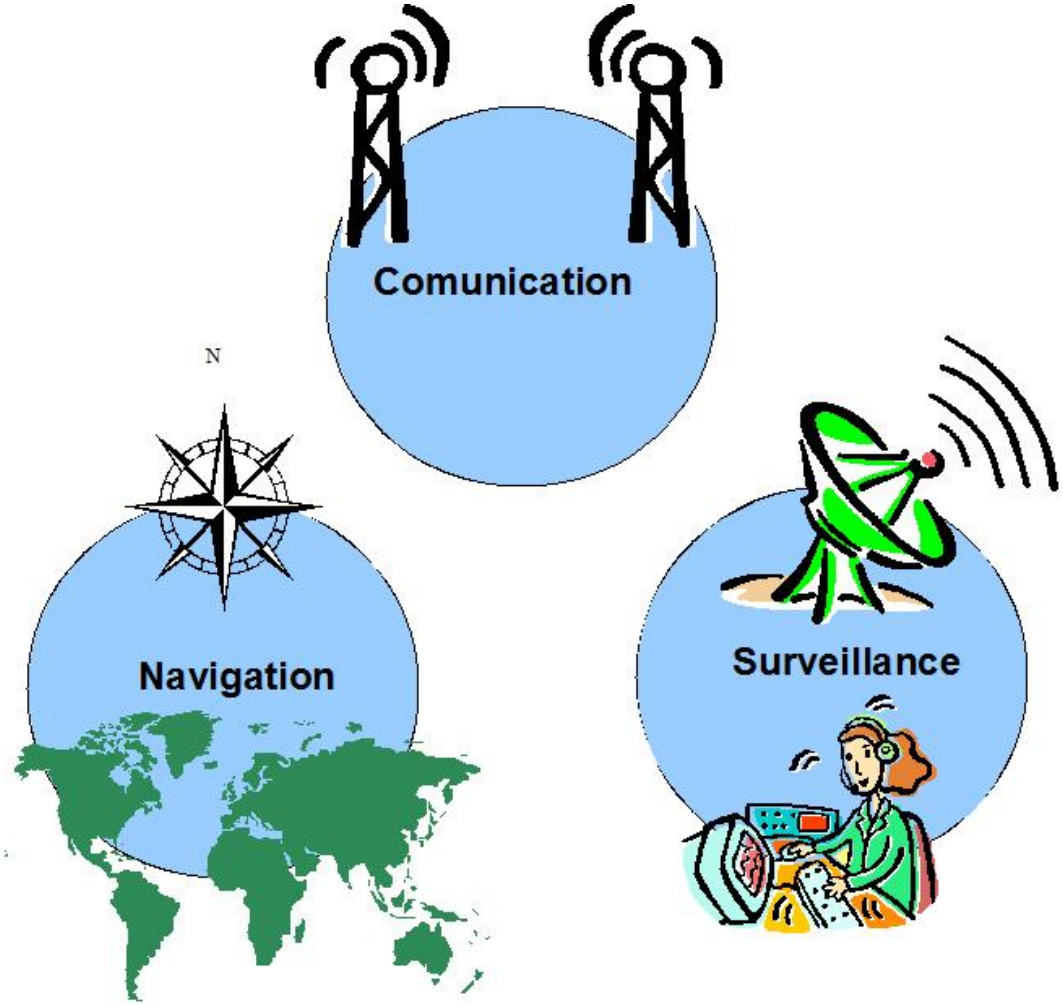

Figure 1.6: Independence among legacy CNS technologies

Figure 1.6, symbolizes the independence among CNS functionalities as well as among the system and technologies that implements the functionalities.

1.2.1 Communication

Communications employed by ATCos and ATCOs are, mainly, analogical voice communications over different frequencies (VHF and HF).

The analogical nature of the voice transmission makes those communications specially vulnerable, both against intended and unintended interferences for the current

human interlocutors but when trying to adapt to the UAS (Unmanned Aerial System) communications the interpretations of the analogical transmission as orders becomes a problem of Natural Language interpretation with all the associated complications.

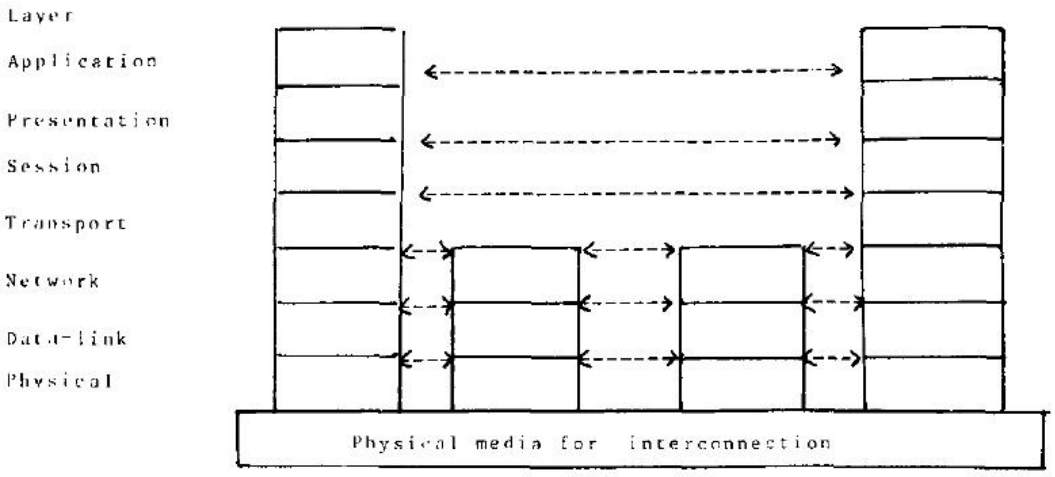

Figure 1.7: OSI Model, H. Ziemmermann

The OSI model (31) is broadly known in telematics communications. Figure 1.7 shows the decomposition in levels from the application layer at the top of the model until the physical layer at the bottom of the model.

ICAO promulgates norms and recommended methods to ensure the interoperability of the aircraft at world level. The aeronautical application layer is defined as communication protocols in (32). The systems implementing the OSI tower are specified in (33). Finally, the radiofrequency spectrum (physical layer) to be employed are compiled in (34)

The architecture employed for the implementation of the communication function depends closely on the kind of missions envisaged with the aircraft in their concept of operations (CONOPS). The requirement of being able to operate in BLOS conditions requires communication means quite different that the employed in VLOS conditions. The acceptable communications implementations for a UAS with an operating range of 200 NM will be completely different than the acceptable for a UAS with a range of 10.000 NM; being both UAS in BLOS conditions one could rely in ground infrastructure and the other must require satellite communications.

In (35) is shown how different operational ranges (VLOS and BLOS) are required

and different architectures are proposed using different means (direct communications, terrestrial datalinks, satellite communications...etc)

Improvement of communications is not a UAS exclusive problem. Is rather a transversal activity through the aviation. Some of the envisaged improvements of both SESAR(36), (17) and NEXTGEN (19) programs require characteristics that could not be found in the current communications.

In conventional aviation, there are different sources of information (radar surveillance, flight plans, meteorology, capacity...etc) that are employed differently by each actor (airlines, airports, ANSP, pilots, ground personnels...etc). currently, these communication needs are solved separately for each pair producer-consumer (see (37)).

These telecommunications improvements could be grouped in the concept SWIM (System Wide Information Management) that groups the different producers of aeronautical information (meteorology, airlines ...etc) feeding the same information system. This way, consumers could access to a single information system where they can found whatever they need in function of its user profile that allows an automated and structured exploitation.

This approach is shared between FAA and Eurocontrol (see (37) and (38)), reason why any new communication requirement in aeronautics shall be contemplated under the prism of future SWIM.

The future interoperability as been studied jointly by the main actors of the global Air Transportation System. (39) summarizes the recommendations of Eurocontrol and the FAA for the Future Communications, assessing aspects as the Spectrum bands for new systems or identifying the communication roadmap.

A more updated general overview of the current aeronautical communications (mainly based in voice communications), as well as the envisaged (mainly Datalinks) to cope with the frequency depletion is offered at (40).

The compatibility of the legacy aeronautical infrastructure in L-Band (e.g: DME, TACAN) with the envisaged physical layer for the aeronautical data-link (L-DACS1) has been evaluated in (41). The proposed combination of Orthogonal Frequency Division Multiple Access (OFDMA) and Time-Division Multiple Access (TDMA) shows an absence of interference problems.

The envisaged Medium Access to the physical layers requires a clock synchronization among the data-link users that is directly related with the performances of such data-

links. Synchronism mechanisms for the clock are not considered in this study assuming accuracies in line with existing technologies, see (42). Synchronism precision of COTS (Common Off The Shelf) devices varies among a deviation from UTC of 5ns for time reference stations, 20ns for rackeable devices and 100ns for computer cards available in the most common embedded forms as VME or PCI .

1.2.2 Navigation

The aircraft navigation is based on the use of analogical radiofrequency emissions sent from known positions (the radio navigation aids) and the interpretation of the emission on board (flight instruments). These radio navigation aids are specified by ICAO in (43) for ensuring the interoperability of the systems across the globe.

Legacy Navigation The classical navigation based on radio navigation aids is based on a point to point trajectory where each point is a Radio Navigation Aid. The navaids commonly employed in this kind of navigation are:

- VHF Omnidirectional Range (VOR). the difference between two modulations of the signal indicates the angle between the north and the line that contains both the radionavigation aid and the aircraft.
- Distance Measurement Equipment (DME). The period of time elapsed between the emission from the aircraft of a train of impulses and the reception of the answer emitted by the radionavigation aid is employed to calculate the distance between aircraft and navaid.
- Non Directional Beacon (NDB). The Automatic Direction Finder (ADF) shows the direction from the aircraft where can be found the NDB emitter.
- Instrument Landing System (ILS). The difference in the modulation allows the identification of the alignment with the runway and with the glide slope.

These navaids could be interpreted with analogical instruments, presenting an advantage at the deployment decades ago. Today the use they made of the radiofrequency spectrum could be interpreted as inefficient from the point of view of the air transport system. From an aircraft designer, each technology requires a dedicated equipment

with its own antenna on the fuselage. In terms of weight, consumption or electromagnetic compatibility this multiplicity of equipments represents additional problems to be solved during the design.

RNAV and RNP The large amount of Navigation systems at today's aircraft has motivated studies about the integration and fusion of different navigation sources as (44) where different architectures providing Navigation solution are evaluated. These architectures take advantage of the redundancy of legacy Navigation sources (INS, GPS) for providing Fault Tolerance Information.

The prospective of the Navigation includes some advanced operational concepts derived from the integration of the CNS as the Cockpit Display of Traffic Information (CDTI) Enabled Delegated Separation. (45) states the results of the MITRE Corporation Center for Advanced Aviation System Development Human in the Loop Study of CDTI Enabled Delegated Separation which is based on the availability in the cockpit of the surrounding traffic information.

Table 1.1: Required Navigation Accuracy Values (in NM)

	Flight Phase					
	En Route		**Arrival**	**Approach**		**Departure**
Navigation Spec.	Oceanic remote	Continental		Initial, Intermediate, Missed	Final	
RNAV 10	10					
RNAV 5		5	5			
RNAV 2		2	2			2
RNAV 1		1	1	1		1
RNP 4	4					
Basic-RNP 1			1	1		1
RNP APCH				1	0.3	

Independently of the Navigation source (legacy, new system, integration...) a common agreement of the navigation accuracy shall to be fulfilled to guarantee the safety of the operations. ICAO stated in its Performance-Based Navigation (PBN) manual (46) the performance requirements for the different phases of Flight, which are applicable for aircrafts, airspace and navigation services. RNP improves RNAV adding

other performances than accuracy e.g: Integrity. A newer version of the document (47) updates the required values. Table 1.1 summarizes the accuracies, in NM, that must be fulfilled the 95 % (2σ) of the time. ICAO states that the error in positioning shall be decomposed into along track error e_{at} (advance or delay) and cross track error e_{ct} (besides the trajectory)(see appendix E).

RNAV and RNP presents a more flexible approach where the definition of waypoints permits its location arbitrarily, without the need to be co-located with a navaid. Additionally, more flexible trajectories are possible.

The most employed navaid for RNAV an RNP is the GNSS who gives positioning information all over the globe with enough accuracy to achieve the strongest area specification. Nevertheless, the low SNR (Signal to Noise Ratio) at the GNSS receivers makes them vulnerable. The vulnerability of GNSS is assessed by the Volpe National Transportation Systems Center in (48), where is analysed the vulnerability of the transport system (aerial, maritime, ground and river) in USA. The signal of the GPS is analysed and how augmentation systems provides a valuable information of integrity but do not solve the vulnerability weakness against interference, spoofing or jamming. Among the conclusions can be found the recommendation of keeping backup systems and to impose the formation on these systems to the flight Crews.

The vulnerability of the satellite positioning systems is also evaluated by Eurocontrol in (49) to discard the decommissioning of existing navigation infrastructure as the existing infrastructure presents a lower susceptibility. The low susceptibility of datalinks, provided by features as anti-spoofing or anti-jamming, makes datalinks an interesting candidate to act as backup for satellite navigation systems.

The integrity of GNSS is partially provided by Satellite based Augmentation Systems (SBAS) as EGNOS which can alert of large scale unavailability of GNSS. The European Space Agency announced the availability of the open service in (50) and later on the availability of the SoL (Safety of Live) dependant services in (51).

The mentioned impact of the GNSS susceptibility could be appreciated in the Eurocontrol road map civil/military (52), in which part of the navigation infrastructure is kept beyond 2020. In figure 1.8 could be observed how the deployment of new navigation infrastructure do not imply the decommissioning of current systems.

In spite of the large amount of advantages provided by SBAS systems, still remains vulnerabilities at small scale as intended or unintended jamming caused by electronic

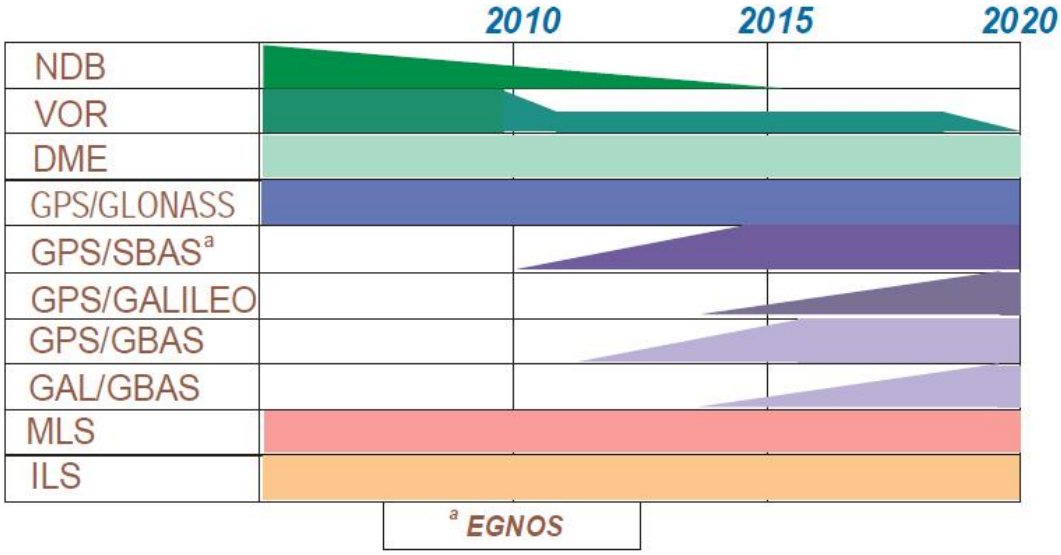

Figure 1.8: Roadmap for Navigation infrastructure, EUROCONTROL

devices (53). These vulnerabilities precluded the use of GNSS as only navigation mean, requiring a secondary navigation mean for support in case of anomalous functioning of the GNSS.

Relative Navigation Using TDMA in the digital communications required by the UAS, the distances between the emitter and the receiver could be measured thank to the ToF (Time of Flight) of the messages, which are emitted from known positions.

Figure 1.9 shows how is calculated the position of the aircraft using the ToF of the messages received from different locations.

This technique is known as Relative Navigation (RelNav) by the military which implement it in they tactical Datalinks. Those datalinks employed by military are designed to be employed in hostile scenarios with features as anti-spoofing protection and anti-jamming. These features decrease the vulnerability of the systems, which is one of the weak point of satellite based systems (48).

1.2.3 Surveillance

ICAO defines in (54) the different technologies employed in surveillance for ensuring the interoperability or aircraft and surveillance systems across the globe.

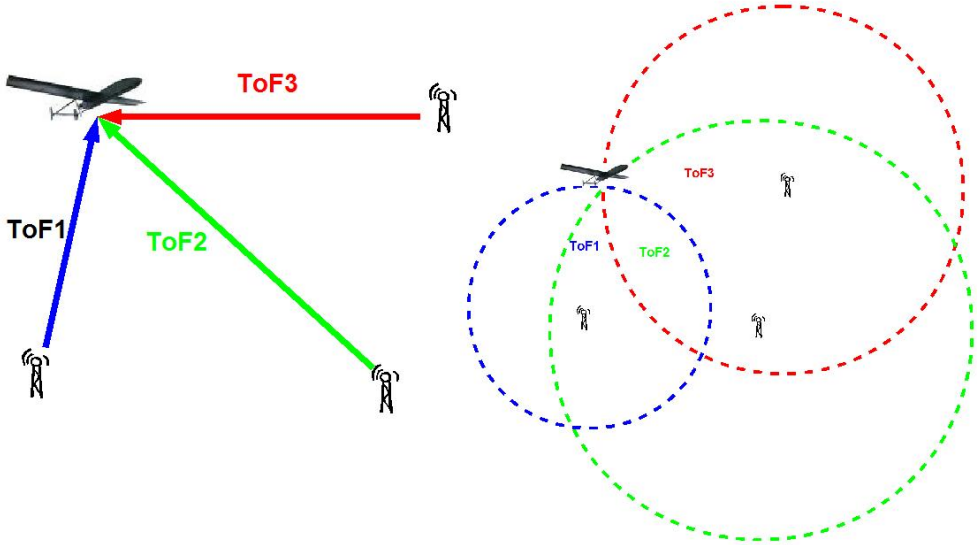

Figure 1.9: Relative Navigation on Tactical Datalinks

Radar Current surveillance services are based on the Primary Surveillance Radar (PSR) and Secondary Surveillance Radar (SSR). Both technologies have the same base: a directional antenna sends a pulse of electromagnetic energy that impacts at the aircraft emitting an echo that is captured by the radar antenna. The radar system employs the time elapsed between the emission of the pulse until its reception to calculate the distance separating the antenna and the aircraft. Thanks to this distance and the orientation of the antenna, could be obtained the position in polar coordinates of the aircraft.

The fundamental difference between PSR and SSR is the employment of a transponder in SSR to increment the Signal Noise Ratio of the echo. A specific AMC for the transponder could be found in (55). Thanks to the collaborative nature of the civil airspace users, the system becomes more precise and reduces the spurious detections.

ADS Even with the simplification that the use of transponders on board brings to the radar installations, the mechanical complexity (moving parts associated to the antenna) and the location restrictions (requires straight line of sight between aircraft and antenna) motivates big costs. In (52) different technologies (e.g: Automatic Dependent Surveillance, Multilateration) are being considered as alternatives for the future that

could reduce these costs.

The high cost of the conventional SSR hardware and the difficulties to apply radar technologies to some unpopulated areas, as the mountain canons in Alaska motivate the development of a different surveillance technology: the Automatic Dependant Surveillance. The ADS-B (Broadcast) concept is based in a datalink that transmits the own aircraft position (ADS-OUT). It is very often associated to the transponder using its capability to operate in mode S (56) to transmit the position.

The aircraft could receive the position of the aircraft in the neighbourhood if the aircraft is adequately equipped (ADS-IN). This information could be broadcast directly between aircraft or (in ADS-C) could be collected by a central processing facility that integrates the information and sends a consolidated image through a Traffic Information Service (TIS-B) (57).

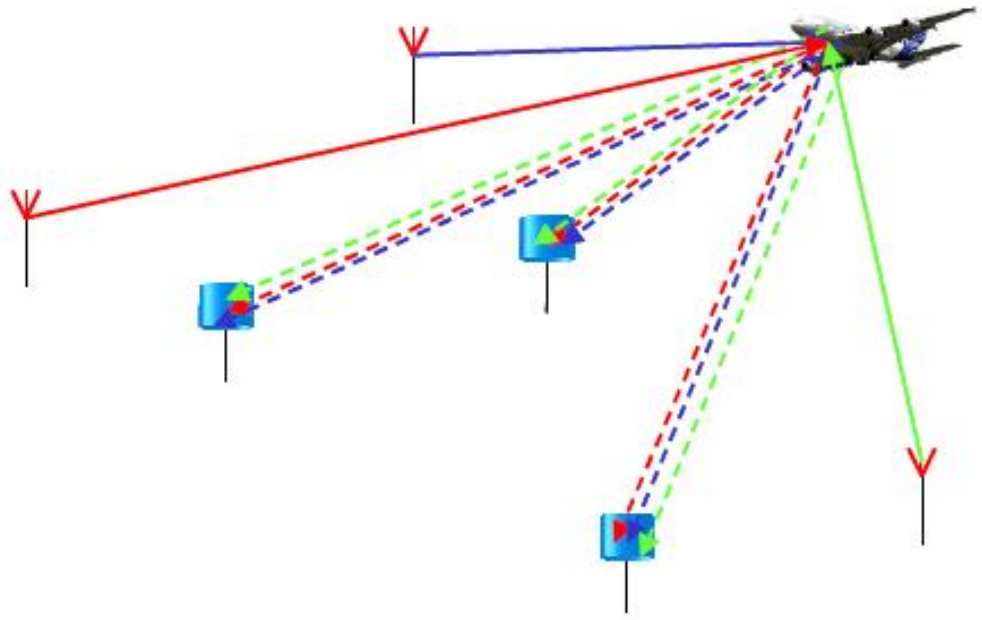

Figure 1.10: Multistatic detection principles, ICAO

Multilateration Multilateration is based in the use of omnidirectional antennae instead of the directional antennae of the primary and secondary radar systems. Figure 1.10 shows hows the omnidirectional antennae sends a signal and receives the echo of

the own signal as well as the echo of the rest of emitter antennae. With the time of emission of a signal and its time of reception at another antenna could be calculated the hyperbole where the aircraft is located. Different pairs of emitter-receivers produces different hyperboles that constitutes a system of equations that serves to calculate the position of the aircraft. With this technique, the sensor is not longer a directional antenna and becomes a network of antennae incrementing the resilience of the system thanks to the capacity of add a new node, remove a node or move a node from a location to another.

The ICAO communication panel has evaluated its viability in (58) as well as dutch NLR in (59).

An operational example of employment of multilateration could be found in the deployment program for RVSM in Europe (60) where was employed to monitory the flight altitude of the aircraft.

The correlation of the DME impulses received at different location for its use with multilateration purposes has been explored in (61).

Required Surveillance Performance The performance to be required to a surveillance system includes different aspects of the system behaviour: rotation period of the radar antennae, latency between sensor acquisition and display, position accuracy, availability continuity... etc.

This work will focus on the required position accuracy taking two references: the Lincoln Laboratory of the Massachusetts Institute of Technology and EUROCONTROL.

The Lincoln Laboratory analyses the Required Surveillance Performance (RSP) accuracy for support the separation of 3-Mile and 5-Mile in (62). Using a reference system approach simulates the accuracy to be retrieved from the radar currently available in the USA and validates these simulations with actual flight tests.

EUROCONTROL states in (63) the Surveillance performance to be required at any surveillance system that support the air traffic management.

Table 1.2 summarizes the indicators retained for the analysis in both 3-mile and 5-Mile separation spaces from both Lincoln Laboratories and EUROCONTROL. The Lincoln Laboratory requires a geographical position accuracy with a σ of less than 0.2NM for the 3NM separation and a σ of less than 1NM for the 5NM separation.

Table 1.2: Required Surveillance Accuracy Values

	Separation Required	
	3NM	**5NM**
Geographical Position accuracy (62)	$\sigma < 0.20NM$ (370m)	$\sigma < 1NM$ (1852m)
Horizontal position RMS error (63)	$< 330m$ ($< 230m$)	$< 550m$ ($< 350m$)

This geographical position accuracy shows how much variation or dispersion from the average are we facing. It includes the error generated by the delay between position updates originated by the rotational period of the radar antenna, rotational period that is not present in systems based in omnidirectional antennae as multilateration or ADS.

EUROCONTROL requires a horizontal position error of less than $330m$ for the 3NM separation (but recommends less than $230m$) and less than $550m$ for the 5NM separation (but recommends less than 350m). This horizontal position error is a threshold in the distance between the indicated position and the actual position of the track. This distance in straight line differs from the errors required by ICAO for RNP.

ASTERIX No matter the source of surveillance data, the integration of different surveillance data sources provides a integrated air traffic picture that increase its resilience from the individual sources. It exist a protocol to achieve this integration of surveillance data named ASTERIX (All Purpose STructured Eurocontrol SuRveillance Information EXchange)(64).

1.3 Convergent CNS

Conventional CNS means acts isolated; surveillance means performs only surveillance tasks, navigation means performs only navigation task as well as communication means only performs communication tasks. There is a tendency to take advantage of the synergies between communication, navigation and surveillance, making them converge.

The different CNS means are the link between the ground (where ATC is located) and the air (where the aircraft is located). This link is substantiated by the radiofrequency spectrum that the civil aviation has assigned.

The radiofrequency is assigned to its exclusive use in different application to avoid the interference that different applications could create when accessing simultaneously

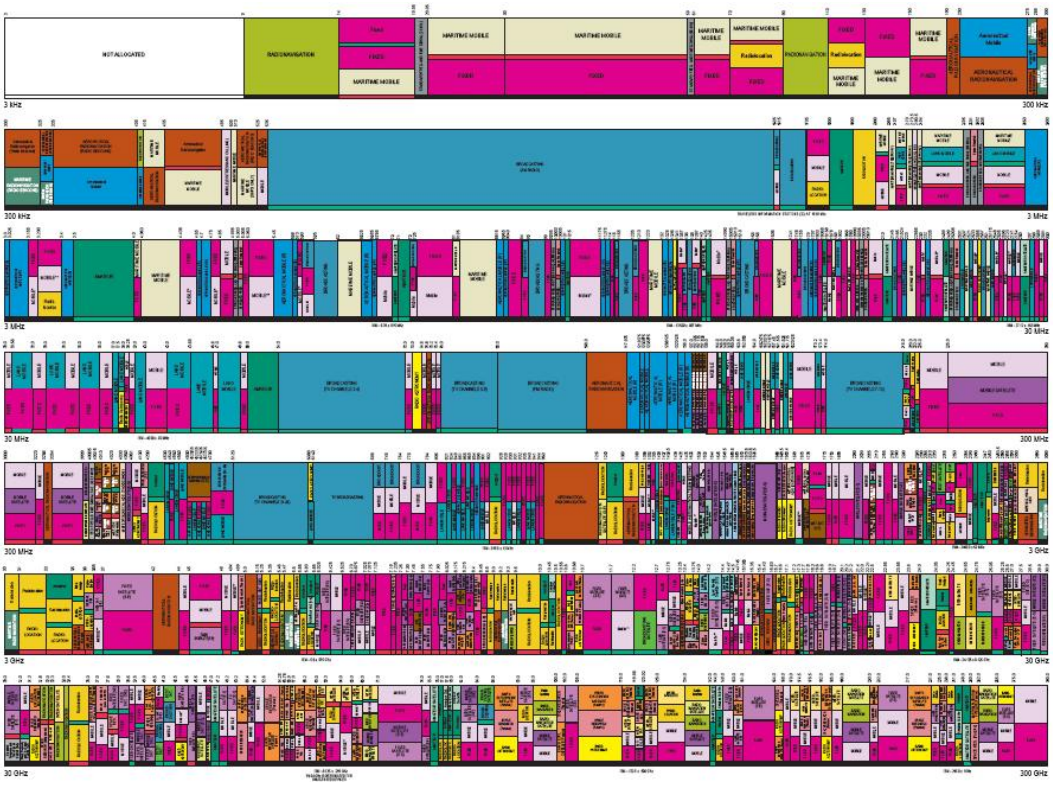

Figure 1.11: Frequency allocations in USA from (2)

to the radiofrequency. Some uses of aviation are defined at international level by ICAO in (34) to ensure the interoperability of aircraft and systems at international flights.

Nevertheless, each country has sovereignty over its radiofrequency spectrum, assigning the rest of the spectrum at his own convenience. As a consequence, there is a lack of unassigned spectrum that could be employed for UAS. As an example of this lack of spectrum could be seen in figure 1.11 from (2) which represents the spectrum assignment in USA. The rest of modern countries has the same problem with minor changes in some assignments. The absence of unassigned frequencies difficult the deployment of new technologies for CNS (38). One of the strategies to cope with the lack of unassigned frequency is the shift from analogical to digital communications that enhances the efficiency of the communications.

UAS have extra demand of radiofrequency as they require additional systems for remote Command & Control and Sense & Avoid (replacing human See & Avoid). Eurocae WG-73 on UAS and RTCA SC-203 agrees on the requirement for demanding

new assignments of radiofrequency for the implementation of these new functionalities to the ITU, considering this assignment a keystone for the deployment of civil UAS.

In this scenario of lack of assignable frequencies and exigence of new systems requiring radiofrequency, the optimization of the assigned frequencies becomes a catalyst for the new functionalities.

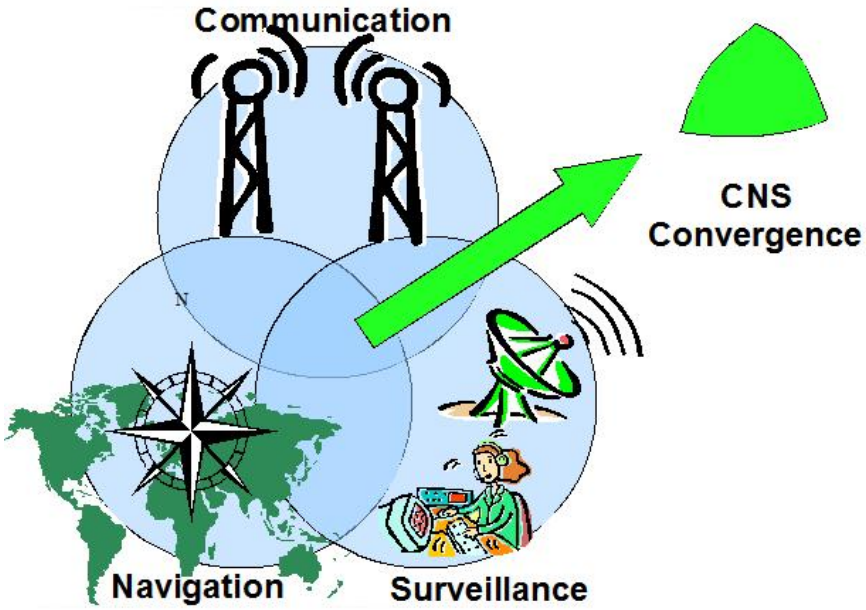

Figure 1.12: CNS functions Convergence

The current use of radiofrequency by the CNS means enables different synergies providing CNS support in different aspects convergently such as:

- SSR mode S. The radar interrogation and the transponder response (Surveillance) could be employed as datalink exchanging information (Communication).
- DME. The pulses sent by the interrogator (Navigation) could be employed on ground to obtain the position of the aircrafts by multilateration (Surveillance).
- ADF. The emission of a dedicated beacon is employed to locate the direction since the aircraft (Navigation). It also could be used with conventional radio stations (communications).

In (65), there are different techniques to obtain CNS information from datalinks. Eurocontrol has evaluated the use of a specific system called MIDS (Multifunctional

Information Distribution System). In (66), Eurocontrol details the result of its study about the use of MIDS as support for ADS-B. A premise of the study was the employment of the Euromids to reduce costs thanks to the economy of scale. Nevertheless, the massive employ of MIDS could create some problems of frequency saturation which results unacceptable as MIDS is an element of the defence in modern Armies. The interest of European Armies in the convergent capacities of MIDS as support for the Civil/military interoperability has its counterpart on USA (67).

Despite the unfavourable result of (66), Eurocontrol considers MIDS as susceptible of being used in ATM in its Civil-Military CNS/ATM Interoperability Roadmap (52). This document has as objective to ensure the interoperability of current and future military and civil CNS systems. This interoperability is reflected on the assumption of common requirements for Navigation (RNP), Communication (RCP) and Surveillance (RSP).

Eurocontrol also mentions in (52) the need of rationalization for the CNS infrastructure as well as the increasing demand on security aspects that the terrorist menace imposes.

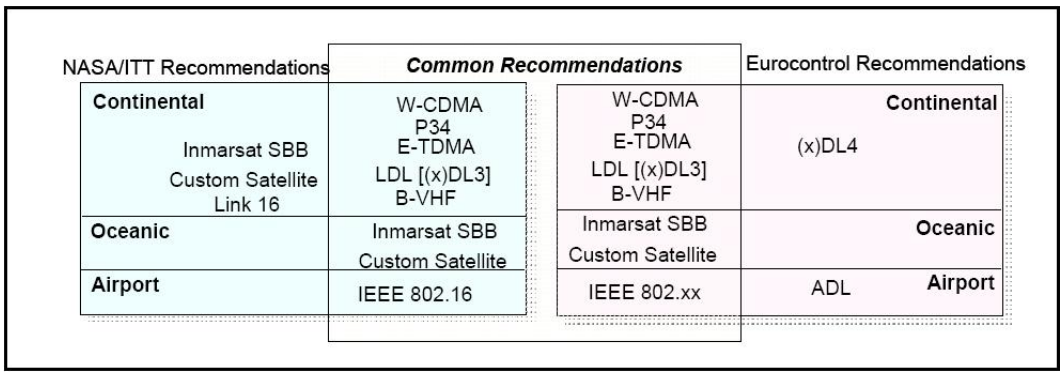

Figure 1.13: NASA and Eurocontrol recommendations

Nasa performed a technology screening program ((68), (69) and (70)) searching for candidate technologies for future communications systems. In its document Identification of technologies for Provision of Future Aeronautical Communnications ((69)) the evaluation of Link 16 as candidate technology to support the evolution of CNS means in aviation, as can be seen in Figure 1.13.

1.4 Overview

This thesis is divided in seven chapters: Chapter 2 gives an overview of the concerns for UAS operations. Chapter 3 states the objectives of this thesis. Chapter 4 describes the positioning methodology employed. Chapter 5 describes the simulation environment developed for testing the proposal. Chapter 6 analyses the results obtained in navigation. Chapter 7 analyses the results obtained in surveillance. Chapter 8 presents the conclusions and future developments.

Some additional information has been placed in 6 annexes: Annex A develops the linearisation of the measurements equation in order to emploi a linear estimator. Annex B explains briefly the structure of the extended kalman filter employed. Annex C summarizes some relevant statistical information. Annex D explains the ICAO methodology employed for computing the confidence level for GBAS, which is the same employed in our analysis. Annex E describes the error considered by ICAO in navigation (e_{at} and e_{ct}) and how to calculate it. Annex F describes the clock model employed in the simulations.

To improve our knowledge
we must learn less
and contemplate more.
René Des Cartes (1596 - 1650)

2

UAS Concerns

UAS are aircraft without human flight crew on board. A common misunderstanding about UAS is to consider them as a simplified versions of existing aircraft, just because are not loaded with people on board. Actually, the concept of UAS goes beyond the limits of conventional aviation in different aspects; comprises different levels of human flight crew dependence; requires new systems; support more functionalities and have more typologies than in conventional aircraft.

Unmanned Aircraft Systems (UAS) is in fact a misleading acronym. While the theoretical concept includes from radio-controlled air models to intelligent self controlled aerial artefacts, the envisaged regulations limits its autonomy keeping always a man in the control loop. Other acronyms that better represents this limitation are RPAS (Remotely Piloted Air System) or ROA (Remotely Operated Aircraft) .

Civil aircraft operations regulation states that the Pilot In Command (PiC) is the responsible of the safety of the aircraft, the life of the occupants and people in ground. The absence of human pilot on board has impact on the design of the aircraft being responsible of the creation of new systems to comply with functionalities performed by humans in conventional aviation, e.g:

- Air traffic detection in VFR,
- Remote operation of the Aircraft.

In this chapter some limitations on UAS operations are identified and it is stated the point of view of main standardization and regulatory bodies

2.1 Access to airspace

There is a broad consensus that UAS civil airspace access shall be obtained with a safely seamless integration, independently of which mission will be performed in which airspace type. UAVNET proposes in its roadmap (71) the need of stablish long term strategic lines in Europe and to stablish an excellence center coordinating the involved actors in civil UAS research.

Main problem for civil operations of UAS is the lack of regulation ensuring a safety integration with the rest of airspace users. There are examples of political impulse as (72) in USA that emphasizes the need of integrate UAS in the airspace, or (73) in Europe, but the lack of acceptable means to achieve the objective impedes in fact its accomplishment.

Some examples of an apparently normality in the use of UAS around the globe could be found in: (74), (75), (76), (77), (78) or (79). Nevertheless, the examples mentioned are operated as state aircraft. Shall be kept in mind the difference in the operation between military UAS, where some regulation is already published (see (80) and (81).) and civil UAS where the regulation applicable to the sate aircraft are no longer applicable.

Figure 2.1 shows how state aircraft (surrounded by blue dots) are controlled by a mission dedicated controller. The military controller is the responsible of maintaining the separation with the rest of airspace users, using military means (surveillance, communications, Navigation) and providing the directives exclusively for the state aircraft. The problems that the absence of pilot on board could be then solved by controller. The most usual tool for achieving a UAS operation is to segregate the airspace around the UAS (impeding the access to the rest of airspace users), which is usual in war environment, but is not feasible in a civil environment where the UAS shall coexist with the rest of airspace users.

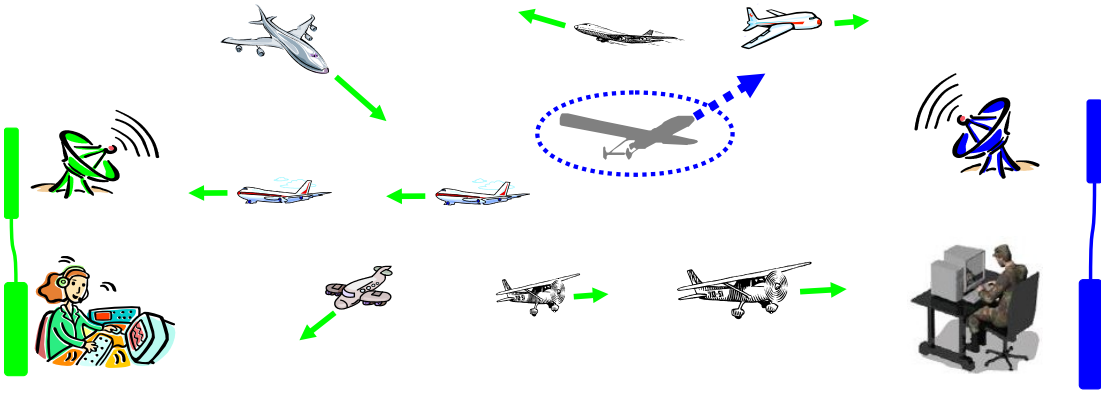

Figure 2.1: Military UAS control

State aircraft have applicable regulations both for the UAS itself (80) as well as for the pilots in command (81). Eurocontrol has already published specific regulations (82) for the use of state UAS as operational air traffic (OAT) outside segregated airspace.

Figure 2.2 shows how civil controllers are shared by all the users of a section of the airspace. This approach requires a seamless integration of UAS where the unmanned or manned nature of the aircraft does not suppose any difference to the controller in contraposition of military controllers (see fig. 2.1) which could pay special attention to a UAS.

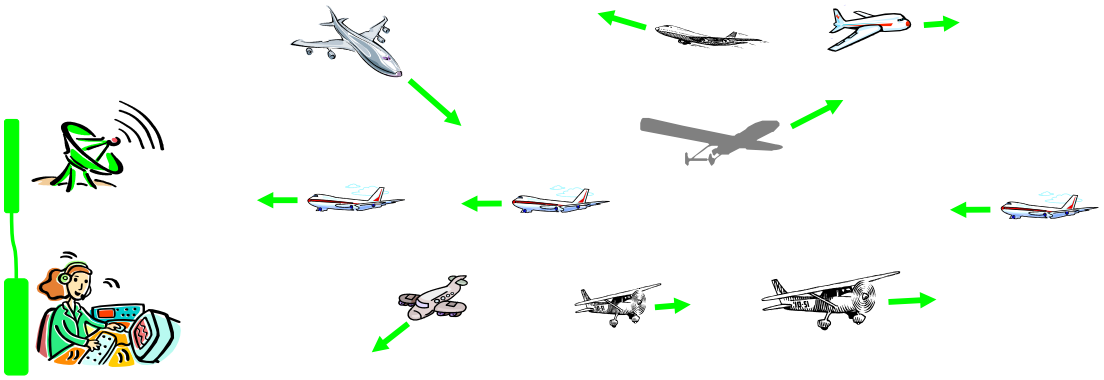

Figure 2.2: Civil UAS control

The difference between air control performed by civil (figure 2.2) and military controllers (figure 2.1) is that in a civil environment, the controller does not manage a mission but a section of the airspace and its use by the airspace users (commercial jets, general aviation, business aviation...).

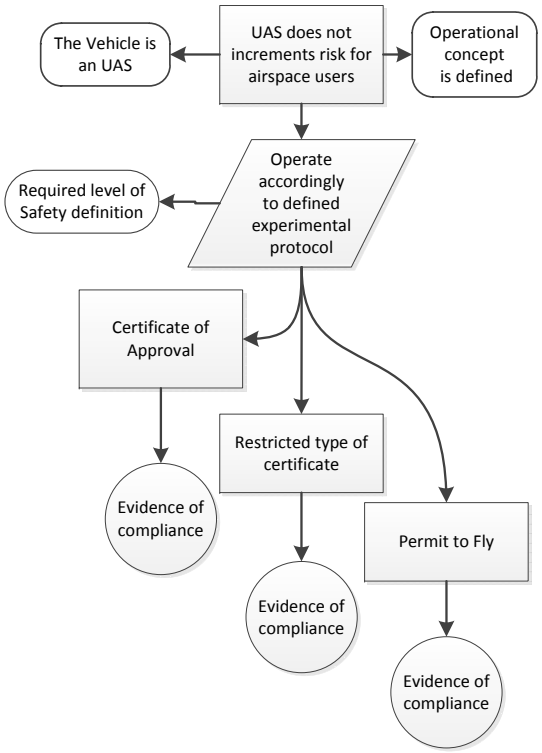

Figure 2.3: Experimental Access to Airspace

Figure 2.3 states the different mechanism to allow UAS to access to the USA national airspace using GSN Goal Structured Notation ((83) and (84)). The lack of UAS flight experience motivates a recommendation to provide access to airspace. The Regulatory bodies offer two different mechanisms to allow UAS to access the civil airspace:

- Restricted type certificate with an airworthiness certificate,
- Special Permit to Fly.

FAA developed an additional interim procedure(85) for U.S. Governmental institutions grouping the requirements of:

- Aircraft Certification Service;
  - Unmanned Aircraft Program Office (UAPO) (AIR-160);
  - Production and Airworthiness Division (AIR-200);

- Flight Technologies and Procedures Division of the FAA Flight Standards Service (AFS-400); and
- Air Traffic Organisation Office of System Operations and Safety, (AJR-3).

This procedure describes how to obtain a COA (86) aimed at granting access to UAS into the U.S. National Airspace. Includes indications on airworthiness, flight operations and personnel qualifications.

Restricted Type Certificates allows an aircraft produced accordingly to obtain a Restricted Certificate of Airworthiness which is valid only if the aircraft is operated in segregated airspace.

EASA proposes to include a statement in the aircraft flight manual limiting the operations to segregated airspace, unless mitigation measures (e.g: S&A (87)) have been accepted by the responsible authority granting access to the airspace volume in which the UAS will operate.

FAA proposes, alternative methods to the conventional compliance of FAR Part 61, which tackles certification for pilots, flight and ground instructors; and part 91, which deals with the general operating and flight rules.

In case the aircraft cannot meet the previous certification requirements, but is still capable to perform a safe flight under defined conditions, a Permit to Fly can also be granted. This could be the case of the majority of UAS. The eligibility conditions for a Permit to Fly may be different among countries e.g: Access to European airspace for UAS under 150 kg of operating mass must be granted by the national authority of the state in where the UAS will carry on the operations.

Australian Civil Aviation Safety Authority (CASA) published UAS specific regulations in the Civil Aviation Safety Regulation (CASR) Part 101: Unmanned aircraft and rocket operations limiting the UAS access to airspace only to IFR flights (if conveniently equipped) unless sufficient visual cues are provided to the UAS pilot.

(88) explains the spiral life cycle of the development of the Global Hawk navigation system. The developers used a stepped approach for the flight test with the navigation systems located in a conventional aircraft who flight near the UAS. Thanks to this separation between the airframe and the navigation systems, the eventual deadlocks of the navigation system does not implies the destruction of the airframe.

2.1.1 Certification recommendations

The newness of the UAS motivates an absence of applicable certification recommendations that impedes obtaining a Type Certificate and, consequently, a Certificate of Airworthiness. The different kinds of UAS and its operation opens the field of technical solutions to a broad spectrum of partial solutions which will be only acceptable under specific circumstances. (89) analyses the current framework for the UAS airworthiness and concludes that the type category alone does not define the UAS airworthiness category. It proposes the use of both the system type and the kind of operation to define the airworthiness in an Airworthiness Certification Matrix (ACM) .

(90) gives an overview of existing regulations and standards on S&A for UAS, highlighting the current issues and challenges that S&A systems will have to face in a future regulatory frame.

ICAO has an Study Group dedicated to the UAS: the UASSG . In (91) proposes to create a circular that must be refined towards a manual. Further development of SARPs and PANS is envisaged but not yet started.

A Restricted Type Certificate can be granted under defined and limited conditions, providing that the actual conditions of use are restricted to those in which the Certification Specification applicability is not compromised. E.g: operations assumed in segregated airspace justifies the absence of the S&A capability.

Non-governmental UAS developments must obtain a Restricted Airworthiness Certificate from FAA for its operation in USA following the specific regulations to issue Experimental Certificates(FAR §21.191).

To operate in airspace a UAS, must comply with the required equipment proving to be safe to any other user. The use of S&A systems must be accompanied by a safety case showing its adequacy to the intended airspace. In (86), FAA discards current onboard cameras or sensors as only mitigation means to comply with the see part of the S&A requirements because they have not yet shown enough maturity (specially sensing non-collaborative airspace users)

The European Authority for granting airworthiness & permit to fly is EASA (see (92)). EASA published in 2009 its certification policy for UAS (87), based on its own A-NPA of 2005 (93). The publishing date for the AMC for UAS is undefined and EASA does not envisage working on certificability for UAS before 2014 (94). EASA assumes in

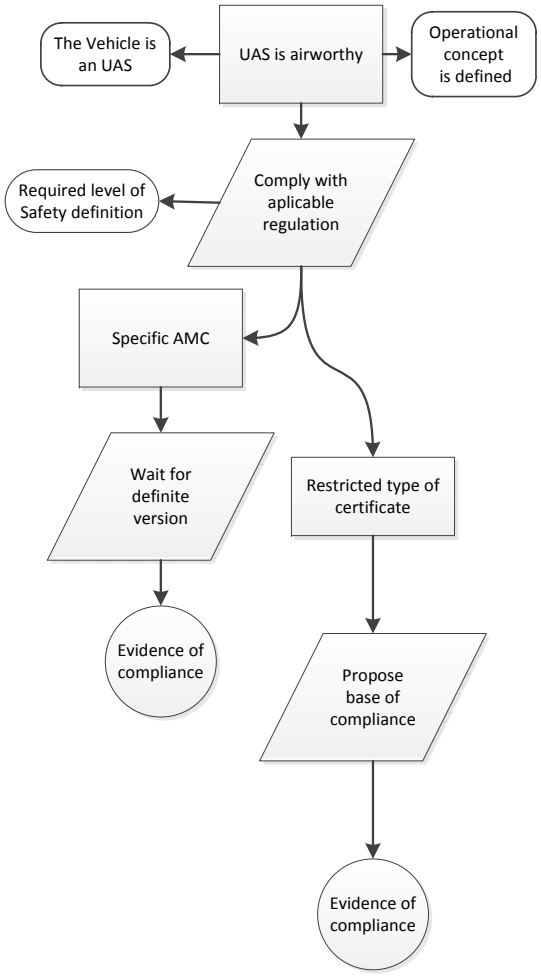

Figure 2.4: Applicable Regulation

its Policy Statement on Airworthiness Certification of Unmanned Aircraft Systems (87) that more experience is needed to publish a dedicated Acceptable Mean of Compliance (AMC) document on UAS. Figure 2.5 shows the proposal of EASA: the interim use of the existing CS-21 , subpart B (type certificates)(95) modified with some guidance on special conditions according to the general means (96) to allow the obtention of type certificate. CS-LUAV CS-UAV 25 UAS with an operating mass below 150 kg, aircraft explicitly designed for research, experimental or scientific purposes are excluded from EASA Authority.

The transport Canada Civil Aviation established in(97) a program design working group aiming to develop different deliverables from 2011 to 2016 concerning, among

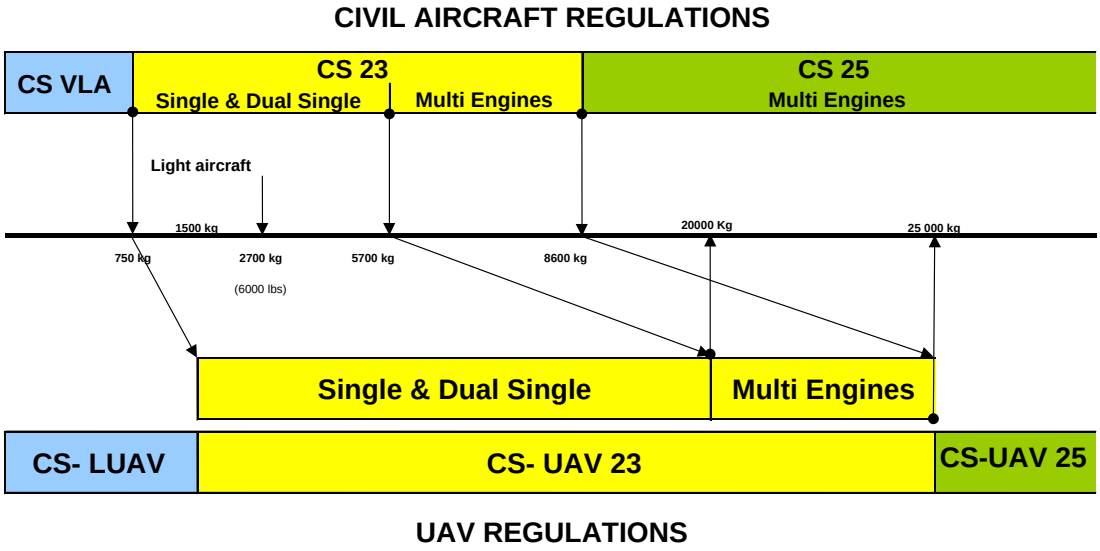

Figure 2.5: EASA proposed equivalence of CS

several objectives, S&A technologies.

(90) offers a survey of existing manned and unmanned regulations world-wide, along with recommendations on UAS integration.

All the existing protocols for flying UAS requires especial attention to S & A emphasizing in the use of human observers. Human observers provide see capabilities but it also provides navigation and surveillance in an integrated picture: situational awareness.

2.1.2 Standardisation bodies

The Acceptable Means of Compliance (AMC) accepted by EASA or FAA for aircraft certification are based on standards produced by organizations as EUROCAE, RTCA, ARINC, SAE etc. Those organisations constitute working groups, with representation of the different interests, that works for the adoption of an agreement.

The set of standards that UAS community could use as AMC are currently under definition process. RTCA in USA and EUROCAE in Europe have working groups dedicated to discuss the future applicable regulation.

EUROCAE Working Group 73 (WG-73) addressing the standards required for civilian UAS to fly in non-segregated airspace is subdivided in:

- SG-1: operations and sense and avoid (98),

- SG-2: airworthiness and continued airworthiness (99),
- SG-3: command and control, communications, spectrum & security (C3SS) (100),
- SG-4: UAS below 150 kg for visual line of sight operations (15)..

The light UAS in VLOS operations are seen as the simpler way to accumulate operational experience

RTCA Special Committee 203 (SC-203) is developing standards for UAS aiming at helping the safe, efficient and compatible operation of UAS with other vehicles. They are coordinated with FAA, Eurocae WG73 and Eurocontrol (101).

RTCA Do 320 (102) proposes an initial assessment of the applicability of existing standards to UAS. For S&A identifies as baseline existing standards on Automatic Dependent Surveillance (ADS) concepts, Traffic Collision Avoidance Systems (TCAS), Traffic Information Systems (TIS), Cockpit Display Traffic Information (CDTI) devices, etc. RTCA is developing a Minimum Aviation System Performance Standard (MASPS) for S&A for UAS.

ASTM International Committee F38 on UAS, is devoted to standards including the design, manufacture, maintenance and operation of UAS, training and qualification of personnel; is divided into different subcommittees:

- F38.01 Airworthiness Standards
- F38.02 Operations Standards
- F38.03 Pilot & Maintenance Qualifications

ASTM has a standard for the design and performance of UAS S&A systems (103) stating high-level design requirements.

The different standardization bodies work aligned with the aviation authorities and, consequently the concerns about the situational awareness appears with the special dedication to the Sense & Avoid.

2.2 Operations

2.2.1 Flight extension

A conventional aircraft operation could be represented as a decomposition in phases of a standard flight: Pre-flight inspection, Taxi, Take off, Climb, Cruise, Approach, Landing, Taxi, Post-flight inspection.

Those phases summarizes the flight plan, but there is also a previous work for each flight which could be present or not depending on aspects as the configuration of the aircraft and the storage of the aircraft. In conventional aviation, these works are not part of the flight plan and are considered as maintenance tasks or even production tasks (e.g: an airliner is assembled only once at the start of its operational life). These previous works could be divided into tactical and strategic phases.

Tactical phases includes: packaging, transport, unpacking, assembly, adequacy, disassembly.

Where: Packaging comprises the compilation of all the required equipment for the mission. Shall be kept in mind that the distance from the storage to the airfield could motivate the abortion of a mission in case of lack of some equipment.

Transport comprises the transfer from the home storage to the airfield. Unpacking comprises the extraction of the equipment from its transport. Assembly comprises the assembly of the aircraft and associated equipments. Adequacy comprises the organization of both material and human crew. Disassembly comprises the disassembly of the UAS. Those phases are usually avoided by conventional aviation users as the aircraft are assembled at the factory and remains assembled on the hangar between flights. The manipulation of the aircraft and its parts beyond its normal use during a flight is reserved to people and organizations certified with the part-145 and part-M.

There is the exception of some very light aircraft (see (104)) which are designed to be towed in a trailer by the owner from its home storage to the airfield. Nevertheless, this towing exception does not contemplate the full spectrum of UAS configurations that requires some kind of manipulation /assembly before the each flight.

Additionally to the tactical phases, the experimental nature of the UAS flights motivates an additional set of phases dedicated to the planning of the mission and obtaining the required authorizations: Operational environment planning, Flight plan planning, Emergency response planning, Payload planning.

This eventual reorganization of the flight phases could have some safety considerations as it relocates some activities from a domain (e.g: maintenance) to another (flight operations) but these are problems that have been already addressed.

2.2.2 Human Crew Roles definition

The responsibilities of the human flight crew are defined in the function assignment process (see (1)) adopting the responsibilities of the aircraft functions that systems are not assuming entirely. As explained before, UAS goes beyond the conventional aviation concept in many aspects. These different aspects motivate the adoption by the flight crew of some additional roles that came from other aspects of the aviation Operations chief, Assembly coordinator, Ground Segment Coordinator, Air Segment Coordinator, Safety Officer.

Operations Chief coordinates the entire mission. In conventional aviations is usually assigned to the Pilot in Command as he is the ultimate responsible of the aircraft and the life of its occupants.

Assembly coordinator is a role usually performed in conventional aviation by a Production Organization that holds a Production Organization Approval or POA (see ref (105)). Due to the large spectrum of UAS configurations, part of the assembly could be performed during the mission. E.g: Assembly of the wings and the fuselage that has been towed in a trailer.

Ground Segment Coordinator comprises responsibilities that are usually performed by flight crew and also by the ground personnel at airfields. Notably, the role of ground observer that ensures the separation with the rest of airspace users are usually performed on board by the flight crew itself in conventional aviation. By the side of airfields operators, the coordination among the deployed personnel on ground is part of the responsibilities of the airfield operator.

Air Segment Coordinator is a role usually performed by the Pilot in Command when airborne. The displacing of the flight crew to the ground enables richest interactions among different mission actors and could require a skilled coordinator understanding both the complexities of the mission and the constraints of flying.

Safety Officer is a role usually performed by the Pilot in Command when airborne as he is the ultimate responsible of the safety of the aircraft and its occupants. The

flexibility that gives the location of the mission Crew in ground enhances the possibilities of assignments of this role, being possible the assumption to flight crew as in conventional aviation or find another assignment.

This flexibility applies also to the regulated time of flight for each flight crew. This time of flight is regulate (e.g: (106)) to maintain at an acceptable level the fatigue of the flight crew. This limitation requires different flight crew sets for long flights. In conventional aviation, the different flight crew shall be on board, reducing the cargo capacity whilst in UAV, the different flight crew are placed on the GS.

The amount of additional roles that could be assumed during a UAS mission difficult the definition of the flight crew licenses. It is assumed that a UAS pilot shall have a safety culture but it is not clear the extent of it as well as are not defined the different kinds of licenses.

2.2.3 Network Architectural Approaches

Communications is considered one of the corner stones for the integration of UAS in General Air Traffic (GAT). The additional requirements imposed to communications come from two different circumstances, both derived from the control position split between ground and air:

- New communications internal to UAS (between UAV and GS)
- Adaptation of UAS to legacy communications (between UAS and ATC)

Communication between UAV and GS are motivated by the split of the control position between ground station and air vehicle and includes telemetry (UAV to GS) and control commands (GS to UAV).

The adaptation of UAS to legacy communications are imposed by the integration in General Air Traffic (GAT) where analogical voice communications are used. Those analogical means are very flexible in their use by humans, but difficult its automatic interpretation by UAVs. This interpretation problem and the foreseeable requirement of a human Pilot in command motivate the redirection of such communications to the Ground Station.

The new requirements of communications, both motivated by architecture and new technologies, motivate different architecture depending on the range and the availability

of infrastructure envisaged for the UAS deployment. The range envisaged for the deployment could be divided in two:

- Line of Sight (LoS)
- Beyond Line of Sight (BLOS)

The infrastructure availability could be translated into the availability of wired networks or its absence, in which case the network is usually provided by communications satellites.

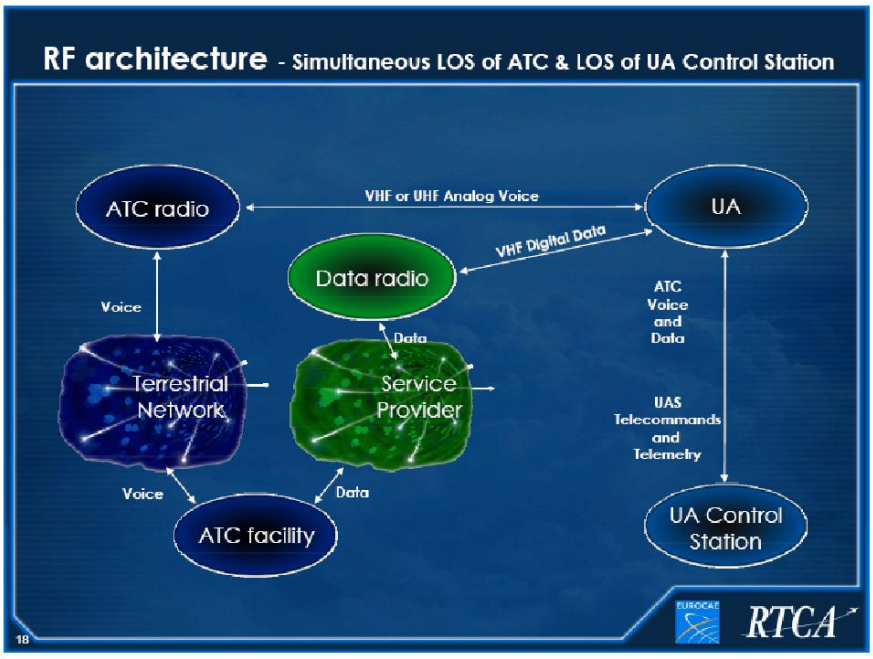

Figure 2.6: RTCA/Eurocontrol proposed RF architecture for LoS operation

Figure 2.6 shows a communications architecture where the UAV receives both voice and data communications from ATC/ATM through RF and redirects it to the GS through a different frequency through RF. This configuration makes indifferent to ATC the fact of managing a UAS or a conventional aircraft. On the other hand the communications are duplicated between ATC and UAV and between UA and GS through RF.

Figure 2.7 shows a communications architecture where the UAV receives both voice and data communications from ATC/ATM through RF and redirects it to the GS

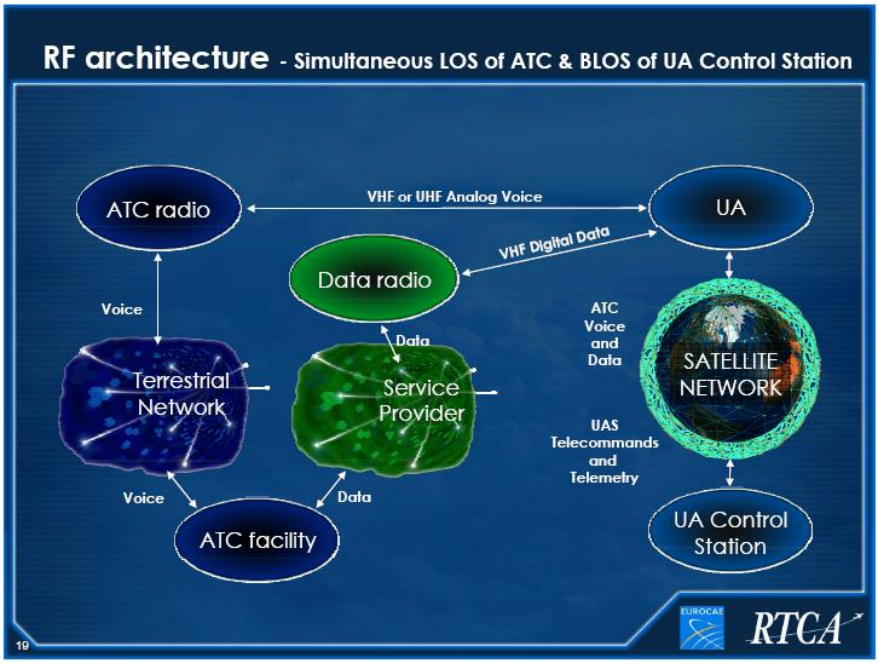

Figure 2.7: RTCA/Eurocontrol proposed satellite architecture for BLoS operation

through a satellite network. This configuration makes indifferent to ATC the fact of managing a UAS or a conventional aircraft. On the other hand the communications are duplicated between ATC and UAV through RF and between UA and GS through satellite network.

These configurations increases the flexibility for UAS deployments in BLOS conditions with the limitations that the Satellite network could impose in terms of data throughput availability (specially when itinerant) or latency (critical for responses in critical situations).

Figure 2.8 shows an architecture for remote UAV where the datalinks between UAV and GS use a satellite network and the communications with ATC and ATM are done through wired networks infrastructure.

This architecture limits the duplications of communications thanks to the existence of a ground infrastructure that allows the exchange of communications through the cable. Thanks to this approach the requirement on satellite data throughput is smaller than the architecture reflected in Figure 2.7 but limiting its applicability to operations over wired territories.

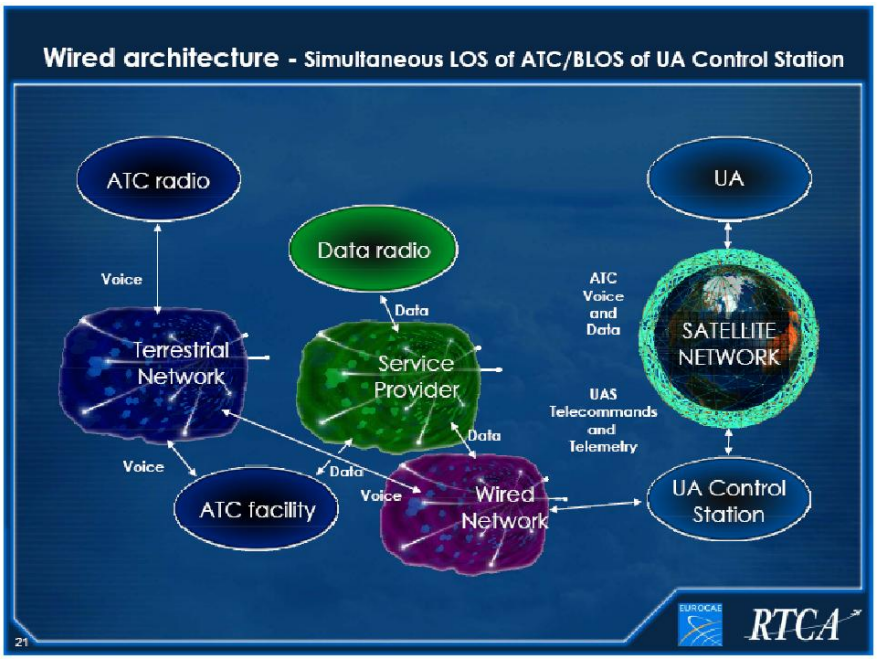

Figure 2.8: RTCA/Eurocontrol proposed wired architecture for BLoS operation

The different comms architectures presented show technical options to fly UAS in different scenarios. The major problem for the comms is the political assignment of radio frequency spectrum, which is a very scarce resource.

2.3 Function assignment

Even with the constraint of keeping a pilot in the loop, there is a high interest in avoid annoyances to the rest of civil airspace users when integrating UAS. This seamless integration requires the fulfilment of the same high level functions that are already implemented by conventional airspace users with a freshly new architecture that displaces the flight Crew to the ground.

Figure 2.9 shows a proposal of functions to be implemented by the UAS. Following the methodology for highly integrated systems of SAE (1), these functionalities shall be assigned to the UAS systems, to the flight crew or to a combination of both. There is not any problem for the majority of functionalities as they are currently implemented in the conventional aircraft.

Nevertheless, problems raise when trying to assign the functionality of See & Avoid

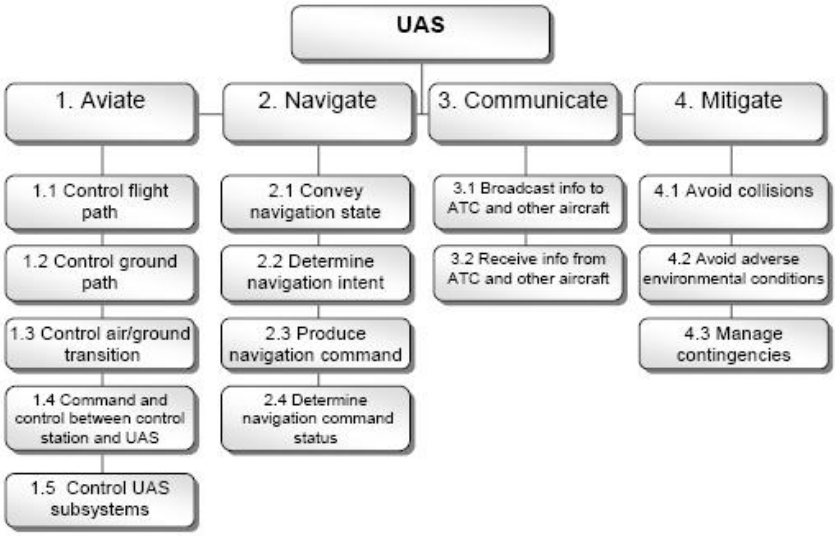

Figure 2.9: Aircraft functions proposed by NASA for UAS

as NASA proposes in (16). In it is assumed that human crew is responsible of the flight safety, especially under Visual Flight Rules (VFR) but the situational awareness capability offered by the flight crew on conventional aircraft is no longer available in UAS. The assumption of this functionality by the flight crew, which is placed on ground, could compromise the safety because of the complexity of transmitting the video information to the ground.

Figure 2.9 shows a proposal of functions to be implemented by the UAS in which the point 4.1 Avoid Collisions contains the see functionality usually performed by human flight Crew in conventional aviation. See&Avoid is the capacity of the human crew to detect and identify other threatening objects or terrain; perform actions to safely separate from them; or perform evasive manoeuvres to avoid collisions as a last resort in case of a loss of separation. See&Avoid appears as one required aircraft function which design shall find the optimal solution for the scenario (mission, airspace, range, architecture...) dividing the function between flight crew and systems.

Following the methodology for highly integrated systems of SAE (1), this responsibility assumption could be extremely difficult to implement in UAS as the complexity of transmitting visual information to the PiC on Ground could decrease excessively the safety margins.

The principal regulatory bodies agree that, the displacement of the flight crew to the ground, should be equivalent (in terms of Safety) with respect to manned aviation. Different methodologies have been proposed to demonstrate this equivalence in the for-coming UAS regulation:

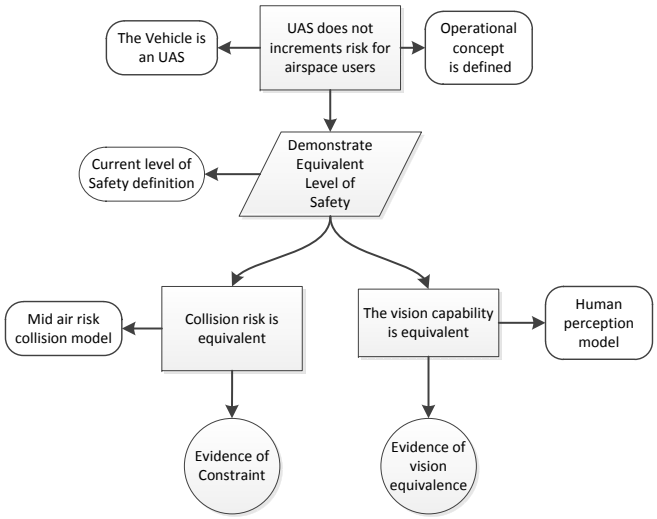

Figure 2.10: Equivalent Level of Safety

Equivalent Level of Safety (ELOS) tries to quantify the risk for human beings of Conventional aviation and provide the same level of Safety in UAS operations.

Figure 2.10 shows the ELOS concept applied to the S&A. Several interpretations of this concept has been done in S&A trying to quantify the human performance for seeing air traffic but the equivalence has not been satisfactorily demonstrated (90).

Target Level of Safety (TLS) specifies the acceptable mean number of collisions per flight hour which could result in fatalities. Figure 2.11 shows the TLS concept applied to the S &A. It is noteworthy the absence of the human models that difficult the adoption of the ELOS concept, nevertheless to show compliance with the target level of safety is not an easy question when there is not an Acceptable Mean of Compliance as is the case for the systems in conventional aviation.

For the S&A case, different studies has been produced for analysing the required performances of the systems implementing such functionality: an interesting model of the end-to-end system performance is shown in (107); a mid-air collision risk-assessment is presented in (108). The estimated number of expected collisions per hour of flight

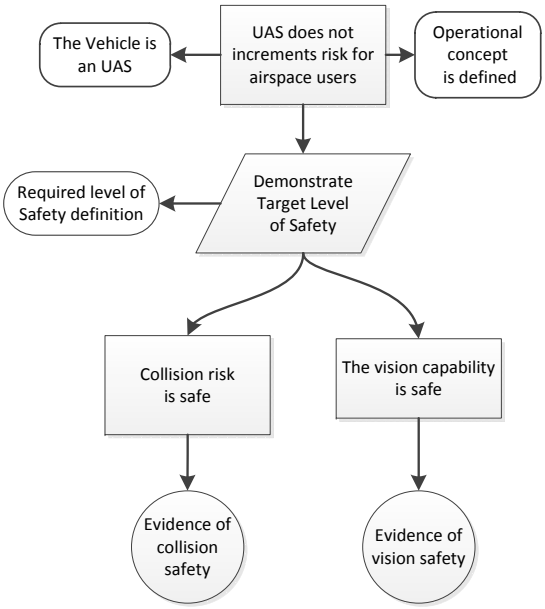

Figure 2.11: Target Level of Safety

could be useful for establishing the minimum performance requirements of S&A systems in different scenarios.

FAA mention in its Certificate of Approval (COA) (86) procedure the use of external observers or equivalent means (such as chase planes). The observers shall be located nearer than 1 NM in the horizontal plane and 3000 ft vertically. Night operations requires a special Safety Case and precludes the use of observers. As explained before, observers have the advantage of providing an integrated situational awareness.

From a technical point of view, (108) presents eight different S&A solutions families grouping by different *sense* technologies. In (109) some conflict detection and resolution algorithms that shall provide the *avoid* functionality are reviewed.

The kind of operations envisaged for the UAS could also determine the development of new system to comply with the aircraft functions more specifically with the navigation functions. Most of envisaged UAS missions are devoted to the territory monitoring requiring a RNP capability. the most usual source of navigation for RNP is GNSS capability, nevertheless, GNSS is vulnerable enough as to require a secondary means of navigation as backup. In conventional aviation this is performed through the use of legacy systems as DME or VOR but the level of situational awareness provided by DME & VOR is very limited as they where developed to provide support to

a system of airway. The performance of legacy systems does not allows its use in most of the precision mission envisaged for UAS requiring an additional backup system for precision navigation.

(110) offers an overview of the system assurance process that the British Royal Air Force (RAF) employ in the Remotely Piloted Air Systems (RPAS) . Regarding navigation, it states that a navigation solution based in GPS as only navigation mean is insufficient and additional navigation means shall be incorporated to the RPAS design.

The specificity of some kinds of UAS could bring to new requirements for already existing systems e.g: the ATC transponder. In conventional aviation, the size of the aircraft allows them to be detected by primary Radars. The small size of some UAS, and consequently its small radar cross section, could difficult its detection by primary radar. This difficulty could be seen as a security problem in the case of intentional absence of ATC transponder on board, but there is also a safety problem as the PSR detection capability could no more be presented as a backup to comply with the certification requirements of the transponder. Additionally, a failure of the SSR transponder affects not only the safety of the UAS, it also affects the situational awareness of the rest of airspace users, reducing their safety levels.

The users of the airspace maintains a separation minima to ensure the safety of flight. Figure 2.12 shows different mechanisms employed to ensure the separation. Any of the presented mechanisms requires a situational awareness in the time scale of the mechanism. While Procedural Separation requires several minutes to ensure the separation, Non-Cooperative Collision Avoidance acts in few seconds.

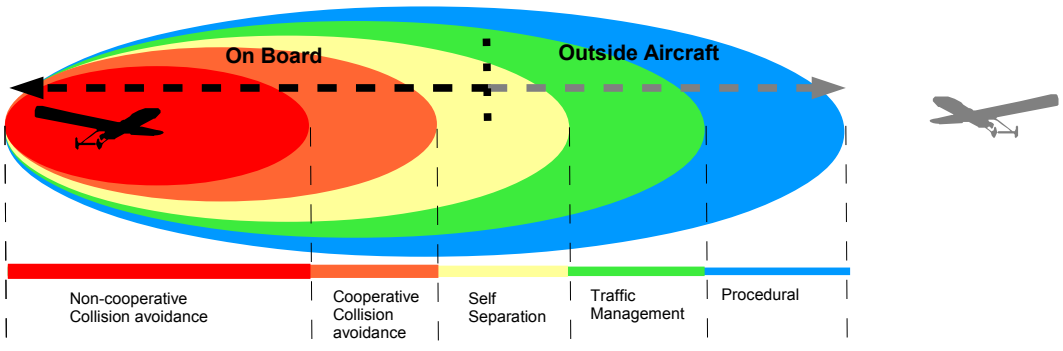

Figure 2.12: Separation and Collision Avoidance Mechanisms in conventional aircraft

Procedural separation requires the knowledge of the airways as well as the airports in

the vicinity to ensure that a new procedure will not create a conflict with the previously existing. Traffic Management requires that ANSP owns some kind of surveillance means providing position and attitude of the different airspace users in an integrated picture to take the adequate decision to avoid conflicts.

Self Separation is performed by the airspace users themselves basically by visually assessing the distance to the rest of airspace users and maintaining this distance between acceptable limits. The visual assessment could be improved by the use of some assistance systems as the Automatic Dependent Surveillance (ADS). Cooperative Collision avoidance includes all the systems between collaborative aircraft as defined by ICAO. Non cooperative collision avoidance refers to such airspace users not equipped with ACAS (Automatic Collision Avoidance System) which position and attitude shall be assessed visually by the pilot.

Errare humanum est,
sed perseverare diabolicum

Lucio Anneo Seneca (2 BC - 65)

3

Thesis Objectives

UAS are composed by the air vehicle itself (UAV) and the ground station (GS). This is a major difference with the conventional airspace users where there is not separation between control and air vehicle (i.e: the pilot is inside the air vehicle). The operation of a UAS requires then telecommunication capabilities to maintain control over the vehicle. This requirement could be derived from the necessity of monitoring the state of the vehicle, control the attitude of the vehicle, monitoring the flight plan status, etc.

The keystone of this PhD is to look at, beyond the current problem of the UAS integration, the benefits that such UAS integration could offer to the airspace users, no matter if manned or unmanned. Such synergies are available in UAS thanks to the loquacity of the communication in both senses: air vehicle (UAV) to ground station (GS) or monitoring and GS to UAV or command & control. This loquacity is absent in conventional aviation where the communication channel (mainly voice radio) is not used during the majority of the flight with the exception of some intense periods (take off, landing, transition between airspace sectors...).

This PhD thesis is focused in evaluating the synergies that UAS C&C communications offers to the situational awareness through the Surveillance and Navigation

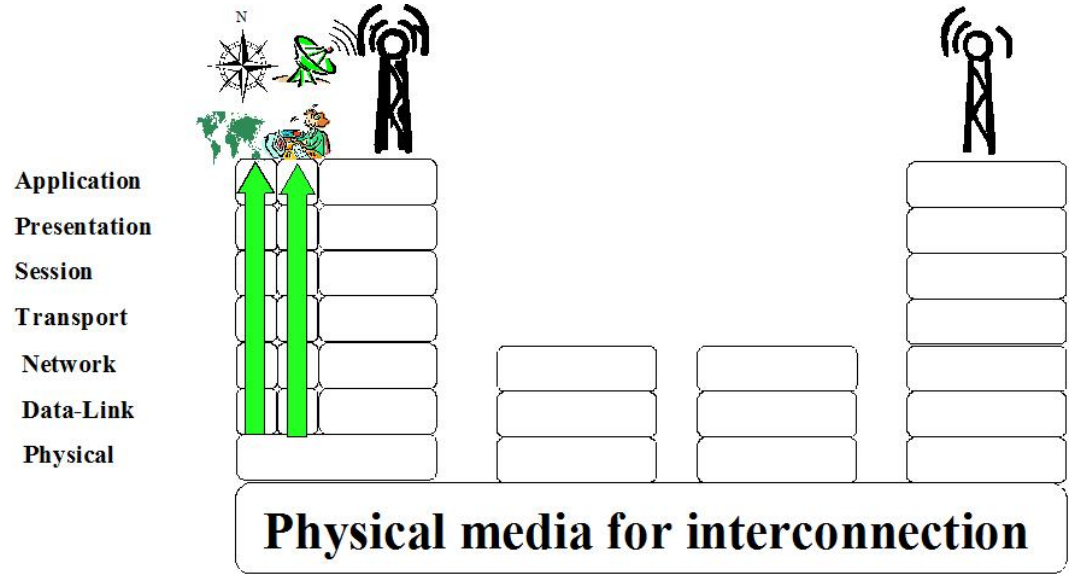

Figure 3.1: Synergy between CNS obtained in the physical layer

functionalities. As these synergies must be available to the rest of airspace users, the performances in both navigation and surveillance shall be in line with the applicable standards to guarantee an homogeneous situational awareness among UAS and conventional aircraft.

The aforementioned synergies are to be retrieved from a common physical layer as seen in figure 3.1 and represent an evolution towards a more integrated interrelation in which UAS are also part of the infrastructure of the air transport system.

3.1 Communication

UAS has shown to require very loquacious communications (see (111), (112) and (113)). This intensive use of radiofrequency in UAS is usually perceived as a drawback; the assignation of a so scarce resource as frequencies is a capital aspect (see (114), (115)). Nevertheless, is this intensive use of the communications (loquacity) in both sense of communication (air to ground, ground to air) that allows us its use in positioning, both in navigation as in surveillance.

The localization, both in navigation and surveillance, is possible thanks to the retrieved information from the physical layer of the datalink. It is assumed the use of

a datalink based on TDMA that allows the measurement of the time of flight of the messages.

This PhD assumes the data throughput described in the literature for Command & Control purposes as the base to calculate the achievable performance in both navigation and surveillance. In addition to the messages required by the command & control and monitoring functions, we propose some specific messages to improve the performance of the positioning.

3.2 Navigation

Navigation capabilities of UAs are usually not retrieved from legacy NavAids, but from GNSS.

Figure 3.2 shows how the aircraft could retrieve navigation information that complement the obtained through the GNSS taking advantage of the messages sent by the rest of users.

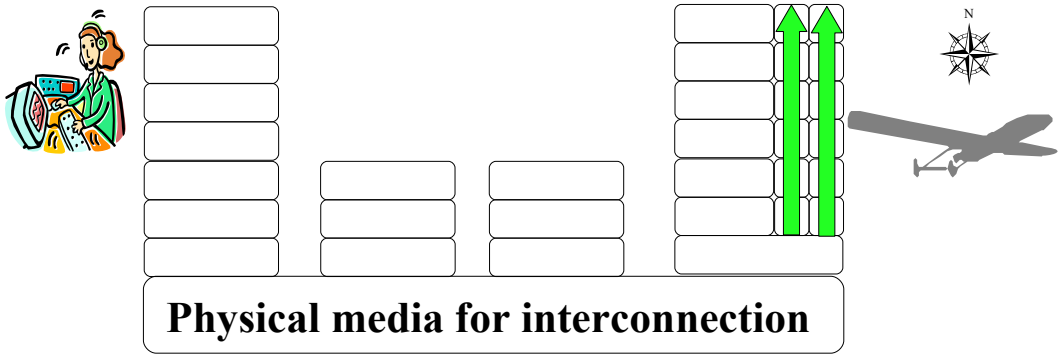

Figure 3.2: Navigation through Communication Synergy

Navigation must show compliance with the performance required by ICAO for RNP. RNP affects several aspects of the flight: the flight crew must have been trained, the operation must be designed for RNP, the infrastructure shall offer adequate performances and the aircraft itself shall be conveniently equipped to perform the designated duty.

ICAO states several performance requirements in accuracy, integrity, continuity and availability for RNP. This PhD will focus on the performance obtained in accuracy as well as integrity.

An important fact to be considered is the direct access to the physical layer for retrieving the navigation data with independence to the semantic content of the messages. This independence opens the possibility to be employed by third users at the same time that the information contained in the messages could be encrypted for security reasons.

3.3 Surveillance

Figure 3.3 shows how the messages sent by the aircraft could by used by ANSP to obtain surveillance data taking advantage of the datalink.

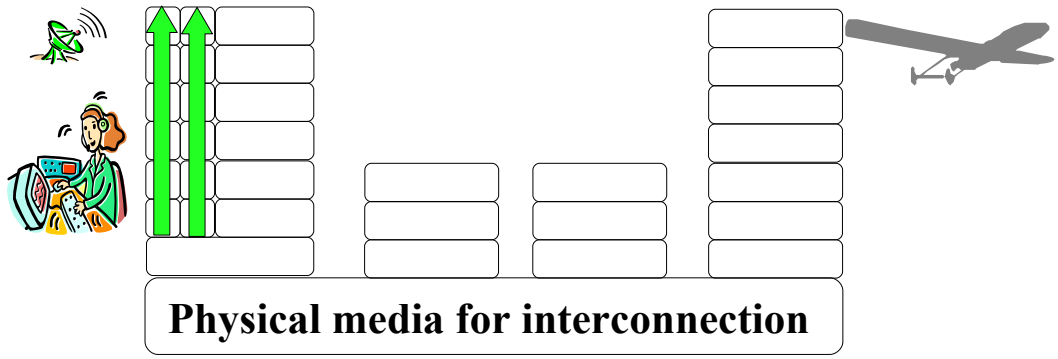

Figure 3.3: Surveillance through Communication Synergy

As in the case of navigation, the Required Based Surveillance has requirements affecting several aspects. This PhD will focus on the performance obtained in accuracy and integrity using as a reference the up to date version of the EUROCONTROL requirements.

As in the case of navigation, the use of the physical layer for surveillance purposes opens the possibility to be employed by third users keeping the content of the messages safe.

Consequently,
good warriors cause others to come to them
instead of going to the other.

Sun Tzu (544 BC - 496 BC)

4

Proposal design

The communications between GS (Ground Station) and UAV shall be in digital format. Voice communications are practical for Standard Aviation which relies in the position on board of a human flight crew that interpret the voice order but increases the complexity of the on board avionics. The communication GS-UAS shall contain at least a datalink that allow the exchange of digital information and orders.

OSI structure for digital applications using telecommunication (which is the case for the UAS control applications) structures each layer using the services provided by the lower layer (an only the immediate lower layer) and providing services for the upper layer (and only to the immediate upper layer). This independence between layers allows improvements in specific layers without affection over the rest of layers but does not allow to the physical layer that we need to measure the ToF of the messages required by the positioning algorithm.

For the purpose of this PhD thesis, it is granted a direct access to the physical layer, where the communication is performed thanks to a generic TDMA over a generic frequency that allow VLOS communication with omnidirectional antennae. The synchronism inherent to TDMA allows the range measurement between emitter and receiver

by just observing the delay at the reception time.

Once measured the ranges , two different kinds of localization are possible:

- The reception of the same message by different receivers offers the capability to obtain the position of the emitter if sharing the ranges measured by each receiver and computing a multilateration surveillance.
- The reception onboard of different messages from different emitters (with known locations), offers the capability to obtain the position of the receiver giving Navigation information.

Initial implementations of UAS Datalinks uses a dedicated datalink. This implementation ensures the control of our UAS at the cost of denying the control of more UAS with the same frequency. The TDMA access allows the sharing of the frequency enabling advance netcentric capabilities. Some information can be shared among different UAV. E.g: Metar, NOTAM.

A shared channel could present security concerns. Those concerns could be controlled using different techniques (e.g: anti spoofing). Nevertheless this PhD is focused in the positioning and does not considers the security issues.

4.1 UAS Communications

The telecommunications to be employed by UAS are currently under discussion among the involved actors in forums as the EUROCAE WG-73 or the RTCA SC-203 where the contributions to the International Telecommunication Unit (ITU) Conference are agreed.

This lack of standardization leads to point to point communications between the ground station and the air vehicle for Line of Sight operations. Figure 4.1 shows a pair of air vehicles communicating with their respectives ground stations isolately. This communications setup has the advantage of the inherent flexibility of a self contained system: flexibility in its design.

Nevertheless, this flexibility is achieved assuming a big cost: the inefficient use of the radiofrequency spectrum that separated links will impose to guarantee the independence of each UAS. For the localization purposes of this PhD presents an additional drawback: there is only one network participant available; grey aircraft sees its grey

ground station but does not sees neither the black aircraft nor the black ground station. The aircraft could be localized combining distance and angle measurements but the accuracy of the obtained position will strongly depend on the measurement errors of only two data.

Figure 4.1: Usual point to point comms in UAS

A way to reduce the effect of the pseudorange errors on the obtained position is to increment the number of measures. This PhD proposes to assume a radio frequency network instead of point to point communications. Figure 4.2 shows how the grey aircraft see its ground station (as in the point to point case presented in fig. 4.1) and also see both the black aircraft and the black ground station thanks to being sharing the radio frequency network.

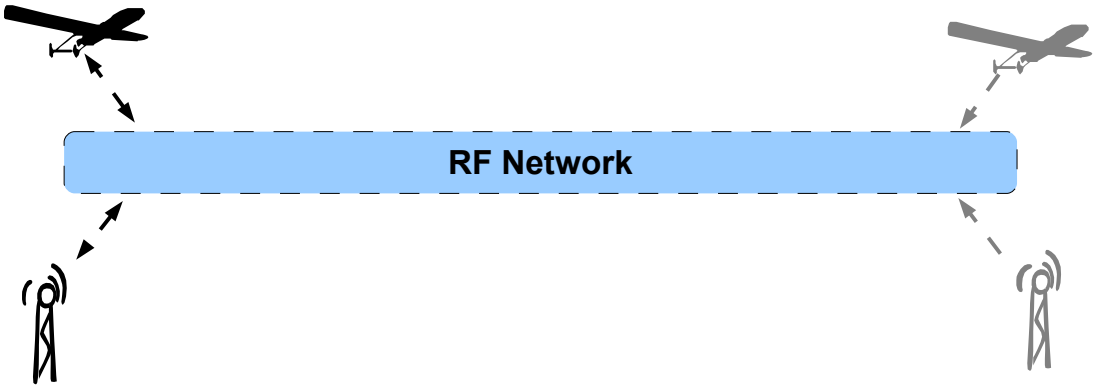

Figure 4.2: Proposed net centric comms

A shared network has the additional advantage of being more efficient in the use of the scarce radiofrequency spectrum compared with the point to point approach. This

improved efficiency makes the shared network the most plausible option once solved the standardization matters.

By interposing the RF network between the aircraft and its control station we increase the available pseudorange measurements which is the main objective, but we are also increasing the architectural options to deploy the UAS.

In unpopulated areas without available communications means there is not big difference with the point to point communication, both the air vehicle and the control station shall have their own communications means. The main difference is that the radio frequency communication supports the protocols of the RF network allowing more participants to cooperate.

In zones with dense availability of communications means and presence of UAS operations, the access to the RF network could be both performed through the control station own means (as in the case of unpopulated areas) or through the use of a communications provider means. This service provider could allow the remote deployment of the pilots (even to BLOS locations) thanks to wired networks who reroute the command&control and the telemetry data from the ground station to the proper antennae and vice versa .

One main difference between conventional aviation telecommunications and UAS telecommunications is the latency between messages. In conventional Aviation, the communications are basically AOC within ATC and airliners. Figure 4.3 shows how the conventional helicopter on the left performs such communications (blue arrows on the bottom) at specific moments of its flight (e.g: at the transitions between parking and taxi, take-off and en route ...) and remaining silent the rest of time.

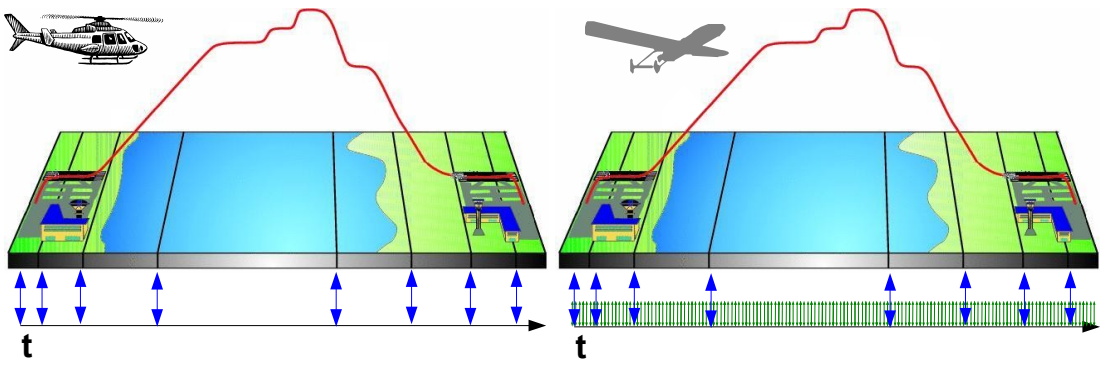

Figure 4.3: Communication events in conventional aviation vs UAS

The UAS architecture, with the flight crew displaced to the ground introduces new communication:

- UAS telemetry,
- UAS command & Control,
- payload monitoring,
- payload control

Payload monitoring and control presents low interest as a Signal of Opportunity as their presence is not guaranteed during all the phases of the flight.

UAS telemetry and Command & Control presents different advantages. Figure 4.3 shows how these communications (green arrows on the bottom) are required during all the phases of the flight for ensuring the flight crew situation awareness as well as the flight crew capacity to take the control of the flight at any moment. The performance required both for situation awareness and for Control imposes a data update rate that ensures periodic range measurements.

Being the communications a keystone for the deployment of the UAS, significant efforts have been directed to the sizing of these communications considering the worst scenario for safety reasons. Whilst the most remarked aspects is the data throughput, some indications about the data update rate could be obtained from different perspectives:

Currently employed communications in generic UAVs are described in (111), excluding the Payload which shall be considered as specific for each mission. It includes an estimation of the data throughput required for the command and status messages.

To cope with the difficulty to legally flight a UAS, some research groups employ conventional aircraft remotely operated with a pilot that could assume the flight control if necessary. This surrogate aircraft have been employed by the NASA's Langley research center and the description of the communications employed are shown in (112). The evaluated communications includes both uplink and downlink for control limited to aviate purposes, being the navigation a envisaged future upgrade.

From a Air Navigation Service Provider perspective, the interesting point becomes the Channel Saturation as they have to avoid this possibility. (113) evaluates the saturation of the UAS Command & Control Channel considering different scenarios.

Table 4.1: Communications Latencies

	Command& Control					**Telemetry**	
	Uplink		**Dowlink**				
Reference	Low	High	Low	High	Default	Low	High
(111)		4Hz		4Hz		1Hz	20Hz
(112)				7Hz	3Hz		
(113)				5Hz			

Table 4.1 summarizes the data rates proposed in different studies for the UAS datalink without the video nor the ATC Voice communications.

4.2 Proposed message catalogue

During a UAS mission, several types of communications are involved: air vehicle Command & Control, air vehicle telemetry, payload control, payload telemetry, ATC, ACARS, TCAS, SSR modes C and S etc... Some of these communications could eventually serve as signal of opportunity to measure pseudoranges and feed the navigation algorithm, improving the performances obtained using the C&C and telemetry. Nevertheless, this PhD focusses on the achievable performance during the entire flight (i.e: using UAV C&C and telemetry), discarding those communications which are not present during the entire flight.

There are initiatives to standardize the command & control communications that copes with the large variety of UAS and missions to propose a common communication core. The USA military has largely standardized the command & control between units. The MIL-STD 6016 (116) has been in use for several years. It defines the messages employed to transmit orders to military units in the battlefield. It defines the semantic content of the messages, the way to interpret those messages and the way to code them taking advantage of the capacities provided by the tactical datalinks as the JTIDS or the MIDS.

For the purpose of this PhD, only the messages employed in the positioning are considered assuming for the rest a data throughput and data rates in line as found in the literature.

Assuming the capability to measure pseudoranges between several points and a common point, it could be calculated the position of common point using multilateration techniques if the position of the rest of point are known. Figure 4.4 illustrates how the position of the black UAV could be calculated as the intersection of two circles of radius the measured pseudoranges ρ_1 and ρ_2 centered on the reported positions of the grey UAVs ((x_1, y_1) and (x_2, y_2)). Then the own position must be reported to enable its use in their positioning by the rest of users.

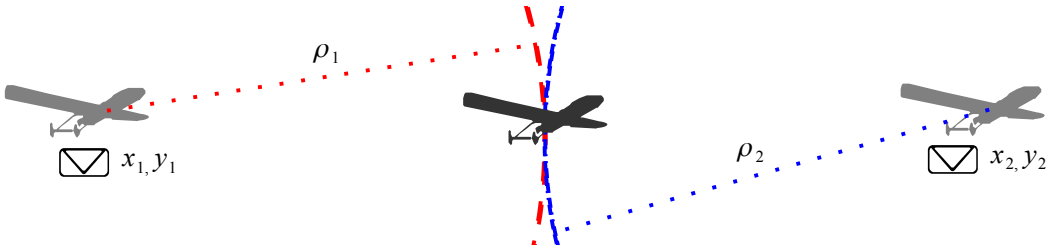

Figure 4.4: Position report required for multilateration

Figure 4.4 shows an ideal example where the pseudoranges ρ_i are equal to the distances d_1 between the communicating network users. Nevertheless, the pseudorange measurement introduces several errors resulting in an intersection similar to the shown in figure 4.5. As the distance is measured with an unknown error, it shall be interpreted not as a circle but as an annulus where the probability of found the UAV is higher. The intersection of two or more annulus no longer provides a single point but an area. Provided that using multilateration we obtain a surface where the UAV could be found with a higher probability, it could be interesting to use additional information to reduce the area provided by the multilateration.

In addition to the multilateration, a better position could be obtained adding a displacement to the previous position. Figure 4.5 shows how such position could be calculated using the speed reported by the mobile $\vec{Sp_i}$ incrementing the last known position (black UAV) to obtain an approach to the current position (green UAV). Such speed could contain measurement errors and is not necessarily constant during the entire period (since the last speed report and the moment where it is being used) but for short periods provides a good approximation. Then, the propagation of the speed through the network provides additional information to improve the positioning. The speed of each aircraft can retrieved from the GPS but also form other sources as the

inertial systems or a combination of compass and speedometer. We will assume that speed is given as a 2 dimensions vector (Sp_{x_i}, Sp_{y_i}).

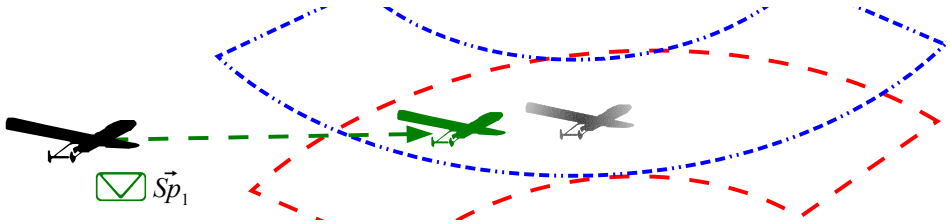

Figure 4.5: Positioning improvement provided by the speed vector

Another mechanism to improve the positioning is improving the pseudorange measurement. Figure 4.6 shows in blue and red how the error in the pseudorange measurement generates a big area. If such pseudorange measurement is improved using clocks with a more accurate synchronism, the area (green annulus) is reduced. Time deviation from the common clock could be calculated as an additional parameter of the positioning algorithm. We will assume that each aircraft and ground station will calculate and propagate its own calculated clock bias. This will result in having estimation of the clock bias of each network user as part of the location algorithm. More detail about the clock model used is given in section F.

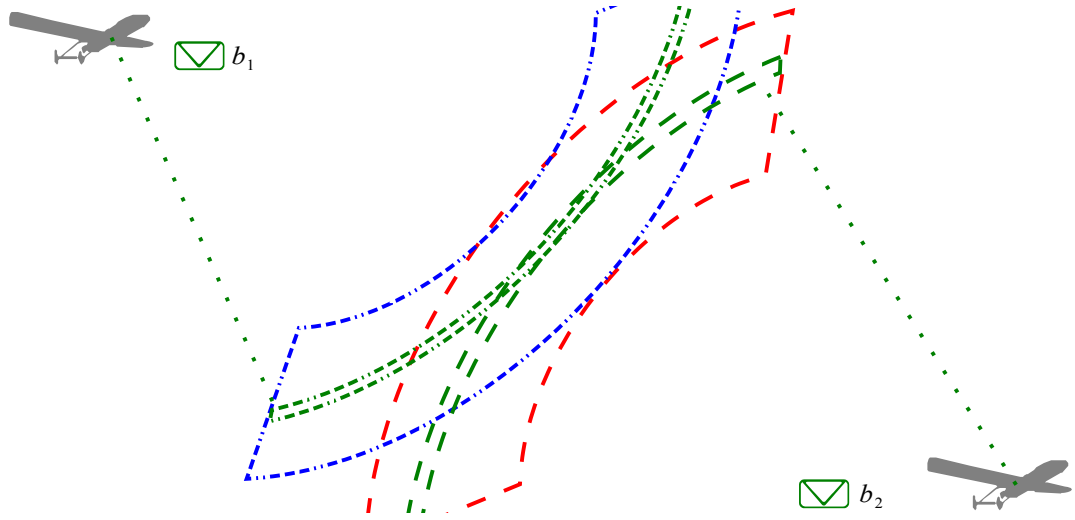

Figure 4.6: Positioning improvement provided by the time bias knowledge

Finally we will assume that all three data (position, speed and clock) are packed in the same message in the low bandwidth scenario (one message per second) defined in

table 4.1 instead of increasing the number of messages and eventually the frequency of communication.

4.3 Physical layer

The time of transmission is structured cyclically over a period. In some data-links technologies (117), (118), (119), this period is assumed to be the same as the radar in order to adjust the dissemination of radar tracks to the capacity of tracking. Even if the mechanical limitations of radars have been solved since long time ago, the cyclical organization of such datalinks remains in use. This cyclical criteria has been kept in the simulation both for simplicity as well as for ensuring some commonality with existing datalink technologies.

Figure 4.10 shows how each node of communication is provided with communication slots which represents the communication capacity available. Those communication slots must then correspond with the communication opportunities offered by the physical layer of the data-link.

Figure 4.7 shows how TDMA allocates the different communication opportunities distributing it along the time in periods of the same duration (T), using all of them the same frequency as carrier. Once consumed the entire period T, a new communication period starts.

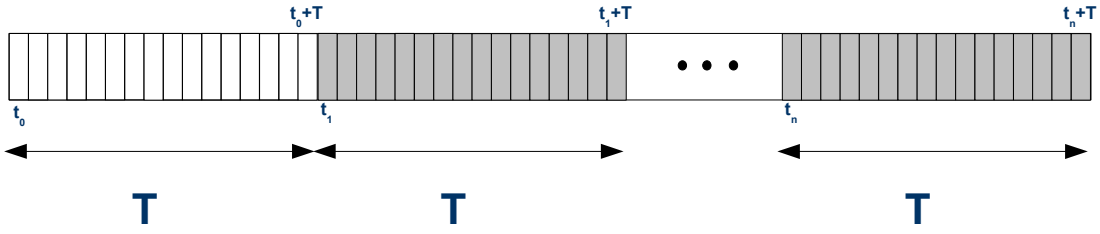

Figure 4.7: Communication Slots organization in TDMA communications

Another significant alternative considered for the access to the physical mean is the OFDMA. Figure 4.8 shows how OFDMA distributes the communication slots along the time as well as along the range of frequencies sub-carriers assigned.

In both technologies (TDMA & OFDM) the communication slots are assigned to a specific time instants in which communication must be performed. Measuring the difference between the assigned time for transmission and the reception of the message

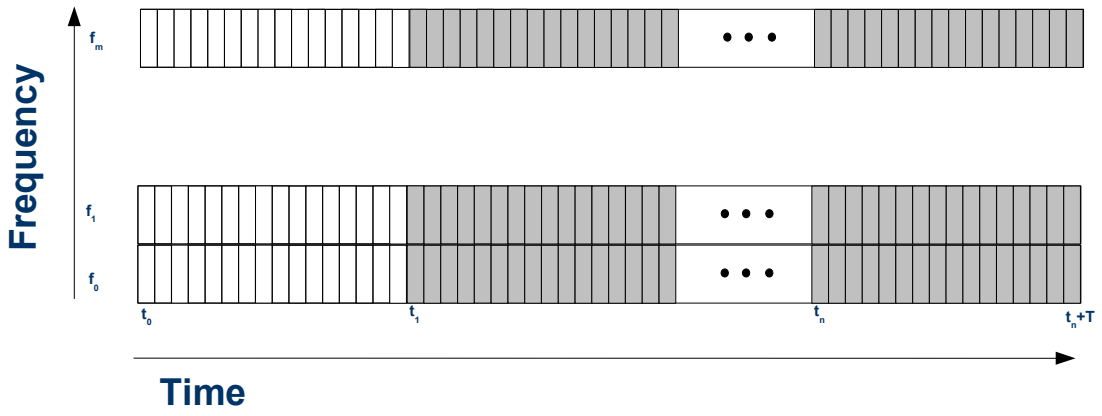

Figure 4.8: Communication Slots organization in OFDMA communications

could be calculated the Time of Flight of the message ToF. This ToF allows the distance measurement between emitter and receiver. Then, for the purposes of this PhD, each communication slot provides a chance to measure a pseudorange, independently of the choice between TDMA or OFDMA.

An interesting comparison between TDMA and OFDMA is given in (120). It proposes the future adoption of OFDMA because of its better use of the radiofrequency spectrum. Nevertheless, it also explains that the already deployed aeronautical communications are based on TDMA.

Then, taking into consideration that:

- ToF measurements could be taken from both TDMA and OFDMA,
- OFDMA is more efficient in the use of radiofrequency spectrum
- OFDMA communications are not yet deployed,
- TDMA communications are already deployed

it has been considered that the access to the physical mean considered in this PhD thesis has been a TDMA.

The identification of the arriving messages and the network users could be performed in many ways. The most evident could be by using a signature in the message to be identified. This technique has the drawback of reducing the available throughput for the message content. Another alternative could be sharing the overall communication slot allocation (see (121)). The assignment of the communication slots allows the

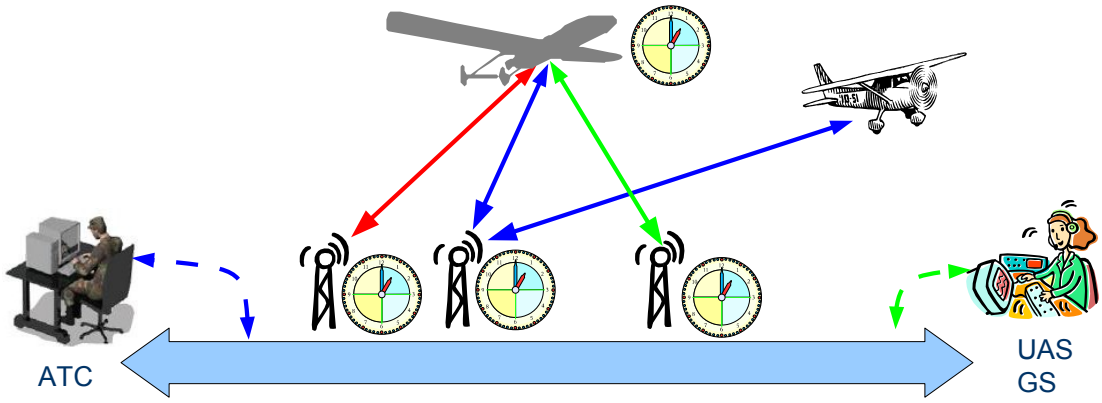

Figure 4.9: Communication Architecture Clock Synchronization

identification of the emitter by the receiver if the allocation takes into account the maximum distance to be travelled by the message to avoid collisions between messages (see at section 4.3.2).

Combining this knowledge of the ranges to the different network users with the knowledge about the positions of these participants could be computed the position of the aircraft.

In fact the range data acquisition and its further processing constitutes new applications, depending on where the range data is processed and exploited:

- if the range data is exploited on ground, it constitutes a surveillance application,
- if the range data is exploited on board, the application becomes navigation
- if the range data is both acquired on board and shared could be obtained Sense & Avoid information

These innovative uses of telecommunications requires a strong synchronization of the network, but not among the different actors. The relevant for range data acquisition is the physical layer not the upper layers. The point that needs to be synchronized are the ground emitter/receiver and the vehicle emitter/receiver which are the end points of the physical channel.

Figure 4.9 summarizes the needs for clock synchronization on the network. The ATC, the UAS ground station and the rest of application layer actors does not need to be strictly synchronized with the network clock, they only need to share data with

the network. The transmitter /receivers that shares the physical channels requires this synchronization to measure the time of flight of the messages from which obtain the range data.

The technology used to achieve the synchronization of the clocks among the network is not considered part of this PhD thesis.

The discussion about the adequacy of TDMA in front of other transmission patterns as CDMA or similar are intentionally considered as out of the scope of this PhD thesis, remaining one interesting field of further developments.

4.3.1 Communication typologies

The integration of the Ground Station into a wider communication infrastructure with the rest of actors (e.g: other UAS, ATC, meteo...) increases the number of communications available for measuring pseudoranges. This advantage comes with a drawback, instead of the simple point to point communications typology required in an isolated scenario, the RF network must be able to implement different typologies:

- point-to-point. Allowing one participant to emission and other to reception.
- point-multipoint. Allowing one participant to emission and several to reception.
- multipoint-point. Allowing several participants to emission and one to reception.
- multipointmultipoint. (aka party line). Allowing several participants to emission and reception.

The instantiation of those multiple communication structures are performed thanks to communication slots assignments that each participants have been assigned by a Network Manager.

A point to point communication is implemented by assigning permission to write in a communication slot to a participant and the right to read the same communication slot to another participant.

Multipoint emissions (present at multipoint-point as well as in multipoint-multipoint) needs a protocol to avoid emission conflicts. This protocol could be based on aloha or token ring concepts. Aloha presents the simplicity of its implementation but does not discard the possibility of conflicts, it only reduces its probability of occurrence. This

probability of occurrence difficult its use in hard real time environments as the C&C is. Token ring concept discards the probability of communication conflict introducing the network administrator that decides at each moment who could write.

Multipoint reception (present at point-multipoint as well as in multipoint-multipoint) could be implemented by assigning to each receiver the same time slot only with read access without requiring further protocols. Point-multipoint communication is implemented by assigning the permission to write in a communication slot to a single participant and the right to read to several participants. Both kinds of communications are free of emission conflicts.

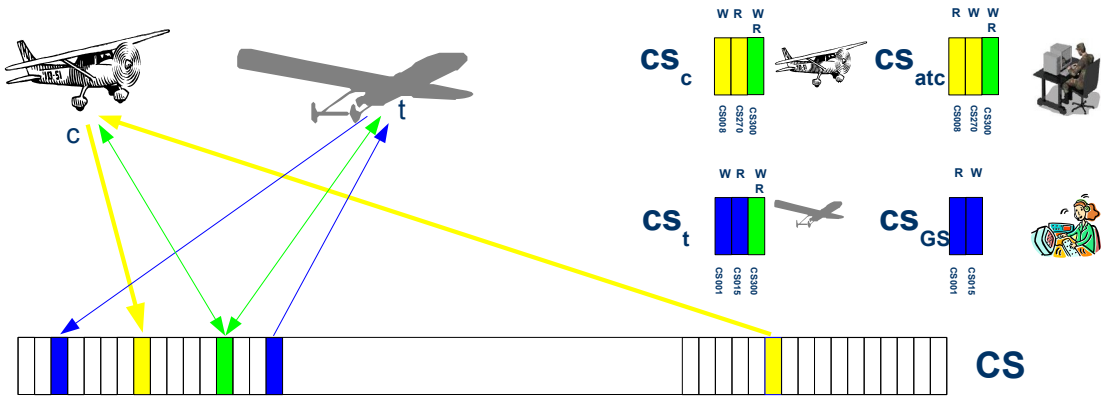

Figure 4.10: Communication Slot Assignment

Figure 4.10 shows how the available communication slots are assigned to the different participant. Each of those participants reflects their communication assignment in their tables of communication slots. In this assignment tables are also reflected the kind of access the participant is allowed by the Network Manager to manage the different kinds of communication required. In the case of fig. 4.10 the conventional aircraft has a communication slot (CS) to talk. This is reflected in his Communication Slot allocation table with the write permission (W). The same communication slot appears in the communication slot allocation table of ATC but their permission is only to read (R). This point-to-point communication is repeated in the case of the grey UAS (blue communication slots). The multipoint-multipoint is performed by assigning the same communication slot (green) with the write and read permission to the three participants that share the party line.

4.3.2 Range Constraints

The size of the communication cell is limited by the visibility of the signal and by the time of flight of the message. The visibility of a signal transmitted between two points depends on the orography but also on the emission power. Figure 4.11 shows how a message transmitted with a specific power is received up to a range R_0. Using more power at the emission, the signal could be received farther, up to R_+. How much far depends on the presence of physical obstacles (mountains, Earth curvature) that could preclude the propagation of the signal in a straight line.

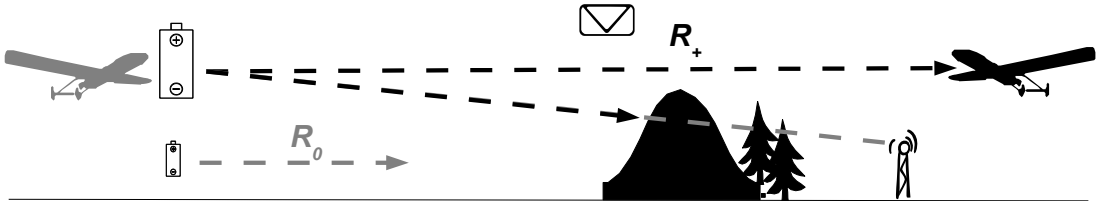

Figure 4.11: Signal Visibility

The distance between the communicating points adds a complexity to the time slot assignment when using TDMA. A message emitted at a time t_0 is not received at the same time by each network user, as the message travels at the speed of the light. This delay is used to measure the ranges in our proposal and should be considered in order to avoid simultaneous reception of messages emitted at different times. The allocation of time slots then takes into account the maximum Time of Flight between two users to add a period of time between consecutive time slots. Figure 4.12 shows a message transmitted between two synchronized network users that expends a time of flight D.

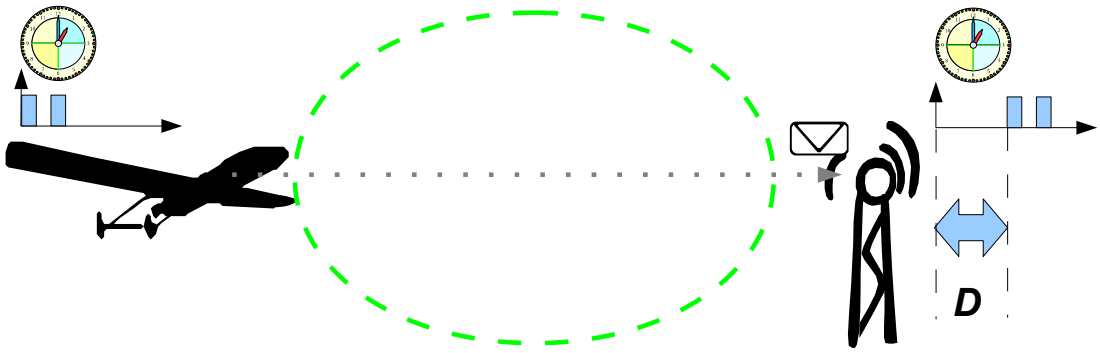

Figure 4.12: Time of Flight of a Message through the entire cell

$$D = \frac{R}{c} \tag{4.1}$$

Equation 4.1 states the delay D to be inserted between time slots as the relation between the range desired for the cell (R) considered as the longest distance between two points in the cell and the speed of the light (c).

Equation 4.1 gives the key to design the time slot assignment of a single communication cell. Adjacent cells must have additional means to avoid messages collisions. This could be performed by using different frequencies. The pattern of frequency assignment must take into account the distance between cells with the same frequency to avoid interferences. Nevertheless, the cell frequency differentiation applies only for bidirectional communications that require the fulfilment of the delays calculated with equation 4.1.

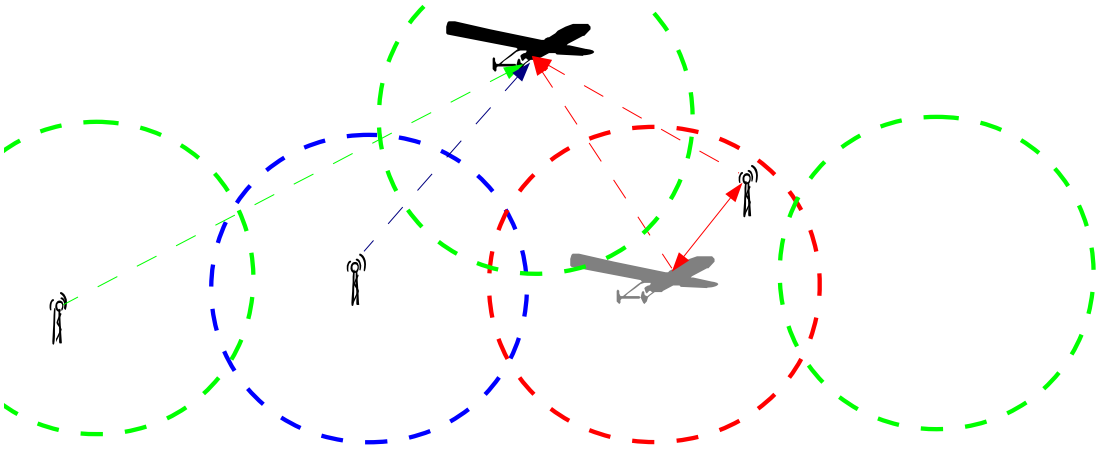

Figure 4.13: Range measurements from outside of the current cell

Figure 4.13 shows how an aircraft placed beyond the radius of a cell could still employ the transmission of the cell to navigate if knowing the time slot allocation, the frequency in which the cell operates and it is not beyond the physical limits of the radio signal propagation. The additional limitation of this use is the difficulty of establishing dialogues using the frequency of the remote cell as it could generate conflicts.

4.4 Pseudo Range Measurement

As seen in table 4.1, UAS are quite loquacious systems that requires a constant throughput to its control. This loquacity allows the measurement of the distance between emitter and receiver at a frequency of 1Hz or more.

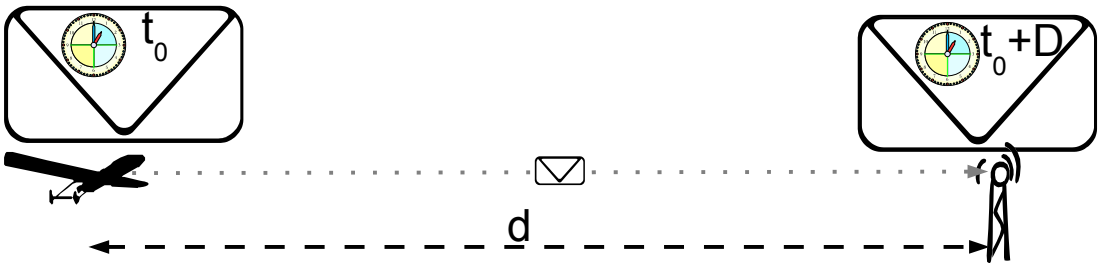

Figure 4.14: Range measurements

Figure 4.14 summarizes the physics beyond the range measurement: a message emitted at an instant t_0 is received at an instant $t_0 + D$. The delay D corresponds to the time employed by the electromagnetic signal in travel the distance d existing between the emission point and the reception point.

$$d = c \times D \tag{4.2}$$

Equation 4.2 explains how to calculate, in ideal conditions, the distance (d) using a time measurement (D) which is multiplied by the speed of light (c).

4.4.1 Pseudo Range Measurement errors

The measured ranges are not exact measures of the distance between emitter and receiver (d_i) as they include some uncertainties derived from the implementation limitations of the equipment. Eq.4.3 reflects some of the errors observed in the distance measurement:

$$\rho_i = d_i + e_{synch} + e_{T^i} + e_{M^i} + e_{proj} + e_{dmt} \tag{4.3}$$

where:

- ρ_i, Pseudorange measurement between target and user i
- d_i, Actual distance between target and user i

- e_{synch}, Range measurement error caused by the synchronism of emitter and receivers clocks
- e_{T^i}, Range measurement error caused by the Troposphere between target an user i
- e_{M^i}, Multipath component; Range measurement error caused by the different trajectories that the signal could take between target an user i
- e_{proj}, error of projection; error in the distance measurement due to the use of 3D measures in a 2D model
- e_{dmt}, different measurement time error; error in the distance measurement due to the use of measures taken at different instants of time between network users which have relative positions evolving in the time.

4.4.1.1 Synchronism error (e_{synch})

The clocks of each Network User are synchronized to the same time reference but with a certain level of precision that affects the accuracy in the range measurement. $c(dt^0 - dt^i)$ Fig. 4.15 tries to summarize how an error in the synchronism affects at the

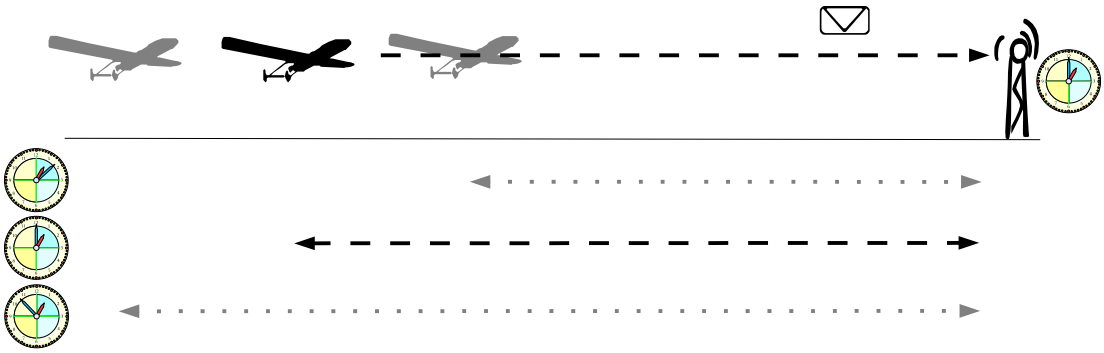

Figure 4.15: Range Measurement Error generated by synchronism

measurement of the distance and generates an error in the measurement. The black aircraft and the black antennae represents two network users perfectly synchronized. The time of emission at which the message is sent by the aircraft is known by both users and then the difference between the time of emission and the measurement of the time

of arrival of the message multiplied by c should give the distance between both users. This is true for the black aircraft which is perfectly synchronized with the receiver.

If the clock of the aircraft is advanced, the message will be sent in advance and consequently the difference between the theoretical time of emission and the time of reception will represent a smaller magnitude than if the clocks where perfectly synchronized. This results in considering the aircraft nearer than it really is (grey aircraft at the right of the true position of the aircraft, represented in black).

If the clock of the aircraft is delayed, the message will be sent later on and consequently, the difference between the theoretical time of emission and the time of reception will represent a bigger magnitude than if the clocks where perfectly synchronized. This results in considering the aircraft farer than it really is (grey aircraft at the left of the true position of the aircraft, represented in black).

4.4.1.2 Troposphere error (e_{T^i})

Figure 4.16 shows how the content of water in the atmosphere could affect the transmission of the signal modifying the speed at which the message travels. The black line represents the straight line travel of a signal through an atmosphere with a low content of water vapour. The gray line represents the same travel in straight line but this time through an atmosphere with a high content of water vapour. The higher content of water vapour, the lower speed of transmission for radio-frequency signals. This lower speed produces a delay in the arrival of the signal which is transferred to the range estimation as a bigger range than the real.

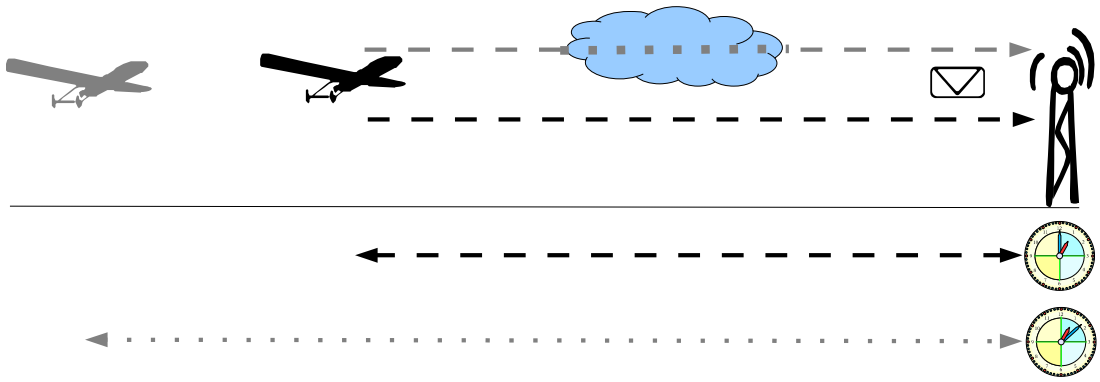

Figure 4.16: Range Measurement Error generated by troposphere content of H_2O vapour

The value of the water vapour content in the atmosphere varies slowly with a time scale of hours producing biases in the range measurement that could not be filtered and requiring its estimation. It could be estimated thanks to the meteorological information available at the region if distributed through the network. It could also be estimated as an additional variable of the equations, requiring in this case more range measurements.

Being its effect considerably big for the scale of the problem, and considering that could be estimated with already existing means, it has been omitted from this thesis.

4.4.1.3 Multipath error (e_{M^i})

Figure 4.17 shows how the signal travels in a straight line (black line) from the emitter to the receiver. As the signal is emitted in all directions, it could also arrive to the receiver after rebounding in some surfaces (gray dotted line). These rebounded signals travels a bigger distance than the one that has travelled in straight line generating an error in the range measurement as the receiver could have difficulties to identify when is arrived the correct signal.

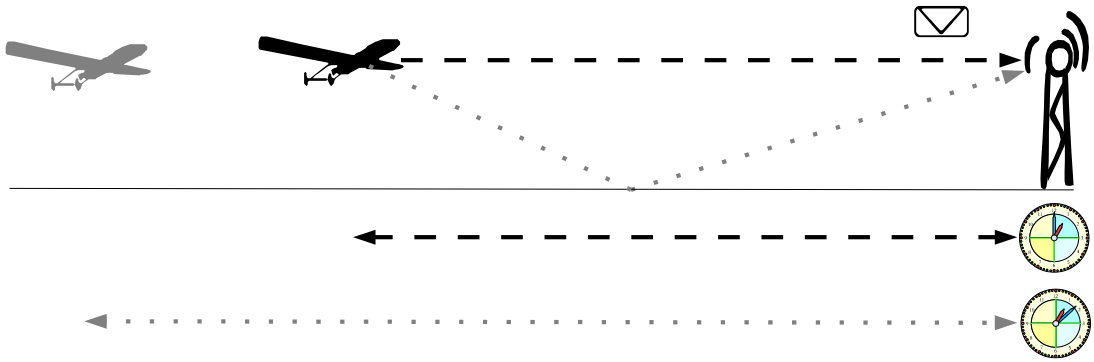

Figure 4.17: Range Measurement Error generated by multipath

This multipath error presents big inconveniences for its use in navigation. It introduces biases that endure over time, preventing its filtering. This is a common problem for localization based on radiofrequency.

This multipath error presents a behaviour attached closely to the characteristics of the location. Different materials (e.g: lakes vs forests) have different reflections as well as different terrain shapes (e.g: urban canyons vs extensive agriculture). . The behaviour of the multipath effect also depends on the frequency employed for the transmission which, for the case of the UAS, are still under discussion.

Being the multipath effect a very complex item which depends of aspects still to be defined (e.g: the frequency employed), its characterization has been deliberately omitted in this Phd thesis.

4.4.1.4 Error of projection (e_{proj})

Fig. 4.18 tries to summarize how the measures obtained in the 3 dimensional space introduce an error when translating to 2D. The position to be considered when using 2 dimension representation of the space is the projection of the aircraft position (black aircraft) over the plane containing the receiver (intersection of the segmented black line and the horizontal dotted line), whilst if using the distance d as the distance between receiver and projected position what we are considering is a different projection at a longer distance (gray aircraft) with an error of projection e_{proj} indicated as a red dotted line.

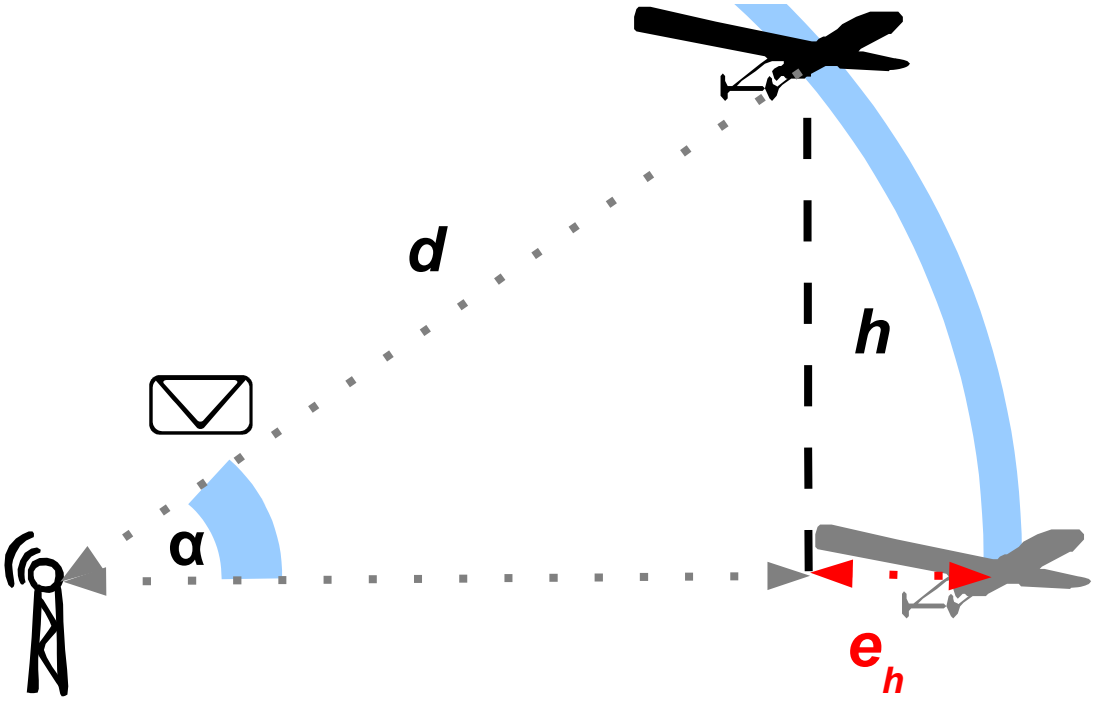

Figure 4.18: Range Measurement Error generated by 2 dimensional problem statement

The distance between receiver and the projected position could be calculated as in eq. 4.4.

$$d_{proj} = d \cos \alpha \tag{4.4}$$

Then, eq. 4.5 states the error introduced in the distance measure by the fact of assuming that a measure taken in a 3 D space could be employed in a 2 D model.

$$e_{proj} = d - d_{proj} = d - d\cos\alpha = d(1 - \cos\alpha) \tag{4.5}$$

Applying the definition of arcsin to the figure 4.18 results in Eq. 4.6.

$$\alpha = \arcsin\left(\frac{h}{d}\right) \tag{4.6}$$

Applying eq.4.6 to eq.4.5 results in eq.4.7.

$$e_{proj} = d\left(1 - \cos\arcsin\left(\frac{h}{d}\right)\right) \tag{4.7}$$

where could be observed that increments in the distance between users decrement the e_{proj} whilst increments in the difference between altitudes increment e_{proj}.

4.4.1.5 Different measurement times (e_{dmt})

The use of messages sent at different times for retrieving navigation data introduces an error in the calculated position. Figure 4.19 shows how a message sent by the helicopter at a time t_0 to the UAV provides the opportunity to measure a pseudorange ρ_1. Using this pseudorange and the communicated position of the helicopter could be created a linearized equation as shown in par. A

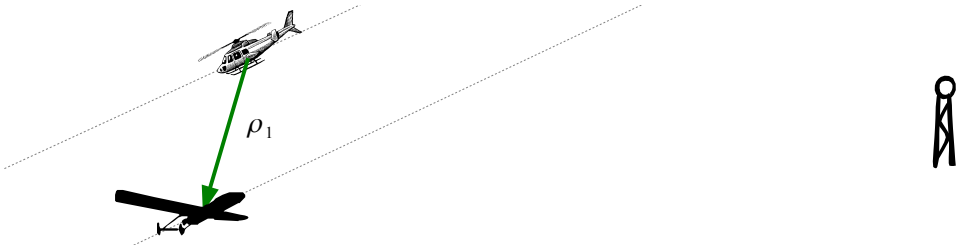

Figure 4.19: Range Measurement at t_0

Figure 4.20 shows how another message coming from a communication tower is employed later on by the UAS to measure a new pseudorange (ρ_2) and to create another equation describing UAV's position. At this instant UAV could describe its position with two equations related to two pseudorange measurements: The equation describing the position of UAS at t_0 (helicopter, arrow and UAV in grey) and the equation describing the position at t_1 (helicopter, arrow and UAV in black).

Equations retrieved at t_0 and t_1 describe different positions of the UAV. Describing the UAV position with these two equations and find an approximation, we are assuming that the UAV is somewhere in between the UAV position at t_0 and the UAV position at t_1. The difference between the position calculated and the current due to the use of equations constructed at different times is represented in this PhD as e_{dmt}

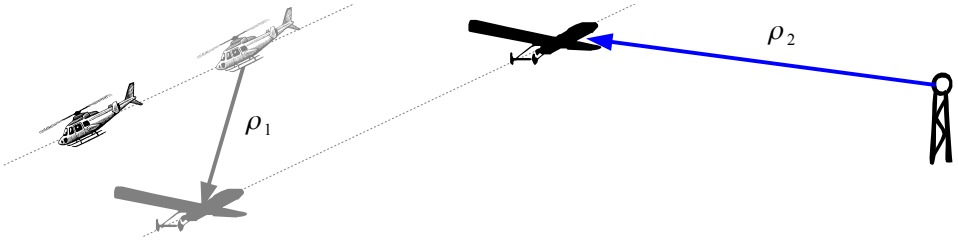

Figure 4.20: Range Measurement at t_1

It should be taken into account that e_{dmt} is present only if pseudorange measurements of different times are used as belonging to the same instant. In the case of a surveillance implementation, a unique message could be received at different places. In this case, all the equations retrieved from the reception of the message describe the position of the UAV at the instant of emission and consequently its $e_{dmt} = 0$.

The simplicity of using measures retrieved at the same intant of time as shown by the surveillance approach is not always applicable to the navigation due to the difficulty of receiving different messages at the same time. Nevertheless, a complementary strategy to minimize this effect could be employed if additional information is shared through the network. Figure 4.21 shows the speed vectors of each user (Sp_1 for the aircraft and Sp_0 for the own UAV speed) are shared through the network.

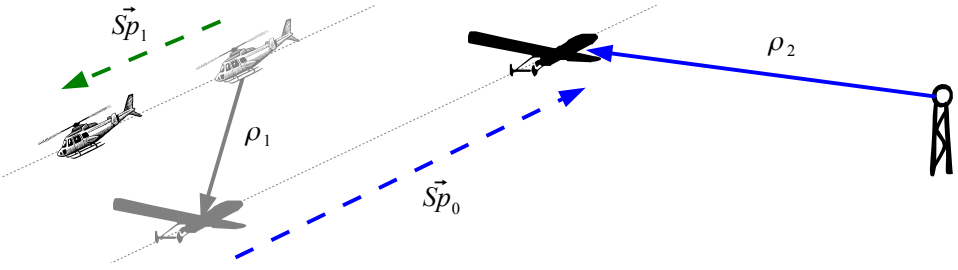

Figure 4.21: Pseudorange improved estimation at t_1

Figure 4.22 shows how the knowledge of both $\vec{Sp_0}$ and $\vec{Sp_1}$ does not provides a new measure of the pseudorange ρ_1 but gives the opportunity of estimating more accurately

different informations as: current positions of both the helicopter and the UAV, the pseudorange ρ_{1_0} from the estimated positions as well of having a better idea of the direction at which the UAV is located.

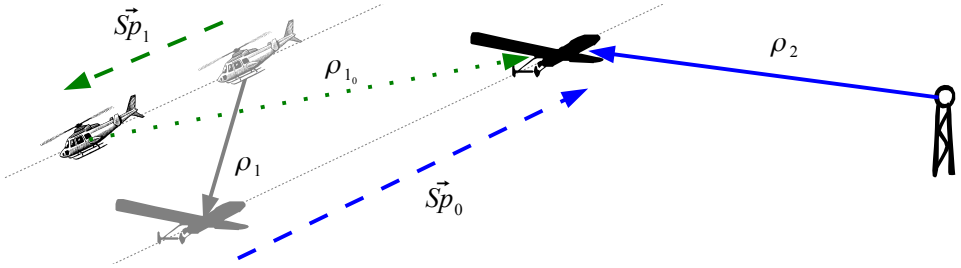

Figure 4.22: Range Measurement at t_0

4.5 PoCoLoCo Methodology

The transmission of messages through the TDMA network provides the opportunity to measure the range between emitter and receiver. The loquacity of the communications is given in both directions, from aircraft to the ground station (telemetry) and from ground station to the aircraft (command & control).

Figure 4.23: PoCoLoCo capabilities

Figure 4.23 shows the two different alternatives to measure the ranges:

- The grey UAS in the left sent a message that is received by several Network Users on ground. In this case the positioning could be performed sharing the range measurements in the ground, providing surveillance information.
- The black UAS in the right of the figure receives different messages from different network users. In this case, the range measurement is performed on board and

the positioning obtained thanks to these range measurements provides navigation information to the UAS.

In both cases (Surveillance and Navigation) what we obtain is a set of range measurements from a point to several other points which position is known that could be exploited using the same technique.

Each distance from a known position could be expressed as in equation 4.8, which describes the distance between two point in a plane.

$$d_i = \sqrt{(x - x_i)^2 + (y - y_i)^2} \tag{4.8}$$

Nevertheless, what we can measure is not the exact distance, but a pseudorange, as expressed in equation 4.3 that contains different error generated by different sources as explained in section 4.4.1. Assuming that we can not get the real distance d_i and in fact we use the pseudorange ρ_i, we combine equation 4.8 with the formulation of the pseudorange expressed in equation 4.3 and we obtain equation 4.9.

$$\rho_i = \sqrt{(x - x_i)^2 + (y - y_i)^2} + e_{synch} + e_{T^i} + e_{M^i} + e_{proj} + e_{dmt} \tag{4.9}$$

Some of the errors stated in equation 4.9 can be estimated. Using these error estimations results in a more accurate ρ_i. This approach is as good as the models employed for estimating the errors could be.

In the case of e_{T^i} the content of water vapour in the troposphere could be retrieved from the meteorological reports and be employed to fix the error generated. This error is not modelled (nm).

e_{M^i} becomes more conflictive as it depends notably on several aspects as the orography, the carrier employed as well as the method employed to detect the arrival of a message. Being the carriers to be assigned for UAS communications still under discussion, this effect has not further be modelled in the simulations.

For the e_{proj}, the barometric altitude of the flight could be employed as a model of altitude reducing the error introduced. Being an easy to fix error that increases the complexity of the simulation, it has been obviated (nm) by placing the network users in very near altitudes.

The e_{dmt} is modelled in different ways depending on the knowledge about the trajectory of the emitter as explained later on section 4.5.3.

$$\rho_i = \sqrt{(x - x_i)^2 + (y - y_i)^2} + e_{synch} + \cancel{e_{T^i}}^{nm} + \cancel{e_{M^i}}^{nm} + \cancel{e_{proj}}^{nm} + e_{dmt} \quad (4.10)$$

Then, applying the estimation of the error we can formalize each range measurement as:

$$\rho_i = \sqrt{(x - x_i)^2 + (y - y_i)^2} + e_{synch} + \epsilon_i \quad (4.11)$$

ϵ_i accounts for all non modelled propagation factors, such as multipath.

Given an architecture with n point of known position and the range measurement between those points and the UAS, a set of equations describing each of the individual range measurements can be written. Geometrically speaking, each of these measurements locates the UAS into an annulus defined by a radius equal to the measured range and width depending on the accuracy of the measures. The intersection of more than 2 annulus provide an area where the UAS (x, y) is located. Nevertheless the obtained equations are not linear and consequently, the complexity of solving the system difficult its use.

To simplify the resolution, equation (4.11) is linearised using Taylor theorem (more details in A) around an approximate position (x_0, y_0):

$$\rho_i \simeq \rho_{i_0} + \frac{x - x_i}{\rho_{i_0}} dx + \frac{y - y_i}{\rho_{i_0}} dy + dt \quad (4.12)$$

where ρ_{i_0} is the estimated range for station i: $\rho_{i_0} = \sqrt{(x_0 - x_i)^2 + (y_0 - y_i)^2}$; and deviations from this approximated position are given by $dx = x - x_0$, and $dy = y - y_0$.

Writing the previous equation for all the n receiver measurements in matrix form leads to:

$$\begin{bmatrix} \rho_1 - \rho_{1_0} \\ \vdots \\ \rho_n - \rho_{n_0} \end{bmatrix} \simeq \begin{bmatrix} \frac{x_0 - x_1}{\rho_{1_0}} & \frac{y_0 - y_1}{\rho_{1_0}} & 1 \\ \vdots & \vdots & \\ \frac{x_0 - x_n}{\rho_{n_0}} & \frac{y_0 - y_n}{\rho_{n_0}} & 1 \end{bmatrix} \cdot \begin{bmatrix} dx \\ dy \\ cdt \end{bmatrix} \quad (4.13)$$

where the difference between the measured pseudorange (ρ_i) and the estimated pseudorange (ρ_{i_0}) is related to the corrections (dx, dy, cdt) to be applied through a geometry matrix.

4.5.1 GNSS analogy

Equation 4.13 could be represented more compactly as:

$$Y \simeq H \cdot X \tag{4.14}$$

where adopting GNSS positioning nomenclature, Y is the observables vector, X the unknowns (or state) vector and H the geometry matrix.

In GNSS positioning a single receiver is measuring ranges sent by several emitters (satellites). The emitter clock biases are estimated (with information contained in the GNSS navigation message) while the receiver clock bias is the fourth unknown to be computed along with the receiver position (x, y, z).

Different methods are proposed in the GNSS literature (122) for solving linear equation such as equation (4.13) or (4.14) which are written each time a measurement is performed. The different kinds of information available could lead to the election of a simple method as least squares (if there is only information about the pseudoranges) or a more sophisticate as extended kalman filter that allows the use of complementary information for refining the positioning information.

A parallelism could be observed between GNSS and PoCoLoCo by substituting the satellites of GNSS by network users in PoCoLoCo; in both cases there is a common point and a set of pseudoranges measurements between the common point and other points which position is known. This analogy is valid both if the aircraft receives the messages (navigation), as well as if the aircraft sends messages which are received at a set of network users (surveillance). This parallelism has its limits in the location of all the actors in a relative narrow interval of altitudes (few kilometres) by comparing with the positioning of the GNSS satellites in their orbital planes at heights of thousands of kilometres.

Taking advantage of the GNSS knowledge about positioning present at the literature, PoCoLoCo is proposed offering positioning in 2 dimensions (x, y) and time (t). We assume the clocks of the emitters and the receivers are synchronized with an accuracy in line with clocks available commercially and it is calculated the difference between the aircraft clock and the common clock. The position of the PoCoLoCo network users is shared through the network when available and, depending on the availability of attitude and speed information, estimated between two positions reports.

4.5.2 EKF Basic Setup

The Extended Kalman Filter (EKF) computes the state (X) using the measures (Y) combined with a measurement model (P_Y) and a geometry matrix (H) (that shall be calculated at each iteration) to correct the prevision performed using the process noise (Q) and the transition matrix (A). See Annex B for more in depth explanation. Next, the setup of matrices X, Y, P_Y, H, A and Q is presented:

- The state (X) is defined as the corrections to the estimated position in 2 D and the time:

$$X = \begin{pmatrix} dx \\ dy \\ cdt \end{pmatrix} \tag{4.15}$$

- The measures (Y) are defined as the difference between the estimated and the measured ranges:

$$Y = \begin{pmatrix} \rho_1 - \rho_{1_0} \\ \vdots \\ \rho_n - \rho_{n_0} \end{pmatrix} \tag{4.16}$$

- The measurement model (P_Y) shall bound the total error of each measure. For this purpose we employ the UERE concept (User Equivalent Range Error), widely known in GNSS; assuming that the different sources of error are independent, their σ could be root-sum-squared to obtain an overall value for σ_i.

$$\sigma_i^2 = \sigma_{synch_i}^2 + \sigma_{T^i}^2 + \sigma_{M^i}^2 + \sigma_{proj_i}^2 + \sigma_{dmt_i} \tag{4.17}$$

The sources of error have been previously explained at section 4.4.1. The availability of reliable models for some errors as e_{T^i}, e_{M^i} and e_{proj_i} has been taking into consideration for discarding both simulation and modelling of these errors to concentrate in the core aspects of PoCoLoCo methodology.

$$\sigma_i^2 = \sigma_{synch_i}^2 + \cancelto{0}{\sigma_{T^i}^2} + \cancelto{0}{\sigma_{M^i}^2} + \cancelto{0}{\sigma_{proj_i}^2} + \sigma_{dmt_i} \tag{4.18}$$

The case of e_{dmt_i} requires a more detailed explanation as it is generated by a model of the environment that does not match with the reality. The achievement of a more accurate model depends deeply on the amount of available information in

its situational awareness, information which should be shared in a cooperative way through the messages exchanged through the network.

$$P_Y = \begin{pmatrix} \sigma_1^2 & & \\ & \ddots & \\ & & \sigma_n^2 \end{pmatrix} \tag{4.19}$$

- The geometry matrix (H) is generated using the unitary vectors defining the direction from each network user to the estimated position of the aircraft:

$$H = \begin{pmatrix} \frac{x_0 - x_1}{\rho_{1_0}} & \frac{y_0 - y_1}{\rho_{1_0}} & 1 \\ \vdots & \vdots & \\ \frac{x_0 - x_n}{\rho_{n_0}} & \frac{y_0 - y_n}{\rho_{n_0}} & 1 \end{pmatrix} \tag{4.20}$$

- For the transition matrix (A), we consider the implementation of the navigation algorithm as a random kinematic process(122) results in eq.4.21 .

$$A = \begin{pmatrix} 0 & & \\ & 0 & \\ & & 0 \end{pmatrix}; \tag{4.21}$$

- For the process noise matrix (Q) we consider the dynamics of the system in which the clock offset at each sampling is modelled as a white noise random variable, with a mean of zero and a variance of σ_{dt}^2.

$$Q = \begin{pmatrix} \dot{q}_x \Delta t & & \\ & \dot{q}_y \Delta t & \\ & & \dot{q}_t \Delta t \end{pmatrix} \tag{4.22}$$

where Δt is the time between two consecutive samples and $\dot{q}_j = \frac{d\sigma_j^2}{dt}$ is the spectral density of coordinate j random process ($j = \{x, y, t\}$). $\dot{q}_j = \frac{d\sigma_j^2}{dt}$ could be bounded depending on the available information to obtain more accurate results.

4.5.3 Options of the EKF kinematic model

For the UAS of the simulated Scenario, the White Noise of the kinematic model could be bounded with the knowledge of the own aircraft trajectory and performance as well as the information available about the kind of UAS performing the flights, its

performance and their flight intentions. Different levels of awareness has been selected to simulate its impact on the navigation:

- Basic Scenario,
- Own trajectory,
- Overall Flight Intention,
- Time Bias.

The "Basic Scenario" assumes the maximum speeds of the network users as a common bound for x and y.

The "Own trajectory" assumes that an inertial system is on board and provides an approximation to the aircraft speed which is employed as bound for the kinematic model.

The "Overall Flight Intention" assumes that an inertial system is on board of each network user and the information about speed is propagated through the network.

Finally, the "Time Bias" assumes the existence of an inertial onboard and the propagation of the speed information through the network as well as the propagation of the calculated time bias between own clock and the common clock.

4.5.3.1 Basic Scenario

The strongest assumption for the navigation based on the range measurements is that there is not additional navigation knowledge about own aircraft trajectory neither information about the participants flight intentions. Range measurements are employed as measured without any correction in both Y and H.

In this method, the range measurements are obtained at an instant but could be employed employed for navigation purposes with a delay of Δt_{meas}. The time elapsed since the last position estimation is noted as Δt_{est}.

The maximum speed achievable by the aircraft Spd_{Max} is used to bound Q. Taking a conservative approach motivated by the absence of specific knowledge about the trajectory, the next position could be in any direction at the Spd^0_{Max}: $\dot{q}_x = \dot{q}_y = Spd^0_{Max}\,\mathrm{m}^2/\mathrm{s}$. Moreover, Δt_{est} depends on the elapsed time since the last position calculation. The declared accuracy of the clock clk_{acc} is used to bound the time component of Q. Wrapping up, Q is set up as:

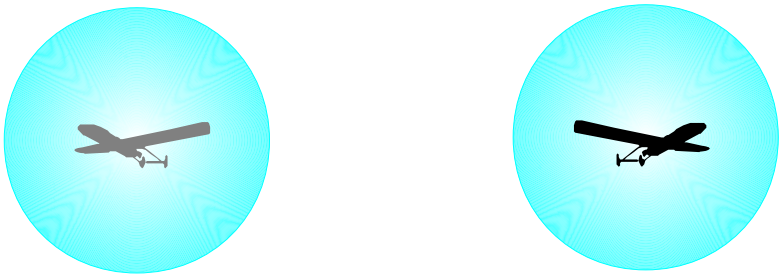

Figure 4.24: Only Navigation Mean

$$Q = \begin{pmatrix} {Spd^0_{Max}}^2 \Delta t_{est} & & \\ & {Spd^0_{Max}}^2 \Delta t_{est} & \\ & & (c \cdot clk_{acc})^2 \end{pmatrix} \tag{4.23}$$

The representation of the range measurement uncertainty in the Kalman Filter employed for navigate is done in P_Y, where we must consider two different sources of error:

- the synchronism error (σ_{synch_i}),
- the measurement delay (σ_{dmt_i}).

Therefore, the P_Y is set up as:

$$P_Y = \begin{pmatrix} \sigma^2_{synch^1_0} + \sigma^2_{dmt^1_0} & & \\ & \ddots & \\ & & \sigma^2_{synch^n_0} + \sigma^2_{dmt^n_0} \end{pmatrix} \tag{4.24}$$

where the synchronism of the common network user ($\sigma^2_{synch_0}$) and the remote user ($\sigma^2_{synch_i}$) are considered:

$$\sigma^2_{synch^i_0} = \sigma^2_{synch_0} + \sigma^2_{synch_i} \tag{4.25}$$

σ_{synch_i} is selected taking into account the synchronism accuracy that COTS technologies can provide nowadays. Among the different technological solutions we have considered the worst case in accuracy: embedded technologies which, in turn, provides the system with more flexibility. Typical synchronism values for these systems are around 100 ns (42), which are translated to range measurement accuracies of $c \cdot 100\,\text{ns} = 30\,\text{m}$.

$\sigma_{dmt_0^i}$ is bounded only by the displacement at maximum speeds of the common point since the last position estimation ($SpdMax_0 \Delta t_{est}$) and the displacement of the rest of users since their last measurement ($SpdMax_i \Delta t_{meas}$):

$$\sigma^2_{dmt_0^i} = SpdMax_0^2 \Delta t_{est} + SpdMax_i^2 \Delta t_{meas} \tag{4.26}$$

4.5.3.2 Own trajectory

Figure 4.25: Own Flight Intention Knowledge

The generically bounded kinematic model represented in eq.(4.23) could be improved by the use of the own trajectory information, which should be available onboard. The trajectory knowledge could be retrieved from different systems or combination of systems(e.g: Compass + inertial) or derived from previous position calculations and is represented as a unitary vector $\vec{r}$.

$$\vec{r} = \begin{pmatrix} r_x \\ r_y \end{pmatrix} \tag{4.27}$$

Using the unitary vector of eq.(4.27) to better adapt the process noise to each component, Q is set up as:

$$Q = \begin{pmatrix} (Spd_{Max} r_x)^2 \Delta t_{est} & & \\ & (Spd_{Max} r_y)^2 \Delta t_{est} & \\ & & (c \cdot clk_{acc})^2 \end{pmatrix} \tag{4.28}$$

If the knowledge of our situational awareness is not limited to $\vec{r}$ and we have access to the speed vector $\vec{Sp}$,

$$\vec{Sp_0} = \begin{pmatrix} Sp_{x_0} \\ Sp_{y_0} \end{pmatrix} \tag{4.29}$$

we can improve the estimation of the own position (x_0^+, y_0^+) by just adding to the position calculated in the previous iteration (x_0^-, y_0^-) the displacement generated by the speed (Sp_x, Sp_y) during the time elapsed since the last measurement (Δt_{meas}).

$$\begin{pmatrix} x_0^+ \\ y_0^+ \end{pmatrix} = \begin{pmatrix} x_0^- \\ y_0^- \end{pmatrix} + \begin{pmatrix} Sp_{x_0} \\ Sp_{y_0} \end{pmatrix} \Delta t_{meas} \tag{4.30}$$

Using own position (x_0^+, y_0^+) as calculated in equation 4.30 could be obtained a better estimation of the pseudorange $(\rho_{i_0}^+)$

$$\rho_{i_0}^+ = \sqrt{(x_0^+ - x_i)^2 + (y_0^+ - y_i)^2} \tag{4.31}$$

and consequently a better value of the measurements vector (Y^+) which is in fact the difference between the estimated range $(\rho_{i_0}$ or $\rho_{i_0}^+)$ and the measured range (ρ_i).

$$Y^+ = \begin{pmatrix} \rho_1 - \rho_{1_0}^+ \\ \vdots \\ \rho_n - \rho_{n_0}^+ \end{pmatrix} \tag{4.32}$$

Once the optimization of pseudorange $(\rho_{i_0}^+)$ is performed and with the optimized own position (x_0^+, y_0^+) as calculated in equation 4.30 an optimized geometry matrix (H^+) is generated

$$H^+ = \begin{pmatrix} \frac{x_0^+ - x_1}{\rho_{1_0}^+} & \frac{y_0^+ - y_1}{\rho_{1_0}^+} & 1 \\ \vdots & \vdots & \\ \frac{x_0^+ - x_n}{\rho_{n_0}^+} & \frac{y_0^+ - y_n}{\rho_{n_0}^+} & 1 \end{pmatrix} \tag{4.33}$$

P_Y could also be improved thanks to the knowledge of the speed of the rest of network users:

$$P_Y = \begin{pmatrix} \sigma_{synch}^2 + \sigma_{dmt_1} & & \\ & \ddots & \\ & & \sigma_{synch}^2 + \sigma_{dmt_1} \end{pmatrix} \tag{4.34}$$

where σ_{synch}^2 remains unchanged as we have not additional information about the synchronism of the clocks. $\sigma_{dmt_0^i}^2$ is changed to reflect the better knowledge of the estimation of the pseudoranges. The difference between the pseudoranges calculated with the formerly estimated position (ρ_{i_0}) and adding the estimated displacement to

the position ($\rho^{+}_{i_0}$) is used as a component of $\sigma^2_{dmt^i_0}$. As the relative direction of both network users are not known, it is used the estimated displacement of the aircraft since the last position calculation ($Sp_0\Delta t_{est}$) to bound as well the $\sigma^2_{dmt^i_0}$. Finally, the maximum speed of the other network user is also use as bound.

$$\sigma^2_{dmt^i_0} = (\rho_{i_0} - \rho^{+}_{i_0})^2 + Sp_0\Delta t_{est} + SpdMax_i\Delta t_{meas} \tag{4.35}$$

where Sp_i represent the modulus of the speed vector $\vec{Sp_i}$:

$$Sp_i = \sqrt{Sp^2_{x_i} + Sp^2_{y_i}} \tag{4.36}$$

4.5.3.3 Overall Flight Intention

Figure 4.26: Overall Flight Intention Knowledge

The range measurements are obtained through a data link that could also provide the speed vector of each participant ($\vec{Sp_i}$). Alternatively, in an environment where the speed of the participants are not shared through the data link, those speed vectors could be derived from log containing the latest positions.

$$\vec{Sp_i} = \begin{pmatrix} Sp_{x_i} \\ Sp_{y_i} \end{pmatrix} \tag{4.37}$$

we can improve the estimation of the positions of the rest of participants by just adding to the position reported in the last message (x^{-}_i, y^{-}_i) the displacement generated by the speed (Sp_x, Sp_y) during the time elapsed since the last report (Δt_{rep_i}).

$$\begin{pmatrix} x^*_i \\ y^*_i \end{pmatrix} = \begin{pmatrix} x^{-}_i \\ y^{-}_i \end{pmatrix} + \begin{pmatrix} Sp_{x_i} \\ Sp_{y_i} \end{pmatrix} \Delta t_{rep_i} \tag{4.38}$$

Using both the optimized positions (x^{+}_i, y^{+}_i) from eq. 4.30 and (x^*_i, y^*_i) from eq. 4.38 could be obtained a better estimation of the pseudorange ($\rho^*_{i_0}$)

$$\rho^*_{i_0} = \sqrt{(x^{+}_0 - x^*_i)^2 + (y^{+}_0 - y^*_i)^2} \tag{4.39}$$

and consequently a better value of the measurements vector (Y^*) than using $\rho_{i_0}^+$) and the measured range (ρ_i).

$$Y^* = \begin{pmatrix} \rho_1 - \rho_{1_0}^* \\ \vdots \\ \rho_n - \rho_{n_0}^* \end{pmatrix} \tag{4.40}$$

Once the optimization of pseudorange ($\rho_{i_0}^*$) is performed and with the optimized own position (x_0^+, y_0^+) as calculated in equation 4.30 as well as the optimized positions of the rest of users (x_i^*, y_i^*) an optimized geometry matrix (H^*) is generated

$$H^* = \begin{bmatrix} \frac{x_0^+ - x_1^*}{\rho_{1_0}^*} & \frac{y_0^+ - y_1^*}{\rho_{1_0}^*} & 1 \\ \vdots & \vdots & \\ \frac{x_0^+ - x_n^*}{\rho_{n_0}^*} & \frac{y_0^+ - y_n^*}{\rho_{n_0}^*} & 1 \end{bmatrix} \tag{4.41}$$

The other participants trajectories information and the own trajectory knowledge could be employed to bound the Measurement Covariance Matrix P_Y.

$$P_Y = \begin{pmatrix} \sigma^2_{synch_0^1} + \sigma^2_{dmt_0^1} & & \\ & \ddots & \\ & & \sigma^2_{synch_0^n} + \sigma^2_{dmt_0^n} \end{pmatrix} \tag{4.42}$$

where σ^2_{synch} remains unchanged as we have not additional information about the synchronism of the clocks and $\sigma^2_{dmt_0^i}$ is changed to reflect the better knowledge of the estimation of the pseudoranges. The difference between the pseudoranges calculated with the formerly estimated position (ρ_{i_0}) and adding the estimated displacement of both network user to their respective positions ($\rho_{i_0}^*$) is used to bound $\sigma^2_{dmt_0^i}$. It is used the estimated displacement of the aircraft since the last position calculation ($Sp_0 \Delta t_{est}$) and the estimated displacement of the other network user ($Sp_i \Delta t_{meas}$) since the last measurement (t_{meas}) to bound as well the $\sigma^2_{dmt_0^i}$.

$$\sigma^2_{dmt_0^i} = (\rho_{i_0} - \rho_{i_0}^*)^2 + Sp_0 \Delta t_{est} + Sp_i \Delta t_{meas} \tag{4.43}$$

4.5.3.4 Time Bias

Time Bias merits an special consideration. The physics of the clocks employed in communications (see section F) produces a bias that is not filtered by the Kalman

filter. This leads to the estimation of the own clock error to reduce the effect of the e_{synch} over the navigation solution.

If the time bias is shared with the rest of users it could be employed to improve the pseudoranges sustracting the bias of each user.

$$\rho_i^\circ = \rho - c \cdot dt_i \tag{4.44}$$

leading to a more accurate measurements:

$$Y^\circ = \begin{pmatrix} \rho_1^\circ - \rho_{1_0} \\ \vdots \\ \rho_n^\circ - \rho_{n_0} \end{pmatrix} \tag{4.45}$$

A better knowledge of the clock bias motivates also a better bounding of the P_Y as we count on better measurements.

$$P_Y = \begin{pmatrix} \sigma^2_{synch_0^1} + \sigma^2_{dmt_0^1} & & \\ & \ddots & \\ & & \sigma^2_{synch_0^n} + \sigma^2_{dmt_0^n} \end{pmatrix} \tag{4.46}$$

This time $\sigma^2_{dmt_0^i}$ is bounded depending on the situational awareness as described in previous sections. For the component introduced by the synchronism error ($\sigma^2_{synch_0^i}$), the contribution of the common point must be calculated as before, but the component of the rest of users could be reduced to the Allan deviation (σ_{A_i}) of each clock as the bias is shared:

$$\sigma^2_{synch_0^i} = \sigma^2_{synch_0} + \sigma^2_{A_i} \tag{4.47}$$

We dare not to do many things because they are hard,
but they are hard because we dare not.

Lucio Anneo Seneca (2 BC - 65)

5 Simulation setup

A simulation scenario has been designed to test the Surveillance and Navigation capabilities offered by the communications. In this scenario, all the UAS share the TDMA network. Each UAS is composed by an unmanned air vehicle (UAV) and its ground station (GS). Three different UAS are simulated simultaneously:

- Metropolitan area traffic monitoring
- Coastal Lifeguard.
- Vineyard Aerial Works.

The simulation envisaged to validate the concept requires to take into account the number of messages interchanged over the TDMA network, the position reported by each actor, the messages received and the clock accuracies of both the emitter and the receivers.

The algorithm 1 shows how the time slots assignment is employed to structure the simulation. It could be seen how the actors (both UAV and GS) measure the pseudorange when receives a message. Using the position reported in the "Position Report" messages, the position of the actors could be calculated with the methodology

explained in paragraph 4.5. The algorithm 1 simulates the continuous operation of the UAS for a period of 24 hours.

Algorithm 1 Positioning Simulation Algorithm

```
for all TimeSlots do
  for all Actors receiving the message do
    measure distance from Emitter to Receivers in LoS
    if Message is Position Report then
      Store Reported Position
    end if
    Estimate distance from estimated own position to reported positions
    Calculate Distance Difference
    Compute Q
    Compute P_Y
    Feed the Kalman Filter
    Kalman Filter Predict
    Kalman Filter Correct
  end for
end for
```

The positioning capacity of the proposed algorithm is verified using a simulated set of measurements obtained from the different trajectories as shown in Fig. 5.1. To obtain each range measurement the simulation follows the next steps:

- The intended position for the current time slot of the Emitter is computed.
- The intended Emitter position is modified to reflect the uncertainties of the real world,
- The intended position for the current time slot of the Receiver is computed.
- The intended Receiver position is modified to reflect the uncertainties of the real world,
- These simulated positions are used to compute the Actual Range,
- The Actual Range is modified by adding a noise N_s (see fig. 5.1) to simulate realistic Measures.

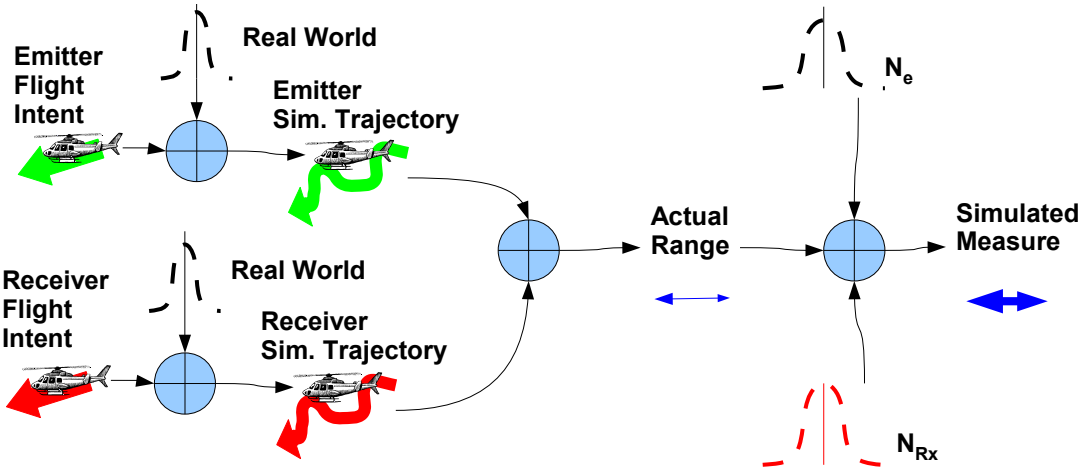

Figure 5.1: Measurements Simulation

.

The Simulated Measure are used as input into the navigation algorithm and the position results are compared with the actual position. The accuracy is test against the required values in two dimensions (see Annex F): along the track e_{at} and cross track e_{ct}. The accuracy obtained is plotted in absolute values and in frequency of occurrence. The accuracy statistics are confronted with the required values for the 95%.

Using the covariances of the Kalman filter, an upper bound for the error is calculated as explained in annex D that serves to guarantee that the error obtained is below the required value on the $1 - 10^{-7}$ of the times. This value is plotted confronted with the actual error showing: the compliance with the integrity alarm values, the integrity of these alarms and how the estimation of the upper bound fits with the actual error.

5.1 Noise of the measures

As explained in 4.4.1, measurements of pseudoranges contain errors (summarized in eq. 4.3) that should be also simulated to obtain realistic results. Before applying the tracking algorithm, the actual ranges are modified with a noise N_i to simulate realistic conditions:

$$N_i = N_{synch_i} + \cancelto{0}{N_{T_i}} + \cancelto{0}{N_{M_i}} + \cancelto{0}{N_{proj_i}} + N_{dmt_i} \tag{5.1}$$

As explained before, e_{T_i}, e_{M_i} and e_{proj_i} are not being simulated in this PhD, then their contributions (N_{T_i}, N_{M_i} and N_{proj_i})to N_i are 0.

Eq.(5.2) shows how N_{synch_i} comprises the error introduced by the emitter (N_e) and the receiver (N_{Rx}).

$$N_{synch_i} = N_e + N_{Rx} \tag{5.2}$$

$$N_e = c * dt \tag{5.3}$$

$$N_{Rx} = c * dt_i \tag{5.4}$$

Eq.(5.3) shows how N_e is composed by the error between emitter and the reference time. dt is simulated as a normally distributed pseudo-aleatory with null mean and a standard deviation of 100 ns, accuracy affordable for existing technology (see (42)) being reasonable accuracies up to 20 nanoseconds if shifting from the embedded devices to a rack device. Considering c, N_e has maximum values of 30 m for each Rx.

Eq.(5.4) shows how N_{Rx} is composed by the error between Rx and the reference time. dt_i is simulated as a normally distributed pseudoaleatory with null mean and a standard deviation of 100 ns, accuracy affordable for existing technology (see (42)). Considering c, N_{Rx} has maximum values of 30 m for each Rx.

e_{dmt_i} is not simulated by adding a noise N_{dmt_i} but by just generating different measures at different times, depending on the time slot allocation of each network participant. In this way, the current measure has an $e_{dmt_i} = 0$, error that is increases as it becomes older because the network users had moved since the measurement time.

5.2 Simulated Flights

A set of three UAS flights has been simulated with trajectories coherent with operations already in use in a metropolitan area:

- Traffic monitoring fig.5.2a,
- Lifeguard supervision of the coastline fig.5.2b,
- Vineyard monitoring fig.5.2c.

A trajectory similar to the some of the main motorways surrounding Barcelona has been simulated in fig 5.2a). The entire flight has been simulated at a constant speed of 40 $\frac{m}{sec}$. In addition to the simulated trajectory, the Barcelona area has more motorways whose monitoring could raise a richer scenario than our proposal.

A lifeguard flight has been simulated in fig 5.2b). The entire flight has been simulated at a constant speed of 20 $\frac{m}{sec}$. The monitoring of the beach areas of the metropolitan area of Barcelona (and the rest of Catalonia) could require several UAS, resulting in a scenario richer than our proposal.

A small vineyard monitoring flight has been simulated in fig 5.2c). The entire flight has been simulated at a constant speed of 10 $\frac{m}{sec}$. There is a lot of wine producers in the area of Barcelona that could require this kind of flights. As in the aforementioned cases, considering more that more than one UAS is monitoring vineyards will result in a richer scenario than our proposal for this simulation.

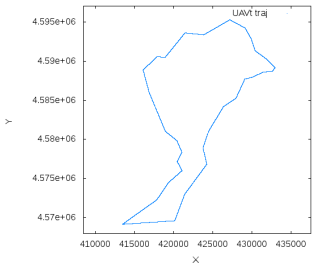

(a) Traffic Monitoring Trajectory UAV_t

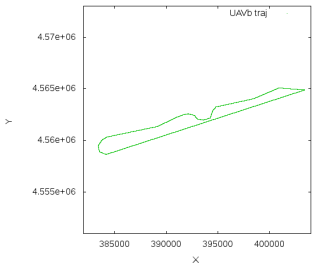

(b) Lifeguard Trajectory UAV_l

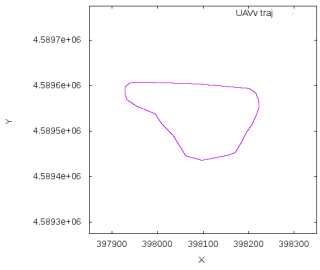

(c) Vineyard Trajectory UAV_v

Figure 5.2: Accuracies of R_x distributions

Once the current position of the intended flight trajectory is computed, it is modified to simulate the inaccuracies that real world conditions could impose. At each sample, all coordinates are modified with a zero mean normally distributed noise with $\sigma = 10m$ for the x and y and $\sigma = 2m$ for the z. Those deviations are introduced with the purpose of stressing the tracking algorithm.

Fig. 5.3 shows the simulated flight paths, without the effect of the aforementioned deviations, over the map. The position of the ground stations are indicated by a triangle of the same color as the UAV trajectory.

Figure 5.3: Flight test and Receiver Stations Rx simulated

5.2.1 Visibility

The amount of measures available for each UAS will depend on the amount of messages produced (which is explained in table 5.4) and on the portion of messages received that could in turn depend on different variables as the distance between actors or the orography.

Table 5.1: Reduced Visibility

	Emitter					
Listener	UAV_t	GS_t	UAV_l	GS_l	UAV_v	GS_v
UAV_t		√	√	√	√	
UAV_l	√	√		√	√	
UAV_v	√		√			√

Table 5.1 summarizes the selected static model of visibility between air vehicle and GS. Subindexes $_t$, $_l$ and $_v$ stands respectively for traffic, lifeguard and vineyard. Each air vehicle could see the other air vehicle and its own GS as a minimum. Additionally UAV_l could see GS_t and UAV_t could see the GS_l.

The visibility model summarized in table 5.1 does not take advantage of all the available transmission to measure distances, discarding good measurements from static positions. In the case of UAV_t and UAV_l the discarded measures correspond to only one GS GS_v.

In the case of UAV_v the measures from two different GS GS_t and GS_l are discarded, keeping two mobile references UAV_t and UAV_l and as the only static reference its own GS_v.

A slightly improved visibility model is also simulated to assess the effect of adding measures to the equation system. The listener has the capability to receive the messages sent by any of the other users (see table 5.2). The number of measures passes for UAV_t and UAV_l from 4 to 5 and in the case of UAV_v passes from 3 measures to 5.

Table 5.2: Improved Visibility

	Emitter					
Listener	UAV_t	GS_t	UAV_l	GS_l	UAV_v	GS_v
UAV_t		√	√	√	√	√
UAV_l	√	√		√	√	√
UAV_v	√	√	√	√		√

The visibility for surveillance purposes has been selected considering that GS communicate among them and UAV do not contribute to the surveillance tasks. Each GS (GS_t,GS_l and GS_v) has the capability to receive the messages sent by any of the air vehicles(UAV_t, UAV_l and UAV_v) (see table 5.3). The number of measures for each UAV remains at 3 (one measure from each GS).

5.3 time slots

Whilst table 4.1 summarizes some typical values of update rates for both the uplink and the downlink, a more conservative update rates of 1Hz for both Uplink and Downlink

Table 5.3: Visibility for Surveillance

	Emitter					
Listener	UAV_t	GS_t	UAV_l	GS_l	UAV_v	GS_v
GS_t	√		√		√	
GS_l	√		√		√	
GS_v	√		√		√	

has been selected to evaluate the accuracy performance in poor conditions. The adoption of 1Hz as transmission rate for the uplink messages, instead of the under demand proposed in different studies, has been selected considering the necessity of detecting the lost of the datalink by the UAS.

Table 5.4: Basic Time Slot Assignment

	Frame																	
	Second 0						**Second 1**							**Second 13**				
Emitter	.15	.25	.35	.5	.75	.85												
UAV_v	•						•							•				
GS_v		•						•							•			
UAV_l			•						•							•		
GS_l				•						•							•	
UAV_t					•						•							•
GS_t						•						•						•

Table 5.4 shows a basic distribution of the Time Slots assigned to each actor in the network where each actor transmits only one message per second. In column **Second 0** is shown how UAV_v transmits its downlink message in second 0 and 150 milliseconds, whilst its ground station GS_v transmits in second 0 and 250 milliseconds; UAV_l second 0 and 350 milliseconds, GS_l second 0 and 500 milliseconds; UAV_t second 0 and 750 milliseconds, GS_t second 0 and 850 milliseconds. For second 1 to 13, the time distribution is repeated. The (•) indicates that the transmitted message contains the position.

Table 5.5 shows a Time Slot assignment similar to the reflected in 5.4 but increasing the position reports of the air vehicles (UAV_v, UAV_l and UAV_t) to two times per second.

Table 5.5: Time Slot Assignment B

	Frame											
	Second 0									Second 1		Second 13
Emitter	.15	.25	.35	.5	.62	.75	.85	.8	.92			
UAV_v	•				•							
GS_v		•										
UAV_l			•					•			...	
GS_l				•								
UAV_t						•			•			
GS_t							•					

5.4 Dilution of Precision

Once decided the architecture of the communication network, a preliminary assessment of the achievable performance must be done taking into account the propagation of measurement errors due to the network geometry. Reference values of DOP can be found in (123); annex D.1 offers a detailed formulation of DOP and a detailed analysis of the lower bounds of DOP can be found in (124). With an optimum of 1, values under 5 could be considered as good DOP values, and values under 10 could be considered as acceptable.

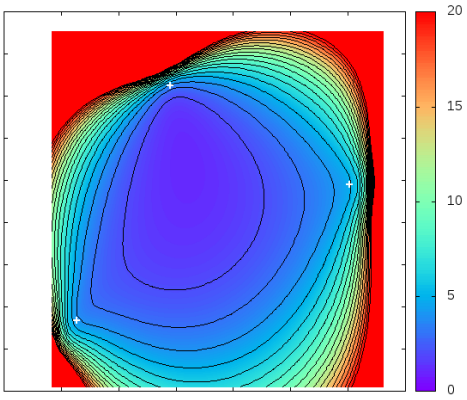

Figure 5.4: HDOP of the GS of the simulated scenario

Figure 5.4 shows the horizontal dilution of precision of a 2D model using only the three ground stations of the envisaged simulation scenario. It could be observed as

the obtained HDOP offer good values in a pseudo triangle with the GS as vertices. Beyond the extension of the pseudo triangle the performance declines gradually up to unacceptable values that are reached nearer in the vicinity of the GS than in between GS.

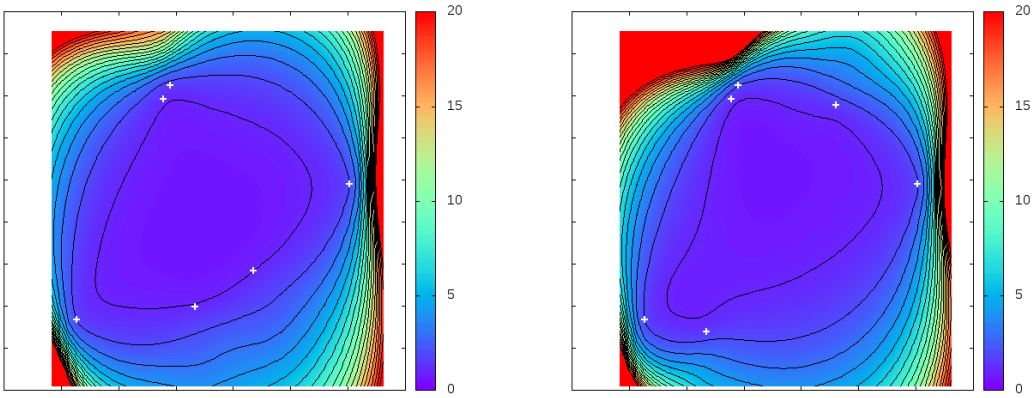

(a) instant 1 **(b)** instant 2

Figure 5.5: HDOP using GS and air vehicles

Figures 5.5a and 5.5b shows the effect of including the measures of the range from the air vehicles in two different instants of the simulation with the air vehicles in different locations. The area with acceptable HDOP is bigger in than in figure 5.4 and the values of the central area are lower (which represents better conditions).

A great sailor can browse
though their sails are for hire.

Lucio Anneo Seneca (2 BC - 65)

6

Relative Navigation Performance

Navigation is not considered as a problem for UAS as a multitude of techniques from the conventional aviation could be employed in UAS. Nevertheless, navigation information could be obtained from the datalink and could be considered as alternative to other navigation means or as backup.

The navigation using information retrieved from the datalink is known as RELNAV. This technique obtains own aircraft position thanks to the known position of the messages emitters and the ToF of these messages.

As in the case of the surveillance proposed in this PhD, there is a synergy between communications and navigation thank to the employ of information retrieved from the physical layer of the datalink. While in surveillance, the position is calculated with the ToF measured in the different receivers for the messages emitted by the aircraft, the navigation position is calculated with the ToF measured on board for the messages emitted by different stations. Figure 6.1) shows how the direction of the message trip is inverse to the direction of the messages employed in surveillance (see Figure 7.1).

The retrieved additional navigation data is independent form conventional navigation means (e.g: DME, VOR) and also from satellite navigation means (e.g: GPS,

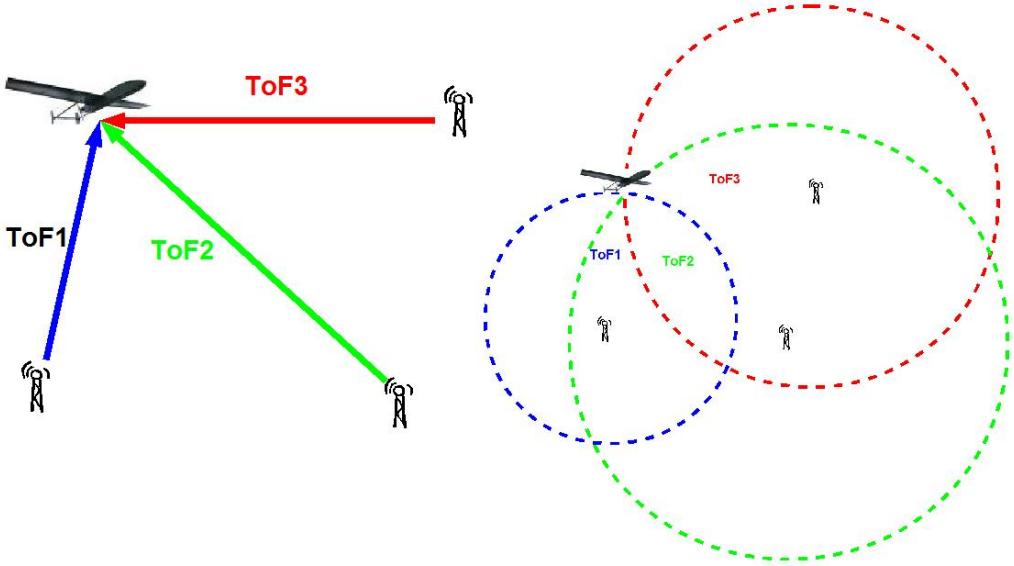

Figure 6.1: Trilateration in RELNAV

GLONASS). This independence provides some additional characteristics:

- Resilience as the position could be computed from different emitters sets (e.g: fall of an emitter).
- Flexibility as aircraft position could be calculated from different sets of emitters with the same result.
- Adaptation as emitters distribution could be easily modified.

Own aircraft positioning by trilateration is not a new concept in aviation. It is already performed with different radio navigation aids, as for example DME. The proposal of using the radiofrequency spectrum already employed in the communication datalink minimizes the radiofrequency employ as there is not additional requirement for the interrogations and responses as in the DME systems.

The calculation of the Time of Flight of messages received onboard from different emitters could provide navigation information. The employment of Signal of Opportunity as source from positioning has been a subject of research in different telecommunications scopes. (125) proposes a methodology for tracking in WLAN Location with TOA Measurements.

The use of communications in UAS as Signal of Opportunity for retrieving localization data has been explored in (126) and (127). They propose a methodology to obtain the localization of a faulty UAV thanks to the range measurements to the rest of UAVs of the same multi-UAS flight. Assumes the capability to obtain a range measurement from the UAV but does not consider the emissions of the ground control stations.

The Air Transportation system is migrating from a technology oriented approach based on legacy systems as VOR, DME, ILS, SSR etc to a Performance based approach where the performances to be fulfilled by the Air Transportation System in Communication (RCP), Navigation (RNP) and Surveillance (RSP) are defined and the support technologies shall comply with. (128) offers the NASA overview of the Required Total System Performance, its decomposition in RNP, RSP and RCP as well as the motivation of its adoption and the benefits that its adoption could provide.

This migration process applies to the legacy systems and technologies as well as the upcoming systems and technologies. As example of Required Total System Performance (RTSP) implications on legacy systems could be mentioned (129) where is analysed the effect of the Required Total System Performance over the Short Term Collision Avoidance Systems.

The prospective of the upcoming technologies and systems supporting current aircrafts and operations are evaluated in (130), offering an overview of the Next Gen ICNS Functional Requirements from the political and socio economic requirements to the technologies passing by the RTSP and by the System Requirements (RSP, RCP and RNP).

Another prospective effort must be done to integrate new kinds of aircrafts currently under development as the UAS or the Very Light Jets (VLJ). (131) explains the results of a study of the impact that new kind of vehicles could have over the National Air Space (USA). The study concludes that the use of UAS for cargo hauling in remote areas will not impact significantly. In this study are considered the requirement over the air space but the advantages are not considered.

The transition from the current Air Transportation Systems to the Next Generation system offers the chance to achieve the envisaged improvements in a more integrated form. (132) analyses the Air-Ground Integration Challenges in NextGen, mentioning: Air-ground Interoperability, Air-ground Information exchange, UAS Integration, and

Mixed Performance. Among the key questions for the UAS integration could be highlighted the UAS interoperability and the Minimum Operational Performance Standard (MOPS) for the data-link between pilot and aircraft.

Figure 6.2 shows in the same frame the simulated trajectories in black and the performed trackings in blue for the traffic monitoring UAV (UAV_t), green for the lifeguard UAV (UAV_l) and magenta for the vineyard UAV (UAV_v).

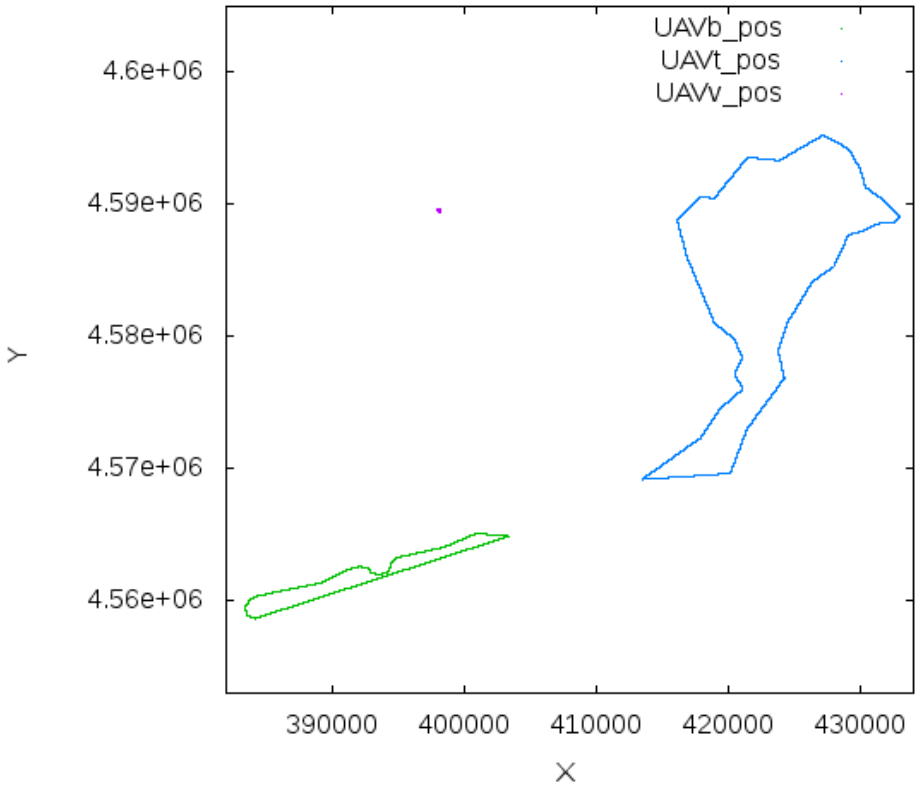

Figure 6.2: Simulated Trajectories and performed trackings

6.1 Basic Scenario

The basic scenario proposed as reference for assessing the improvements achieved by altering time slot allocations or visibilities are based on the visibility summarized in table 5.1 and the time slot allocation of table 5.4.

Along Track Error e_{at} Figures 6.3a, 6.3b and 6.3c, show the e_{at} in the tracking, clearly under the RNP Accuracy performance required by the **RNP APCH** (0.3NM; 555m) shown in Table 1.1.

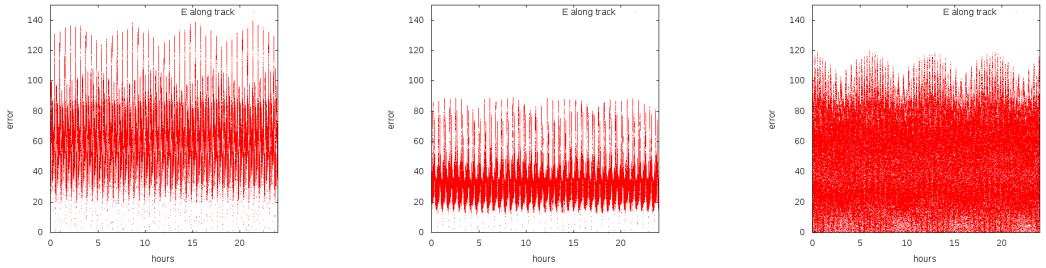

(a) UAV_t **(b)** UAV_l **(c)** UAV_v

Figure 6.3: e_{at}, basic scenario

Figures 6.4a, 6.4b and 6.4c, show the error frequencies.

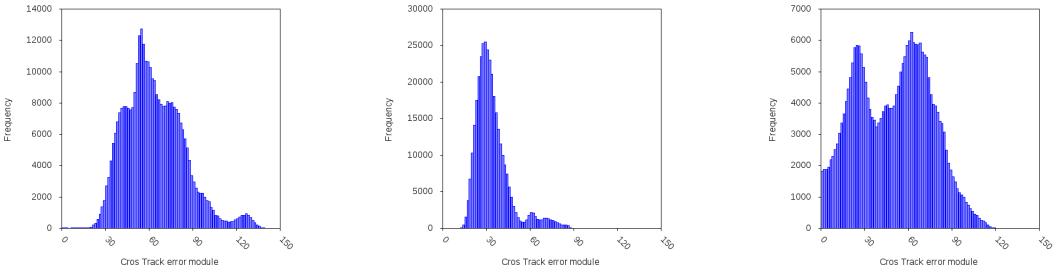

(a) UAV_t **(b)** UAV_l **(c)** UAV_v

Figure 6.4: e_{at} frequencies, basic scenario

Table 6.1: e_{at} Statistics, basic scenario

	Trajectory		
Statistic	UAV_t	UAV_l	UAV_v
$\overline{e_{at}}$	63.74	34.02	49.74
$\sigma_{e_{at}}$	52.00	26.50	37.05
$CDF_{e_{at}}(95\%)$	127.28	64.85	90.69

Table 6.1 summarizes the basic statistics of the e_{at} module. UAV_t has an along

track error mean ($\overline{e_{at}}$) of 63.74 m with a standard deviation ($\sigma_{e_{at}}$) of 52.00 m.

Using the Rayleigh CDF of equation C.12, the required 95 % of accuracy is achieved at a value of 127.28 m for the worst case (UAV_t), which is in fact enough to comply with the most restrictive navigation specification. For the case of the UAV_l and the UAV_v trajectories, their lower $\sigma_{e_{at}}$ ensures also the compliance with the stringent navigation specification (**RNP APCH**).

Cross Track Error e_{ct} Figures 6.5a, 6.5b and 6.5c, show the e_{ct} in the tracking. e_{ct} remains under under the RNP Accuracy performance required by the **RNP APCH** shown in table 1.1 (0.3 NM).

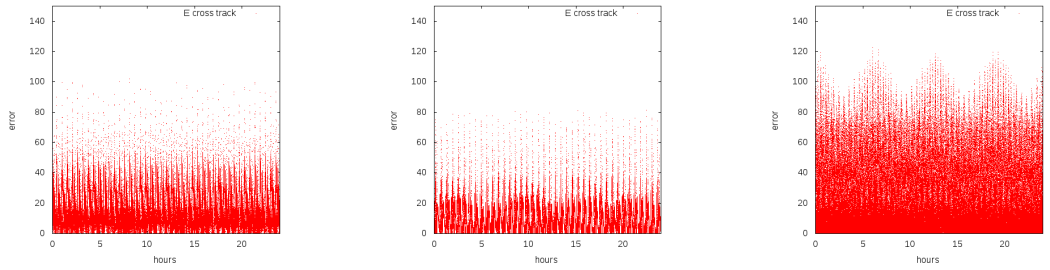

(a) UAV_t **(b)** UAV_l **(c)** UAV_v

Figure 6.5: e_{ct}, basic scenario

Figures 6.6a, 6.6b and 6.6c, show the Error Frequencies.

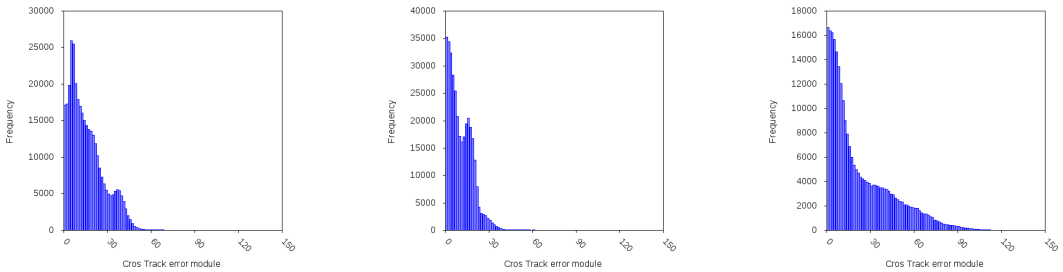

(a) UAV_t **(b)** UAV_l **(c)** UAV_v

Figure 6.6: e_{ct} frequencies, basic scenario

The worst case of table 6.2, UAV_v, has a $\overline{e_{ct}}$ of 22.79 m and a $\sigma_{e_{ct}}$ of 21.63 m. Using the Rayleigh CDF of equation C.12, the required 95 % of accuracy is achieved at a value

Table 6.2: e_{ct} Statistics, basic scenario

	Trajectory		
Statistic	UAV_t	UAV_l	UAV_v
$\overline{e_{ct}}$	15.95	10.45	22.79
$\sigma_{e_{ct}}$	16.09	8.16	21.63
$CDF_{e_{ct}}(95\%)$	39.37	19.98	52.94

of 52.94 m for UAV_v, which is (as for e_{at})enough to comply with the **RNP APCH**. For the case of the UAV_l and the UAV_t trajectories, with lower $\sigma_{e_{ct}}$ the compliance with **RNP APCH** is even improved.

Comparing the values of $CDF_{e_{ct}}(95\%)$ and $CDF_{e_{at}}(95\%)$ trajectory by trajectory, it could be observed the improvement in the accuracy for the e_{ct}, which in fact is the most critical between e_{at} and e_{ct}. This better behaviour of e_{ct} with respect e_{at} is due mainly to the dynamic adjustment that the EKF makes using its Kalman gain to minimize the variance. This adjustment produce position estimations aligned with the trajectory.

UAV_v takes advantage of this EKF dynamic adjustment as well as UAV_t and UAV_l, but its continuous changes in the trajectory reverts in a smaller improvement in the case of UAV_v.

Integrity Figures 6.7a, 6.7b and 6.7c, show the error against the protection level calculated by the Kalman Filter from the noise models.

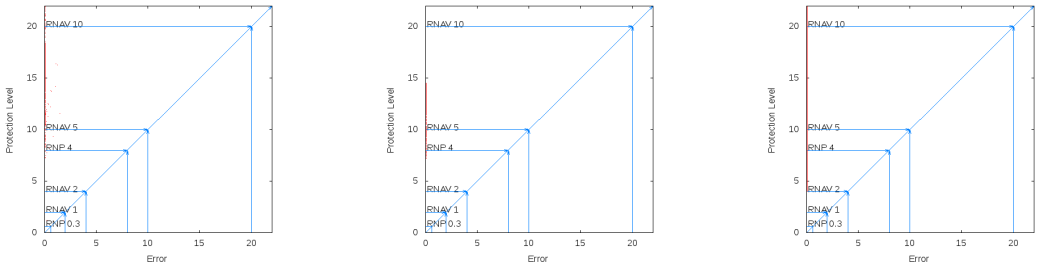

(a) UAV_t **(b)** UAV_l **(c)** UAV_v

Figure 6.7: Integrity Diagrams

The integrity values obtained does not achieved the required values for **RNP 1** navigation specification.

Table 6.3: Integrity Alarm Values Compliance

	Trajectory		
Navigation Specification	UAV_t	UAV_l	UAV_v
RNP 10	0.59	0.75	0.98
RNAV 5	0.09	0.34	0.78
RNP 4	0.02	0.12	0.58
RNAV 2	0	0	0.01
Basic-RNP 1	0	0	0
RNP APCH	0	0	0

Table 6.3 shows the compliance with the navigation specifications of the different trajectories. All the trajectories exceed the limits for RNAV and RNP.

6.2 Own Trajectory

Own trajectory scenario uses the visibility (table 5.1) and time slot assignment (table 5.4) of the basic scenario.

Own trajectory uses the own speed vector to modulate the EKF as explained in 4.5.3.2.

Along Track Error Figures 6.8a, 6.8b and 6.8c, show the e_{at} in the tracking, clearly under the RNP Accuracy performance required by the **RNP APCH** shown in Table 1.1.

Figures 6.9a, 6.9b and 6.9c, show the e_{at} Frequencies.

Table 6.4 summarizes the basic statistics of the e_{at} module. UAV_t has an $\overline{e_{at}}$ of 53.73 m with a $\sigma_{e_{at}}$ of 43.94 m.

Using the Rayleigh CDF of equation C.12, the required 95 % of accuracy is achieved at a value of 107.55 m for the worst case (UAV_t), which is in fact enough to comply with the most restrictive navigation specification. For the case of the UAV_l and the UAV_v

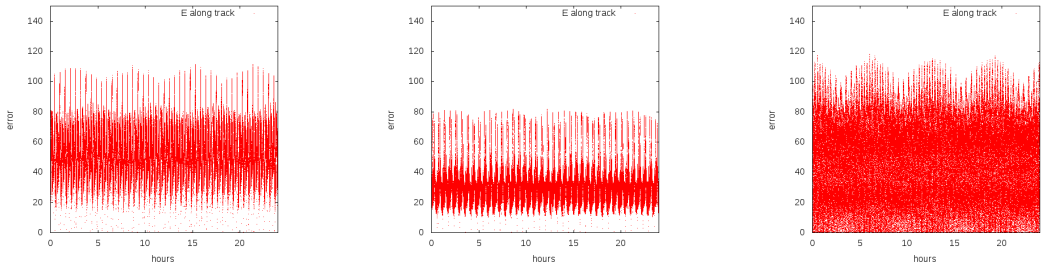

(a) UAV_t **(b)** UAV_l **(c)** UAV_v

Figure 6.8: e_{at}, Hybrid own trajectory

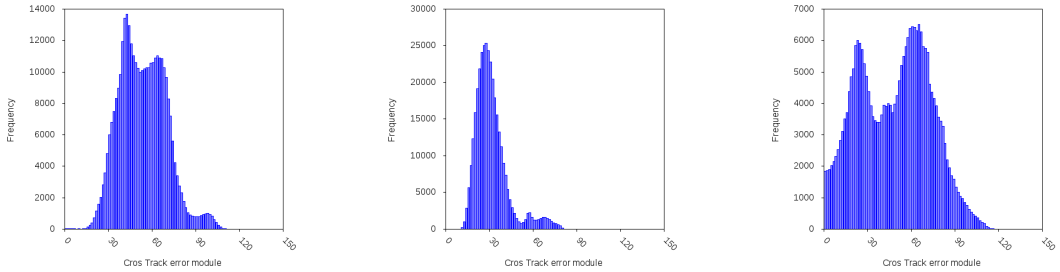

(a) UAV_t **(b)** UAV_l **(c)** UAV_v

Figure 6.9: e_{at} frequencies, Hybrid own trajectory

Table 6.4: e_{at} Statistics, own trajectory

	Trajectory		
Statistic	UAV_t	UAV_l	UAV_v
$\overline{e_{at}}$	53.73	31.43	48.56
$\sigma_{e_{at}}$	43.94	24.24	36.50
$CDF_{e_{at}}(95\%)$	107.55	59.33	89.34

trajectories, their lower $\sigma_{e_{at}}$ ensures also the compliance with the stringent navigation specification (**RNP APCH**).

Cross Track Error Figures 6.10a, 6.10b and 6.10c, show the e_{ct} in the tracking. e_{ct} remains under the RNP Accuracy performance required by the **RNP APCH** shown in Table 1.1.

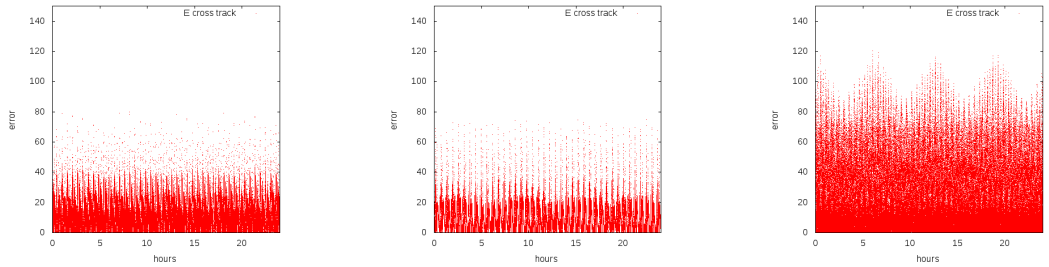

(a) UAV_t **(b)** UAV_l **(c)** UAV_v

Figure 6.10: e_{ct}, Hybrid own trajectory

Figures 6.11a, 6.11b and 6.11c, show the e_{ct} Frequencies.

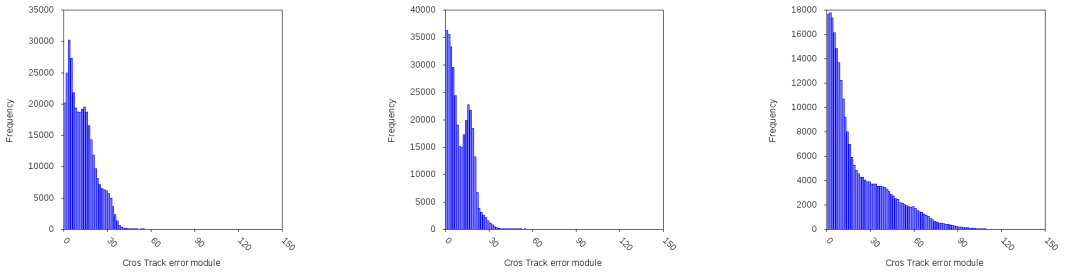

(a) UAV_t **(b)** UAV_l **(c)** UAV_v

Figure 6.11: e_{ct} frequencies, Hybrid own trajectory

Table 6.5: e_{ct} Statistics, own trajectory

	Trajectory		
Statistic	UAV_t	UAV_l	UAV_v
$\overline{e_{ct}}$	12.82	10.16	21.60
$\sigma_{e_{ct}}$	9.24	7.70	20.73
$CDF_{e_{ct}}(95\%)$	22.61	18.86	50.73

The worst case of table 6.5, the UAV_v trajectory, has a $\overline{e_{ct}}$ of 21.60 m and a $\sigma_{e_{ct}}$ of 20.73 m. Using the Rayleigh CDF of equation C.12, the required 95 % of accuracy is achieved at a value of 50.73 m for the worst case (UAV_v), which is (as for e_{at})enough to comply with the **RNP APCH**. For the case of the UAV_t and the UAV_l trajectories,

with lower $\sigma_{e_{ct}}$ the compliance with **RNP APCH** is even improved.

Comparing the values of $CDF_{e_{ct}}(95\%)$ and $CDF_{e_{at}}(95\%)$ trajectory by trajectory, it could be observed the improvement in the accuracy for the e_{ct}, which in fact is the most critical between e_{at} and e_{ct}.

Integrity Figures 6.12a, 6.12b and 6.12c, show the error against the protection level calculated by the Kalman Filter from the noise models.

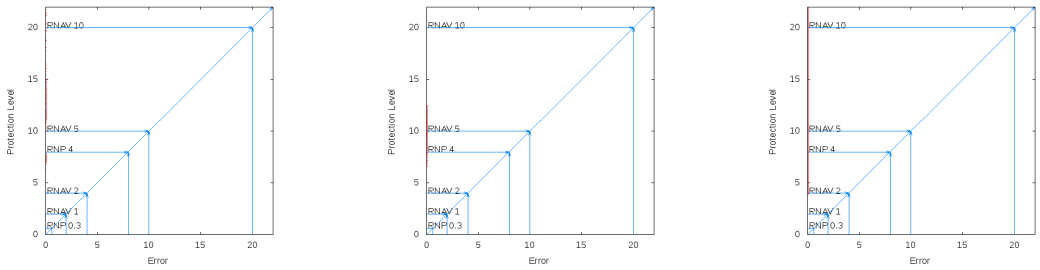

(a) UAV_t **(b)** UAV_l **(c)** UAV_v

Figure 6.12: Integrity Diagrams

The integrity values obtained does not achieved the required values for **RNP 1** navigation specification.

Table 6.6: Integrity Alarm Values Compliance

	Trajectory		
Navigation Specification	UAV_t	UAV_l	UAV_v
RNP 10	0.66	0.79	0.98
RNAV 5	0.28	0.46	0.84
RNP 4	0.13	0.23	0.65
RNAV 2	0	0	0.01
Basic-RNP 1	0	0	0
RNP APCH	0	0	0

Table 6.6 shows the compliance with the navigation specifications of the different trajectories. If there is an improvement comparing with table 6.3 in the percentages of

compliance still all the trajectories exceed the limits of RNAV and RNP.

6.3 Overall Flight Intention

Overall scenario uses the visibility (table 5.1) and time slot assignment (table 5.4) of the basic scenario.

Overall scenario uses the own speed vector and the speed vector of the rest of participants to modulate the EKF as explained in 4.5.3.3.

Along Track Error Figures 6.13a, 6.13b and 6.13c, show the e_{at} in the tracking, clearly under the RNP Accuracy performance required by the **RNP APCH** shown in Table 1.1.

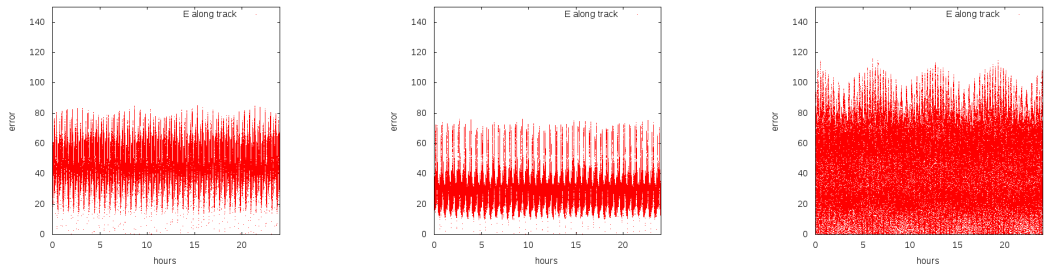

(a) UAV_t **(b)** UAV_l **(c)** UAV_v

Figure 6.13: e_{at}, Hybrid overall situation

Figures 6.14a, 6.14b and 6.14c, show the e_{at} frequencies.

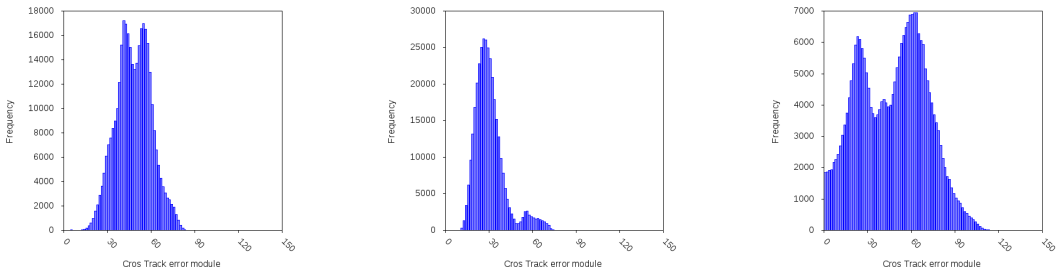

(a) UAV_t **(b)** UAV_l **(c)** UAV_v

Figure 6.14: e_{at} frequencies, Hybrid overall situation

Table 6.7: e_{at} Statistics, overall situation

	Trajectory		
Statistic	UAV_t	UAV_l	UAV_v
$\overline{e_{at}}$	48.16	30.50	47.21
$\sigma_{e_{at}}$	40.67	24.35	35.74
$CDF_{e_{at}}(95\%)$	99.56	59.60	87.48

Table 6.7 summarizes the basic statistics of the e_{at} module. UAV_t has an $\overline{e_{at}}$ of 48.16 m with a $\sigma_{e_{at}}$ of 40.67 m.

Using the Rayleigh CDF of equation C.12, the required 95 % of accuracy is achieved at a value of 99.56 m for the worst case (UAV_t), which is in fact enough to comply with the most restrictive navigation specification. For the case of the UAV_l and the UAV_v trajectories, their lower $\sigma_{e_{at}}$ ensures also the compliance with the stringent navigation specification (**RNP APCH**).

Cross Track Error Figures 6.15a, 6.15b and 6.15c, show the e_{ct} in the tracking. e_{ct} remains under the RNP Accuracy performance required by the **RNP APCH** shown in Table 1.1.

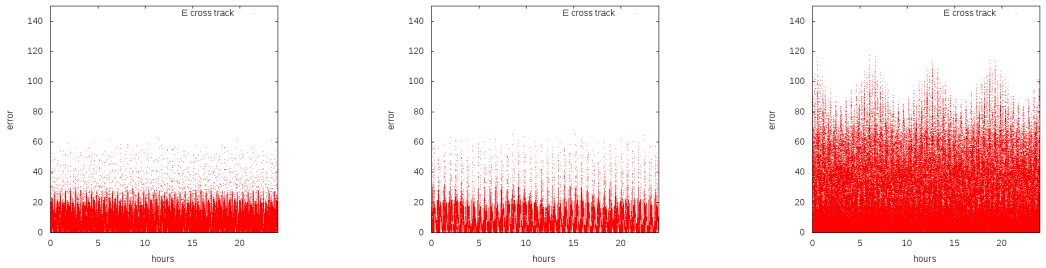

(a) UAV_t **(b)** UAV_l **(c)** UAV_v

Figure 6.15: e_{ct}, Hybrid overall situation

Figures 6.16a, 6.16b and 6.16c, show the e_{ct} Frequencies.

The worst case of table 6.8, the UAV_v trajectory, has a $\overline{e_{ct}}$ of 20.22 m and a $\sigma_{e_{ct}}$ of 19.56 m. Using the Rayleigh CDF of equation C.12, the required 95 % of accuracy is achieved at a value of 47.89 m for the worst case (UAV_v), which is (as for e_{at})enough to

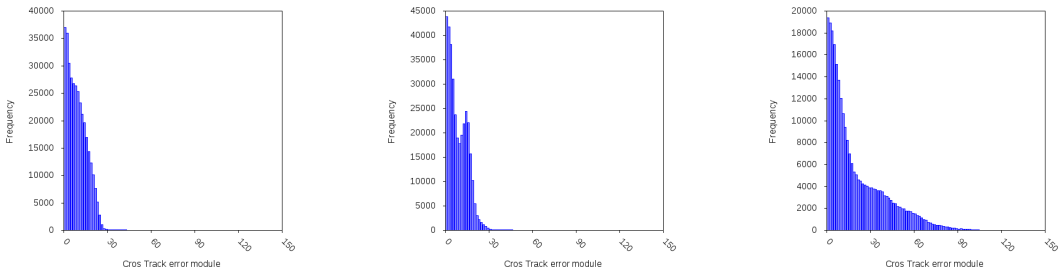

(a) UAV_t **(b)** UAV_l **(c)** UAV_v

Figure 6.16: e_{ct} frequencies, Hybrid overall situation

Table 6.8: e_{ct} Statistics, overall situation

	Trajectory		
Statistic	UAV_t	UAV_l	UAV_v
$\overline{e_{ct}}$	9.28	8.60	20.22
$\sigma_{e_{ct}}$	6.62	6.61	19.56
$CDF_{e_{ct}}(95\%)$	15.23	16.18	47.89

comply with the **RNP APCH**. For the case of the UAV_t and the UAV_l trajectories, with lower $\sigma_{e_{ct}}$ the compliance with **RNP APCH** is even improved.

Comparing the values of $CDF_{e_{ct}}(95\%)$ and $CDF_{e_{at}}(95\%)$ trajectory by trajectory, it could be observed the improvement in the accuracy for the e_{ct}, which in fact is the most critical between e_{at} and e_{ct}.

Integrity Figures 6.17a, 6.17b and 6.17c, show the error against the protection level calculated by the Kalman Filter from the noise models.

The integrity values obtained does not achieved the required values for **RNP 1** navigation specification.

Table 6.9 shows the compliance with the navigation specifications of the different trajectories. There is an improvement in all the percentages (with respect to table 6.6) but still, all the trajectories exceed the limits of RNAV and RNP.

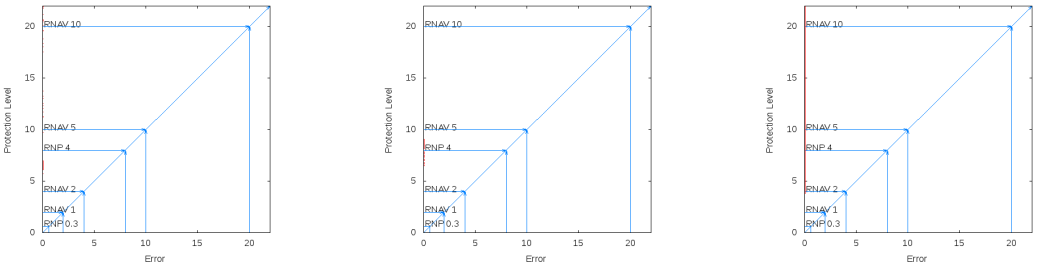

(a) UAV_t **(b)** UAV_l **(c)** UAV_v

Figure 6.17: Integrity Diagrams

Table 6.9: Integrity Alarm Values Compliance

	Trajectory		
Navigation Specification	UAV_t	UAV_l	UAV_v
RNP 10	0.77	0.84	0.99
RNAV 5	0.62	0.61	0.88
RNP 4	0.57	0.45	0.72
RNAV 2	0	0	0.05
Basic-RNP 1	0	0	0
RNP APCH	0	0	0

6.4 Time Bias

Time Bias scenario uses the visibility (table 5.1) and time slot assignment (table 5.4) of the basic scenario.

Time Bias scenario uses the own speed vector, the speed vector of the rest of participants and their shared time bias to modulate the EKF as explained in 4.5.3.4.

Along Track Error Figures 6.18a, 6.18b and 6.18c, show the e_{at} in the tracking, clearly under the RNP Accuracy performance required by the **RNP APCH** shown in Table 1.1.

Figures 6.19a, 6.19b and 6.19c, show the e_{at} frequencies.

Table 6.10 summarizes the basic statistics of the e_{at} module. UAV_t has an $\overline{e_{at}}$ of

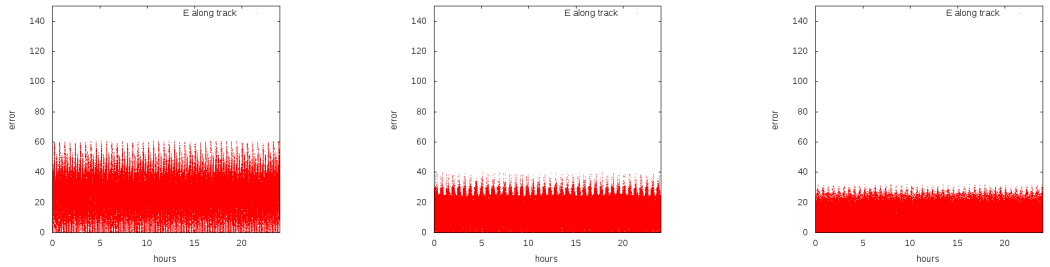

(a) UAV_t **(b)** UAV_l **(c)** UAV_v

Figure 6.18: e_{at}, Time Bias situation

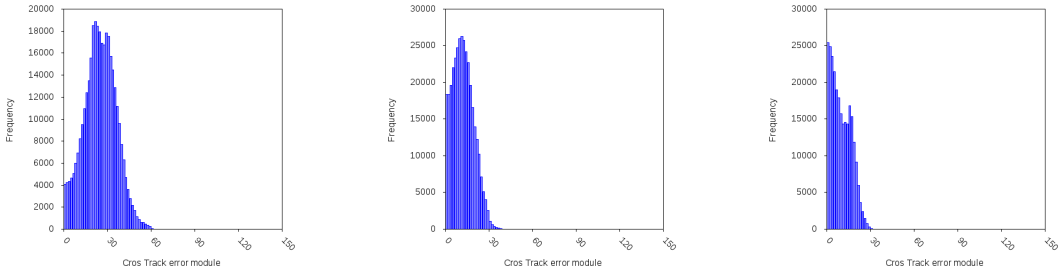

(a) UAV_t **(b)** UAV_l **(c)** UAV_v

Figure 6.19: e_{at} frequencies, Time Bias situation

Table 6.10: e_{at} Statistics, Time Bias situation

	Trajectory		
Statistic	UAV_t	UAV_l	UAV_v
$\overline{e_{at}}$	24.96	12.17	9.80
$\sigma_{e_{at}}$	20.53	10.20	7.55
$CDF_{e_{at}}(95\%)$	50.24	24.96	18.47

24.96 m with a $\sigma_{e_{at}}$ of 20.53 m.

Using the Rayleigh CDF of equation C.12, the required 95 % of accuracy is achieved at a value of 50.24 m for the worst case (UAV_t), which is in fact enough to comply with the most restrictive navigation specification. For the case of the UAV_l and the UAV_v trajectories, their lower $\sigma_{e_{at}}$ ensures also the compliance with the stringent navigation specification (**RNP APCH**).

Cross Track Error Figures 6.20a, 6.20b and 6.20c, show the e_{ct} in the tracking. e_{ct} remains under the RNP Accuracy performance required by the **RNP APCH** shown in Table 1.1.

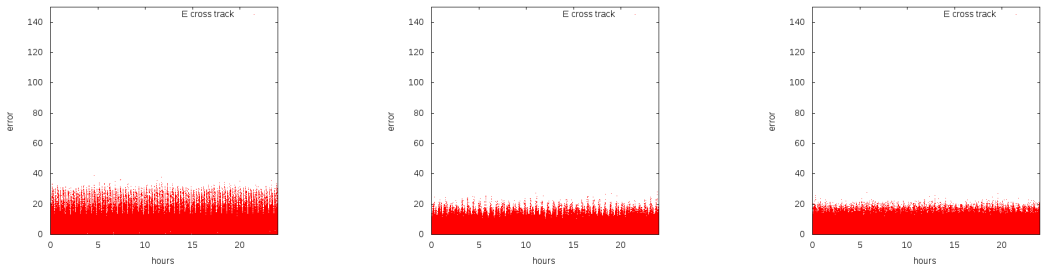

(a) UAV_t **(b)** UAV_l **(c)** UAV_v

Figure 6.20: e_{ct}, Time Bias situation

Figures 6.21a, 6.21b and 6.21c, show the e_{ct} Frequencies.

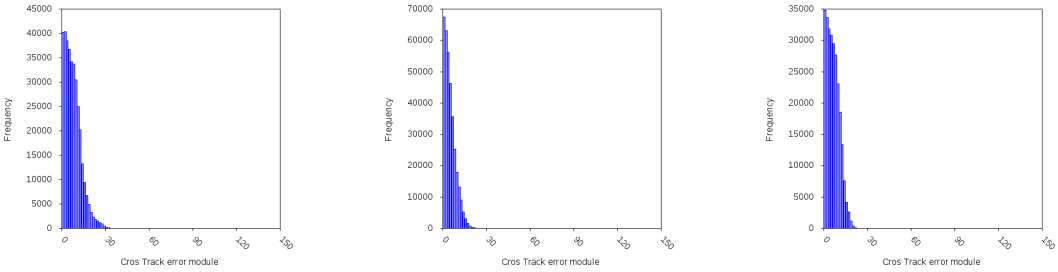

(a) UAV_t **(b)** UAV_l **(c)** UAV_v

Figure 6.21: e_{ct} frequencies, Hybrid overall situation

Table 6.11: e_{ct} Statistics, Time Bias situation

	Trajectory		
Statistic	UAV_t	UAV_l	UAV_v
$\overline{e_{ct}}$	7.59	4.93	6.40
$\sigma_{e_{ct}}$	5.49	3.80	4.26
$CDF_{e_{ct}}(95\%)$	13.45	9.30	10.43

The worst case of table 6.11, the UAV_t trajectory, has a $\overline{e_{ct}}$ of 7.59 m and a $\sigma_{e_{ct}}$ of

5.49 m. Using the Rayleigh CDF of equation C.12, the required 95 % of accuracy is achieved at a value of 13.45 m for the worst case (UAV_t), which is (as for e_{at})enough to comply with the **RNP APCH**. For the case of the UAV_l and the UAV_v trajectories, with lower $\sigma_{e_{ct}}$ the compliance with **RNP APCH** is even improved.

Comparing the values of $CDF_{e_{ct}}(95\%)$ and $CDF_{e_{at}}(95\%)$ trajectory by trajectory, it could be observed the improvement in the accuracy for the e_{ct}, which in fact is the most critical between e_{at} and e_{ct}.

Integrity Figures 6.22a, 6.22b and 6.22c, show the error against the protection level calculated by the Kalman Filter from the noise models.

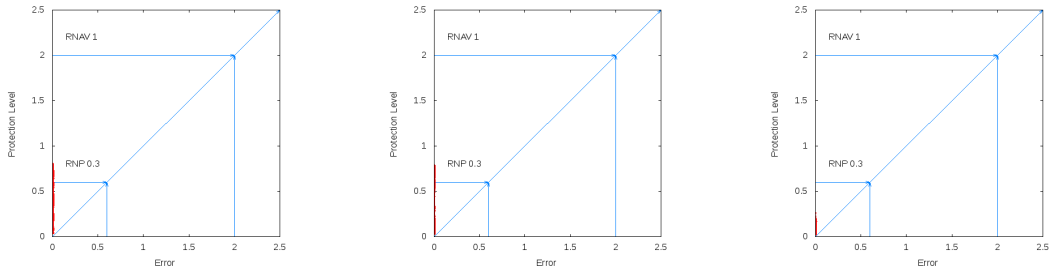

(a) UAV_t **(b)** UAV_l **(c)** UAV_v

Figure 6.22: Integrity Diagrams

The integrity values obtained does not achieved the required values for **RNP 1** navigation specification.

Table 6.12: Integrity Alarm Values Compliance

	Trajectory		
Navigation Specification	UAV_t	UAV_l	UAV_v
Basic-RNP 1	1	1	1
RNP APCH	0.98	0.99	1

Table 6.12 shows the compliance with the navigation specifications of the different trajectories. It could be appreciated a dramatical improvement in the compliance in all the trajectories that drive us to conclude that the control of the Time Bias becomes

a crucial aspect of the PoCoLoCo methodology, independently of the means employed to control this Time Bias.

6.4.1 Loquacity augmentation

Once achieved the target performance in both accuracy and integrity, it raises an interesting question: What happens if the scenario is more loquacious than the presented scenario?

This increment in the loquacity is assessed in two ways: by incrementing the number of time slots per second that each user employs in one hand (Time Slot Assignment B) and incrementing the number of users that each user could listen and consequently employ for positioning in the other hand (Visibility Enhancement).

Seeking to be concise, the results of accuracy have been omitted in the next two scenarios. Both scenarios are compliant in accuracy terms and the accuracy analysis only show slight improvements with respect the scenario Time Bias. Obviating this accuracy results the assessment focus on the integrity improvement, where the improvements are more significant.

6.4.1.1 Time Slot Assignment B

Time Slot Assignment B scenario uses the visibility (table 5.1) of the Basic Scenario but uses the own speed vector, the speed vector of the rest of participants and their shared time bias to modulate the EKF as explained in 4.5.3.4.

Time Slot Assignment B scenario changes the time slot assignment of basic scenario (table 5.4) by another even more loquacious (table 5.5).

Figures 6.23a, 6.23b and 6.23c, show the error against the protection level calculated by the Kalman Filter from the noise models.

The integrity values obtained does achieve the required values for **RNP 1** navigation specification and almost achieve the required performance for **RNP APCH**.

Table 6.13 shows the compliance with the navigation specifications of the different trajectories. It could be appreciated a slight improvement in the compliance of **RNP APCH**.

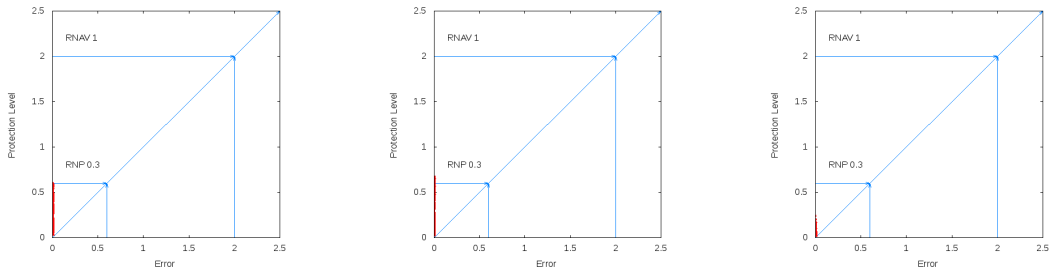

(a) UAV_t **(b)** UAV_l **(c)** UAV_v

Figure 6.23: Integrity Diagrams

Table 6.13: Integrity Alarm Values Compliance

	Trajectory		
Navigation Specification	UAV_t	UAV_l	UAV_v
Basic-RNP 1	1	1	1
RNP APCH	0.99	0.99	1

6.4.1.2 Visibility Enhancement

Once assessed the confidence values achievable with the visibilities of table 5.1, an improved version of the communications has been simulated to asses the effect on the confidence level of a richer scenario. The richer scenario, summarized by table 5.2, has the capability to receive messages from any of the other network user instead of the reduced set of table 5.1.

Figures 6.24a, 6.24b and 6.24c, show the error against the protection level calculated by the Kalman Filter from the noise models.

The inclusion in the EKF of pseudorange measurements coming from more users gives us a better DOP value. This improvement could be observed graphically by comparing figure 5.4 (where only the GS are considered for computing the DOP) with figures 5.5a or 5.5b (where the GS and the UAV are considered for computing the DOP). This better DOP values benefit the three trajectories but the improvement is better seen in the case of UAV_t (fig. 6.24a) and UAV_l (fig. 6.24b) that now complies even with **RNP APCH**.

Table 6.14 shows the compliance with the navigation specifications of the different

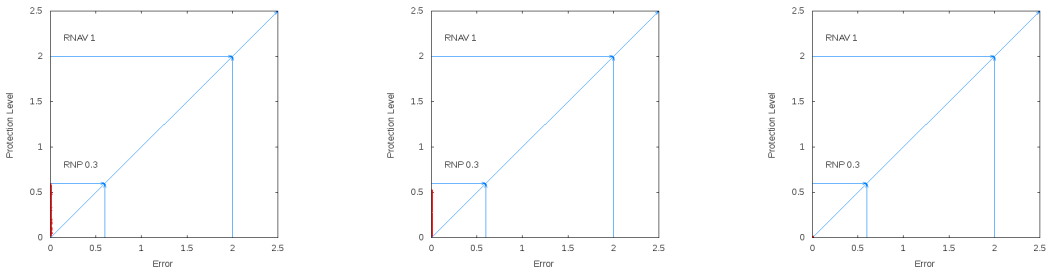

(a) UAV_t **(b)** UAV_l **(c)** UAV_v

Figure 6.24: Integrity Diagrams

Table 6.14: Integrity Alarm Values Compliance

	Trajectory		
Navigation Specification	UAV_t	UAV_l	UAV_v
Basic-RNP 1	1	1	1
RNP APCH	1	1	1

trajectories. It could be appreciated how UAV_t, UAV_l and UAV_v complies now with **RNP APCH**. This significant improvement with respect the shown in table 6.12 is achieved without increasing the data throughput of each user (as it was the case of table 6.13), only taking advantage of the communications of additional users.

This interesting result could be summarized from the point of view of the relative navigation as the more crowded is the scenario, it becomes safer.

There is nothing better hidden
than what is in sight.

Anonymous

7

Relative Surveillance Performance

The expected contribution in Surveillance is to show a surveillance alternative to the conventional surveillance techniques (PSR, SSR, ADS).

This contribution is based on the capacity to compute the ToF of the messages exchanged trough a datalink. The position of the aircraft is obtained by trilateration using the ToF to compute approximate distances from different stations.

Figure 7.1 shows how different Time of Flight for the same message received at different receivers could be employed to calculate the position of the UAS. This is an information already existent in the physical layer that is employed in the application layer.

The surveillance information obtained by this technique is independent from the conventional surveillance sources (PSR, SSR), as well as the positioning data obtained from navigation means based on satellite constellations (GPS, GLONASS). This independence provides some additional characteristics:

- Resilience, as aircraft position (track) could be calculated from different sets of receivers.

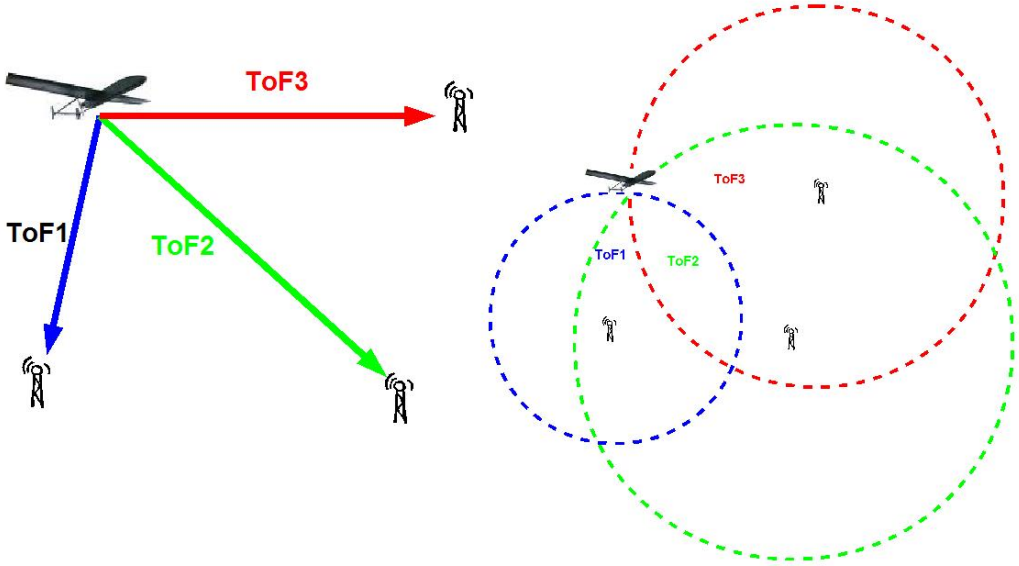

Figure 7.1: Multilateration in relative Surveillance

- Flexibility, as aircraft position (track) calculation could change between different sets of receivers.
- Adaptation, as could be easily reconfigured to different implementations on the ground.

The extension of the RELNAV concept to the multilateration, by using the communication link as source for ToF, represents a synergy opportunity as surveillance data is obtained without requiring adding radiofrequency spectrum employ. The capability to obtain tracking capacities through the communications is aligned with the surveillance strategy of Eurocontrol (133) and does not requires additional spectrum (in addition to the employed in communications) which is one of the problems presented in (134) and detailed in (135).

For surveillance purposes it is assumed that each GS measures the pseudorange between GS itself and each UAV. Those pseudoranges are then shared through a network and the position of each UAV are computed using pseudoranges to the same aircraft obtained from different GS. This positioning could be performed by the GS of the UAV or by a centralized facility, depending on criteria of the system designer for the selected architecture.

The accuracy of the positioning is assessed with the thresholds proposed by (62) and (63), showing the error by components e_{at} and e_{ct} maintaining an analogy with the navigation results shown in chapter 6. This is done in despite of the ICAO requirements, which are stated in linear distance between actual position and calculated position, to better analyse the performance of the methodology. As in the case of relative navigation of chapter 6, the surveillance data presents an asymmetric behaviour depending on the direction of the measurement of the error (e_{at} and e_{ct}). Showing the performance divided into its components allows us to better describe the behaviour obtained.

It should be taken into consideration that (63) specifies a measurement interval of 5 seconds for NM, while recommend 4 seconds interval. In our PoCoLoCo proposal, the measurement update interval is 1 second, improving significantly the required performance.

The integrity threshold for Surveillance is not specified in (62) nor in (63), so it has been selected the values of the separation (3NM and 5NM). These references allows us to show the effect of different error estimation, specially e_{synch}, in the computation of a protection level in spite of the lack of a standard value and maintains an analogy with the chapter 6.

7.1 Basic Scenario

The basic scenario proposed as reference for assessing the improvements achieved by altering time slot allocations is based on the visibility summarized in table 5.3 and the time slot allocation of table 5.4.

Along Track Error e_{at} Figures 7.2b and 7.2c, show an e_{at} under the required by EUROCONTROL (Table 1.2) in the 3NM separation (330m). In fact, it even complies with the recommended value of 230m.

Figure 7.2a shows the performance obtained by the UAV_t which does not comply with the performance required by EUROCONTROL in the 3NM separation and scarcely complies with the performance required in the 5NM separation.

Figures 7.3b and 7.3c, show the e_{at} frequencies of the UAV_l and the UAV_v and how both are under the 230m recommended by EUROCONTROL for the 3NM separation. Figure 7.3a shows the e_{at} frequency of the UAV_t and how does not complies with the

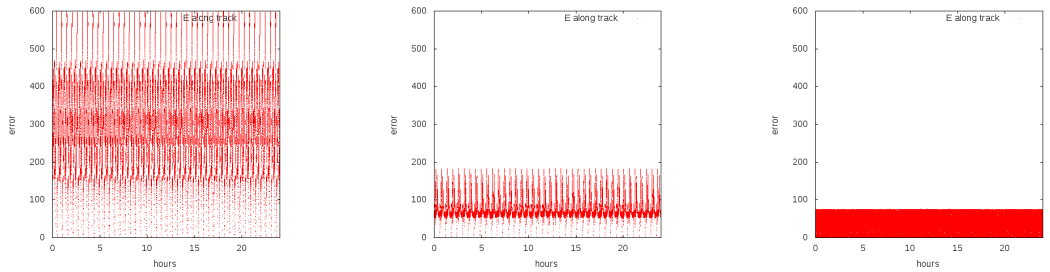

(a) UAV_t **(b)** UAV_l **(c)** UAV_v

Figure 7.2: e_{at}, basic scenario

performance required by EUROCONTROL for the 3NM separation (330m), neither with the recommended performance for the 5NM separation (350m).

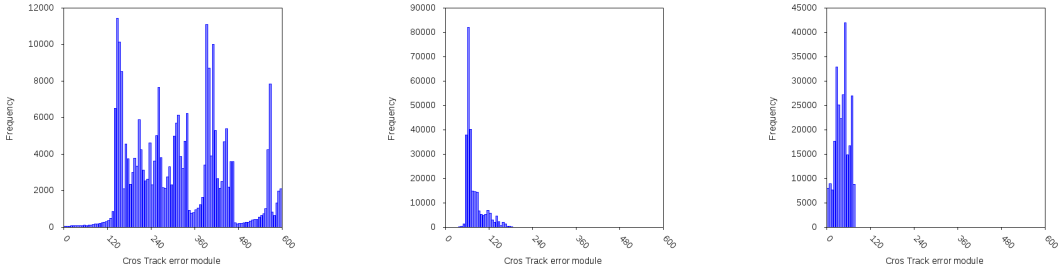

(a) UAV_t **(b)** UAV_l **(c)** UAV_v

Figure 7.3: e_{at} frequencies, basic scenario

Table 7.1: e_{at} Statistics, basic scenario

	Trajectory		
Statistic	UAV_t	UAV_l	UAV_v
$\overline{e_{at}}$	315.51	77.55	42.30
$\sigma_{e_{at}}$	236.69	61.24	32.03
$CDF_{e_{at}}(95\%)$	578.86	149.90	78.40

Table 7.1 summarizes the basic statistics of the e_{at} module. $\sigma_{e_{at}}$ is under the values required by the Lincoln Laboratory (table 1.2) with the premise that the e_{at} is bigger than the e_{ct}, which will be seen next.

The accuracy (95%) of the UAV_l and the UAV_v comply with the required by EUROCONTROL for the 3NM separation but this is not the case for the Traffic monitoring. Traffic monitoring has an along track mean ($\overline{e_{at}}$) of 315.51 m with a standard deviation ($\sigma_{e_{at}}$) of 236.69 m.

Using the Rayleigh CDF of equation C.12, the required 95 % of accuracy is achieved at a value of 578.86 m for the worst case (UAV_t), which is beyond the 550 m required by EUROCONTROL for the 5NM separation.

Cross Track Error e_{ct} Figures 7.4a, 7.4b and 7.4c, show the how the e_{ct} has similar behaviour than the e_{at} but with better values. Figures 7.4b and 7.4c show how the UAV_l and the UAV_v are clearly under the 230m recommended by EUROCONTROL for the 3NM. In the other hand figure 7.4a shows how the UAV_t does not complies neither with the 3NM required accuracy neither with the recommended value for 5NM. Taking into consideration that the 550m required by EUROCONTROL for the 5NM are in fact the module of the e_{at} and the e_{ct} it does not complies neither with the required performance.

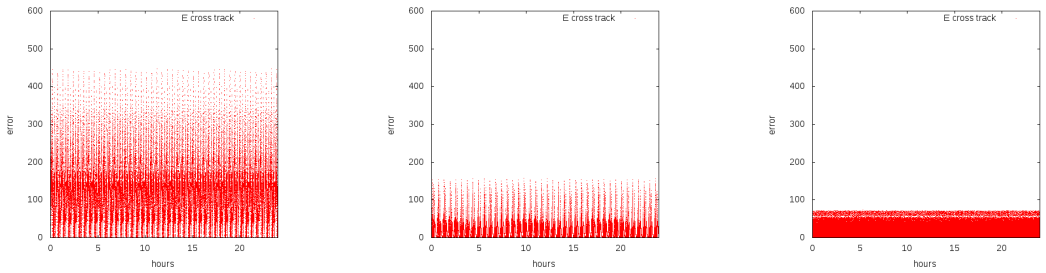

(a) UAV_t **(b)** UAV_l **(c)** UAV_v

Figure 7.4: e_{ct}, basic scenario

Figures 7.5a, 7.5b and 7.5c, show the e_{ct} frequencies. The UAV_l and the UAV_v (figures 7.5b and 7.5c) show an improvement with respect to the e_{at} frequencies remaining under the required values by EUROCONTROL. The UAV_t (figure 7.5a) shows a big improvement with respect to the e_{at} but still remains a long (and thin) queue that goes beyond the required values for the 3NM separation.

The $\sigma_{e_{ct}}$ table 7.2 show values under the 370m required by the Lincoln Laboratory for the UAV_t, UAV_l and UAV_v. For the case of the Traffic shall be kept in mind that

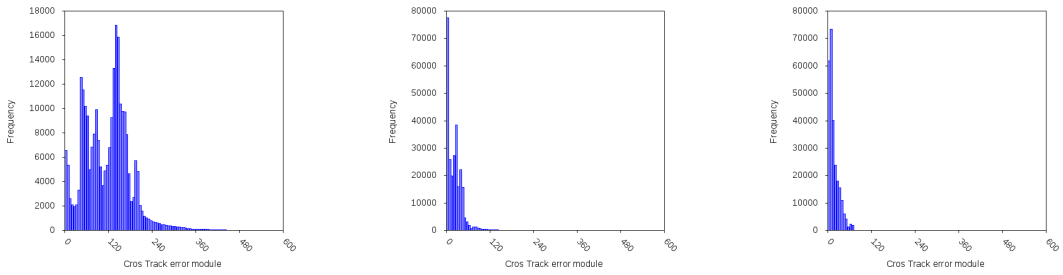

(a) UAV_t **(b)** UAV_l **(c)** UAV_v

Figure 7.5: e_{ct} frequencies, basic scenario

Table 7.2: e_{ct} Statistics, basic scenario

	Trajectory		
Statistic	UAV_t	UAV_l	UAV_v
$\overline{e_{ct}}$	116.83	21.63	16.04
$\sigma_{e_{ct}}$	63.33	19.49	13.84
$CDF_{e_{ct}}(95\%)$	155.01	47.70	33.87

the $\sigma_{e_{at}}$ was already beyond the required performance, making the value of $\sigma_{e_{ct}}$ not valid.

The worst case of table 7.2, the UAV_t trajectory, has a $\overline{e_{ct}}$ of 116.83 m and a $\sigma_{e_{ct}}$ of 63.33 m. Using the Rayleigh CDF of equation C.12, the required 95 % of accuracy is achieved at a value of 155.01 for the worst case (UAV_t), which is enough to comply with the performance required by EUROCONTROL for the 3NM separation. For the case of the UAV_l and the UAV_v trajectories, with lower $\sigma_{e_{ct}}$ the compliance with the 3NM separation is even improved.

Comparing the values of $CDF_{e_{ct}}(95\%)$ and $CDF_{e_{at}}(95\%)$ trajectory by trajectory, it could be observed the improvement in the accuracy for the e_{ct}, which in fact is the most critical between e_{at} and e_{ct}. Nevertheless, the required performance by EUROCONTROL is the linear error not their components. As the e_{at} was already beyond the limits, it remains beyond the limits.

Integrity Figures 7.6a, 7.6b and 7.6c, show the error against the protection level calculated by the Kalman Filter from the noise models.

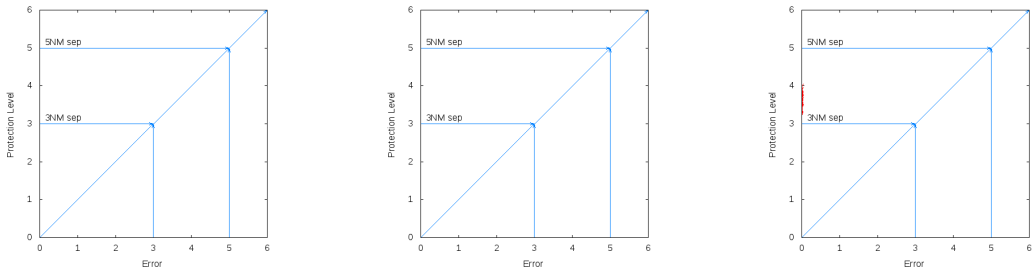

(a) UAV_t **(b)** UAV_l **(c)** UAV_v

Figure 7.6: Integrity Diagrams

The integrity values obtained are beyond the alarm thresholds established for 5NM separation, except in the case of UAV_v.

Table 7.3: Integrity Alarm Values Compliance

	Trajectory		
Required Separation	UAV_t	UAV_l	UAV_v
5NM	0	0	1
3NM	0	0	0

Table 7.3 shows the percentage of compliance with the separation requirements performed by the different trajectories. All the trajectories exceed the limits of **3NM** and only UAV_v, that benefits from a specially good DOP during the entire trajectory, complies with **5NM**.

7.2 Own Trajectory

Own trajectory scenario uses the visibility (table 5.3) and time slot assignment (table 5.4) of the basic scenario.

Own trajectory uses the own speed vector to modulate the EKF as explained in 4.5.3.2.

Along Track Error e_{at} Figures 7.7a and 7.7c, show how the e_{at} of UAV_t and UAV_v comply with the required by EUROCONTROL for 3NM separation (Table 1.2).

Figure 7.7b shows how the UAV_l complies with the performance required by EUROCONTROL for the 5NM ($< 550m$) separation but does not complies with its recommendation for the 5NM separation ($< 350m$).

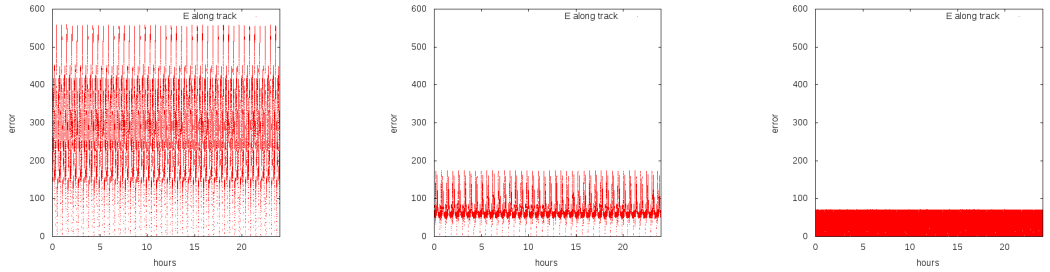

(a) UAV_t **(b)** UAV_l **(c)** UAV_v

Figure 7.7: e_{at}, Hybrid own trajectory

Figures 7.8a, 7.8b and 7.8c, show the how the Error Frequencies of the UAV_t has been significantly improved whilst the frequencies of both UAV_l and UAV_v have a longer tail that offers poorer performance.

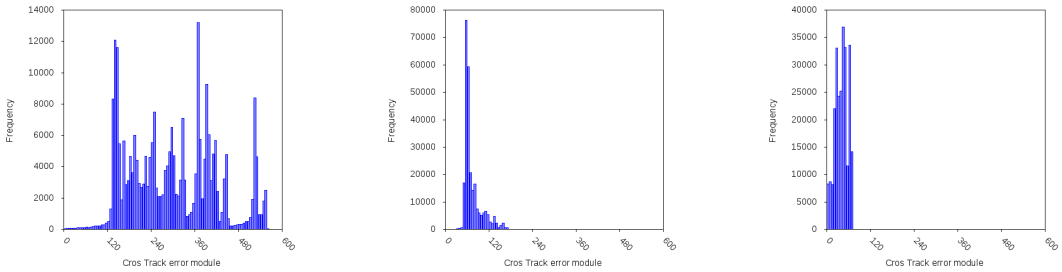

(a) UAV_t **(b)** UAV_l **(c)** UAV_v

Figure 7.8: e_{at} frequencies, Hybrid own trajectory

Table 7.4 summarizes the basic statistics of the e_{at} module. UAV_t improves their positioning accuracy whilst the UAV_l and UAV_v achieve poorer performance. $\sigma_{e_{at}}$ of UAV_t, UAV_l and UAV_v are in line with the accuracy required by the Lincoln Laboratory and the horizontal position error of the traffic and the vineyard comply with the required by EUROCONTROL.

Table 7.4: e_{at} Statistics, own trajectory

	Trajectory		
Statistic	UAV_t	UAV_l	UAV_v
$\overline{e_{at}}$	299.00	73.21	40.39
$\sigma_{e_{at}}$	223.96	57.32	31.04
$CDF_{e_{at}}(95\%)$	548.19	140.30	75.99

Using the Rayleigh CDF of equation C.12 for the UAV_t, the required 95 % of accuracy is achieved at a value of 548.19 m, which is beyond the required by EUROCONTROL for the 3NM separation (330 m) as well as beyond the recommendation for the 5NM separation ($< 350m$).

Cross Track Error e_{ct} Figures 7.9a, 7.9b and 7.9c, show how the e_{ct} achieve poorer results than in the basic scenario; in the case of for UAV_t and UAV_l, going beyond the requirement of EUROCONTROL for the 3NM separation. e_{ct} of UAV_v still complies with the EUROCONTROL requirements but increases is magnitude significantly.

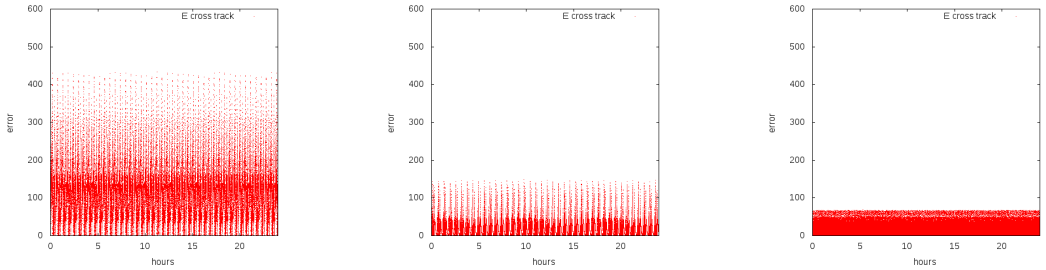

(a) UAV_t **(b)** UAV_l **(c)** UAV_v

Figure 7.9: e_{ct}, Hybrid own trajectory

Figures 7.10a, 7.10b and 7.10c, show how Error Frequencies achieves poorer results in the case of the Lifeguard and the Vineyard and only improves the positioning of the UAV_t.

Table 7.5 shows how the σ_{ct} of the UAV_t, the UAV_l and the UAV_v comply with the Lincoln Laboratoy Requirement. The EUROCONTROL requirement for 3NM

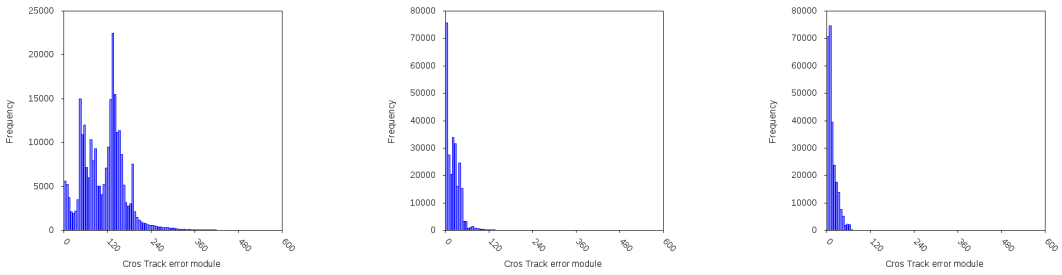

(a) UAV_t **(b)** UAV_l **(c)** UAV_v

Figure 7.10: e_{ct} frequencies, Hybrid own trajectory

Table 7.5: e_{ct} Statistics, own trajectory

	Trajectory		
Statistic	UAV_t	UAV_l	UAV_v
$\overline{e_{ct}}$	110.57	21.24	14.60
$\sigma_{e_{ct}}$	58.57	18.49	12.73
$CDF_{e_{ct}}(95\%)$	143.36	45.25	31.17

separation is achieved by the UAV_t, UAV_l and the UAV_v. Nevertheless, the poor performance obtained in e_{at} by UAV_t discards it use.

Integrity Figures 7.11a, 7.11b and 7.11c, show the error against the protection level calculated by the Kalman Filter from the noise models.

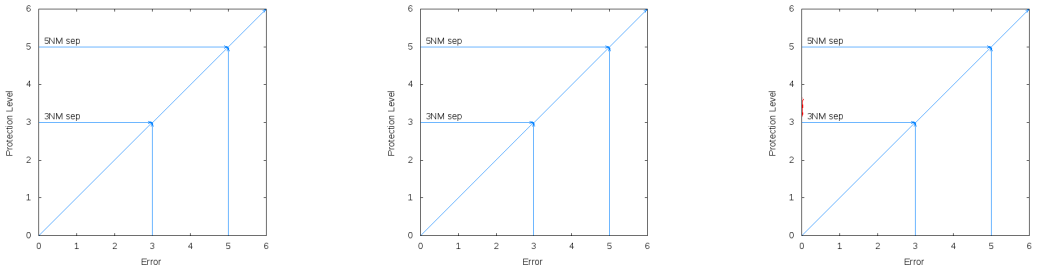

(a) UAV_t **(b)** UAV_l **(c)** UAV_v

Figure 7.11: Integrity Diagrams

The integrity values obtained are beyond the alarm thresholds except in the case

of UAV_v for 5NM.

Table 7.6: Integrity Alarm Values Compliance

	Trajectory		
Required Separation	UAV_t	UAV_l	UAV_v
5NM	0	0	1
3NM	0	0	0

Table 7.6 shows the percentage of compliance with the separation requirements performed by the different trajectories. As in the Basic Scenario, all the trajectories exceed the limits of **3NM** and only UAV_v, that benefits from a specially good DOP during the entire trajectory, complies with **5NM**.

7.3 Overall Flight Intention

Overall Flight Intention scenario uses the visibility (table 5.3) and time slot assignment (table 5.4) of the basic scenario.

Overall Flight Intention scenario uses the own speed vector and the speed vector of the rest of participants to modulate the EKF as explained in 4.5.3.3.

Along Track Error e_{at} Figures 7.12a, 7.12b and 7.12c, show the e_{at} in the tracking, clearly under the Accuracy performance required by EUROCONTROL for the 3NM separation.

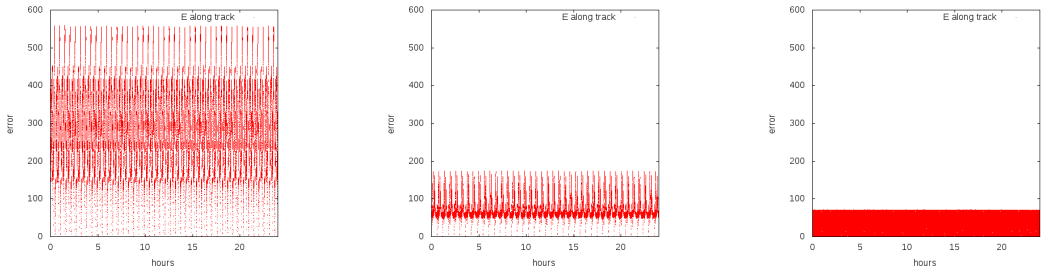

(a) UAV_t **(b)** UAV_l **(c)** UAV_v

Figure 7.12: e_{at}, Hybrid overall

Figures 7.13a, 7.13b and 7.13c show the Error Frequencies of UAV_t, UAV_l and UAV_v.

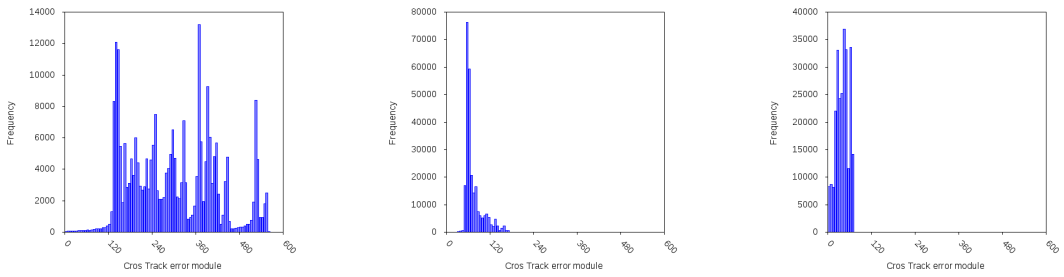

(a) UAV_t **(b)** UAV_l **(c)** UAV_v

Figure 7.13: e_{at} frequencies, Hybrid overall

Table 7.7: e_{at} Statistics, Hybrid overall

	Trajectory		
Statistic	UAV_t	UAV_l	UAV_v
$\overline{e_{at}}$	299.00	73.21	40.39
$\sigma_{e_{at}}$	223.96	57.32	31.05
$CDF_{e_{at}}(95\%)$	548.19	140.30	75.99

Table 7.7 summarizes the basic statistics of the e_{at} module. $\sigma_{e_{at}}$ is under the values required by the Lincoln Laboratory (table 1.2) with the premise that the e_{at} is bigger than the e_{ct}, which will be seen next.

The accuracy (95%) of the UAV_l and the UAV_v comply with the required by EUROCONTROL for the 3NM separation ($< 330m$) as well as for its recommendation ($< 230m$).

Using the Rayleigh CDF of equation C.12, the required 95 % of accuracy is achieved at a value of 548.19 m for the worst case (UAV_t), which goes beyond the required by EUROCONTROL for the 3NM separation.

Cross Track Error e_{ct} Figures 7.14a, 7.14b and 7.14c, show the e_{ct} in the tracking, clearly under the Accuracy performance required by EUROCONTROL for the 3NM separation, improving even the accuracies of e_{at}.

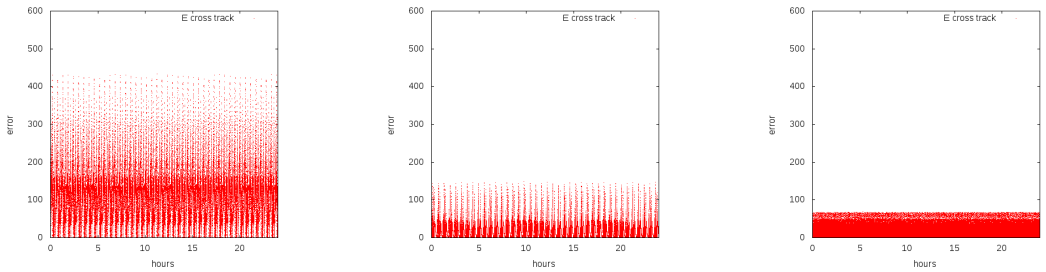

(a) UAV_t **(b)** UAV_l **(c)** UAV_v

Figure 7.14: e_{ct}, Hybrid overall

Figures 7.15a, 7.15b and 7.15c, show the e_{ct} frequencies of UAV_t, UAV_l and UAV_v. It is significant the improvement with respect to the e_{at} frequencies of this scenario.

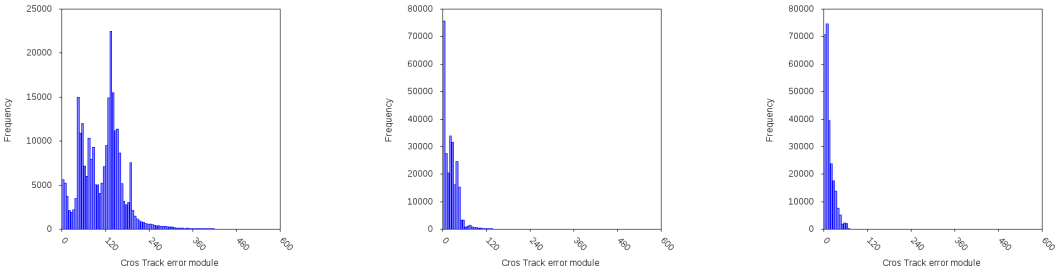

(a) UAV_t **(b)** UAV_l **(c)** UAV_v

Figure 7.15: e_{ct} frequencies, Hybrid overall

Table 7.8: e_{ct} Statistics, Hybrid overall

	Trajectory		
Statistic	UAV_t	UAV_l	UAV_v
$\overline{e_{ct}}$	110.57	21.24	14.60
$\sigma_{e_{ct}}$	58.57	18.49	12.73
$CDF_{e_{ct}}(95\%)$	146.36	45.25	31.17

Table 7.8 summarizes the basic statistics of the e_{ct} module. $\sigma_{e_{ct}}$ is under the values required by the Lincoln Laboratory (table 1.2) complying with the premise that the e_{at} is bigger than the e_{ct}.

The accuracy (95%) of the UAV_t, UAV_l and the UAV_v comply with the required by EUROCONTROL for the 3NM separation ($< 330m$) as well as for its recommendation ($< 230m$).

Integrity Figures 7.16a, 7.16b and 7.16c, show the error against the protection level calculated by the Kalman Filter from the noise models.

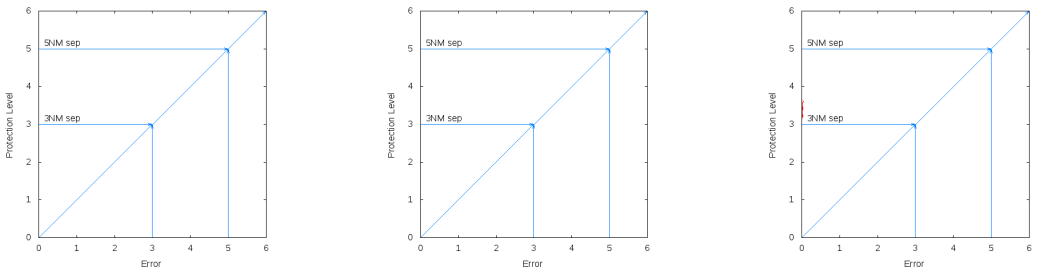

(a) UAV_t **(b)** UAV_l **(c)** UAV_v

Figure 7.16: Integrity Diagrams

The integrity values obtained are beyond 5NM required separation for all the trajectories with the exception of UAV_v

Table 7.9: Integrity Alarm Values Compliance

	Trajectory		
Required Separation	UAV_t	UAV_l	UAV_v
5NM	0	0	1
3NM	0	0	0

Table 7.9 shows the percentage of compliance with the separation requirements performed by the different trajectories. As in the Basic Scenario and the Hybridized with own trajectory scenario, all the trajectories exceed the limits of **3NM** and only UAV_v, that benefits from a specially good DOP during the entire trajectory, complies with **5NM**.

7.4 Time Bias

Time Bias scenario uses the visibility (table 5.3) and time slot assignment (table 5.4) of the basic scenario.

Time Bias scenario uses the own speed vector, the speed vector of the rest of participants and their shared time bias to modulate the EKF as explained in 4.5.3.4.

The improvement on the positioning achieved thanks to the use of the clock biases is as big that the scale of the error has been changed from 0 m to 600 m in the previous surveillance graphics to 0 m to 100 m.

Along Track Error e_{at} Figures 7.17a, 7.17b and 7.17c, show the e_{at} in the tracking, clearly under the Accuracy performance required by EUROCONTROL for the 3NM separation.

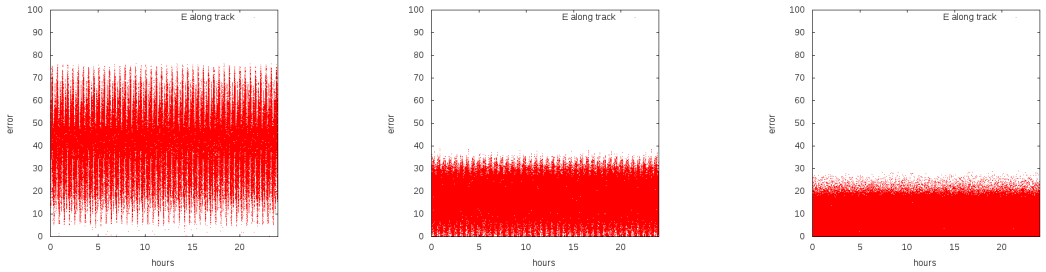

(a) UAV_t **(b)** UAV_l **(c)** UAV_v

Figure 7.17: e_{at}, Time Bias

Figures 7.18a, 7.18b and 7.18c show the Error Frequencies of UAV_t, UAV_l and UAV_v.

Table 7.10: e_{at} Statistics, Time Bias

	Trajectory		
Statistic	UAV_t	UAV_l	UAV_v
$\overline{e_{at}}$	41.32	16.63	9.15
$\sigma_{e_{at}}$	49.26	14.48	7.00
$CDF_{e_{at}}(95\%)$	120.59	35.43	17.13

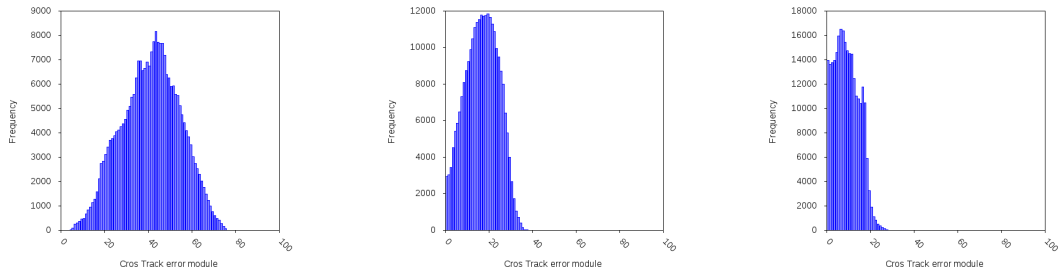

(a) UAV_t **(b)** UAV_l **(c)** UAV_v

Figure 7.18: e_{at} frequencies, Time Bias

Table 7.10 summarizes the basic statistics of the e_{at} module. $\sigma_{e_{at}}$ is under the values required by the Lincoln Laboratory (table 1.2) with the premise that the e_{at} is bigger than the e_{ct}, which will be seen next.

The accuracy (95%) of the UAV_t, UAV_l and the UAV_v comply with the required by EUROCONTROL for the 3NM separation ($< 330m$) as well as for its recommendation ($< 230m$).

Using the Rayleigh CDF of equation C.12, the required 95 % of accuracy is achieved at a value of 120.59 m for the worst case (UAV_t), which complies with the required by EUROCONTROL for the 3NM separation.

Cross Track Error e_{ct} Figures 7.19a, 7.19b and 7.19c, show the e_{ct} in the tracking, clearly under the Accuracy performance required by EUROCONTROL for the 3NM separation, improving even the accuracies of e_{at}.

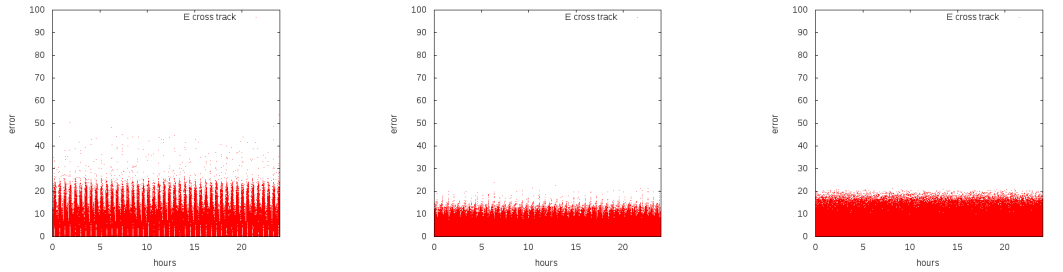

(a) UAV_t **(b)** UAV_l **(c)** UAV_v

Figure 7.19: e_{ct}, Time Bias

Figures 7.20a, 7.20b and 7.20c, show the e_{ct} frequencies of UAV_t, UAV_l and UAV_v. It is significant the improvement with respect to the e_{at} frequencies of this scenario.

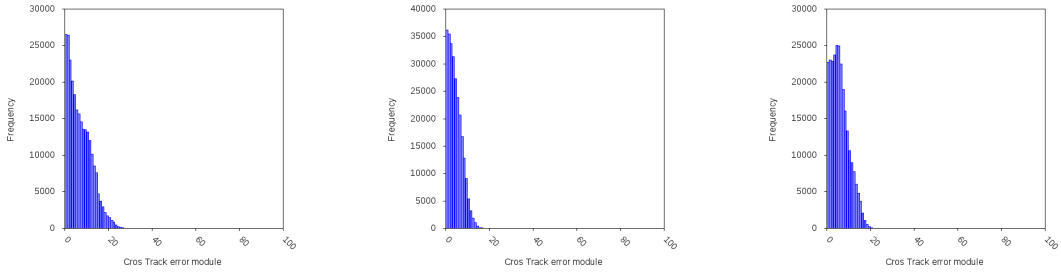

(a) UAV_t **(b)** UAV_l **(c)** UAV_v

Figure 7.20: e_{ct} frequencies, Time Bias

Table 7.11: e_{ct} Statistics, Time Bias

	Trajectory		
Statistic	UAV_t	UAV_l	UAV_v
$\overline{e_{ct}}$	6.99	4.29	6.09
$\sigma_{e_{ct}}$	21.26	3.03	4.50
$CDF_{e_{ct}}(95\%)$	52.03	7.43	11.02

Table 7.11 summarizes the basic statistics of the e_{ct} module. $\sigma_{e_{ct}}$ is under the values required by the Lincoln Laboratory (table 1.2) complying with the premise that the e_{at} is bigger than the e_{ct}.

The accuracy (95%) of the UAV_t, UAV_l and the UAV_v comply with the required by EUROCONTROL for the 3NM separation ($< 330m$) as well as for its recommendation ($< 230m$).

Integrity Figures 7.21a, 7.21b and 7.21c, show the error against the protection level calculated by the Kalman Filter from the noise models.

The integrity values obtained are under the alarm thresholds of 3NM.

Table 7.12 shows the percentage of compliance with the separation requirements performed by the different trajectories. Comparing with tables 7.3, 7.6 and 7.9 could be appreciated a dramatical improvement: all the trajecctories comply not only with

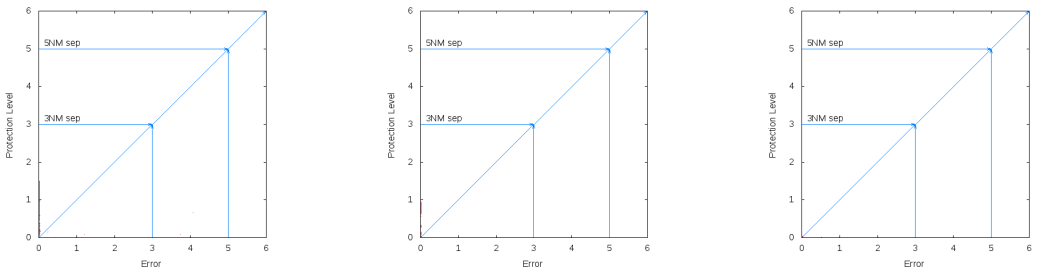

(a) UAV_t **(b)** UAV_l **(c)** UAV_v

Figure 7.21: Integrity Diagrams

Table 7.12: Integrity Alarm Values Compliance

	Trajectory		
Required Separation	UAV_t	UAV_l	UAV_v
5NM	1	1	1
3NM	1	1	1

5NM but even with 3NM separation. As in the case of navigation, the control of the Time Bias of the participants drives to a dramatical improvement in the integrity.

7.4.1 Loquacity augmentation

The enhancement on the surveillance retrieved from increasing the number of measure (i.e: by adding time slots allocation to each participant) is assessed simulating the same visibility than in the basic scenario (table 5.1) but increasing the number of time slots as summarized by table 5.5.

The enhancement on the surveillance retrieved from the improvement on the visibility (i.e: using measures from more actors) has not been evaluated. With the current simulation configuration, the augmentation of the number of actors reporting measures in surveillance implies the use of pseudoranges measured from UAV and its propagation through the radio network. This measures from UAV to UAV complicate the algorithm as it requires an additional set of messages for sharing the measures. It also introduces bigger delays between the measure and the employ of the measures that should be considered for a proper simulation.

7.4.1.1 Time Slot Assignment B

Time Slot Assignment B scenario uses the visibility (table 5.1) of the Basic Scenario and its situational awareness knowledge.

Time Slot Assignment B scenario changes the time slot assignment of basic scenario (table 5.4) by another even more loquacious (table 5.5).

Along Track Error e_{at} Figures 7.22b and 7.22c, show how the e_{at} of the UAV_t, UAV_l and the UAV_v complies with the performance required by EUROCONTROL for 3NM separation (Table 1.2).

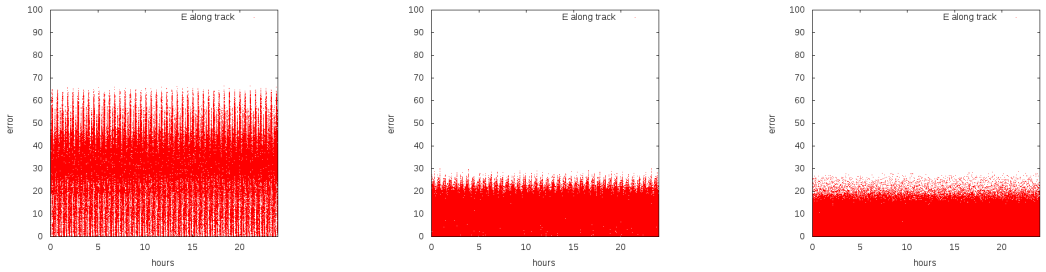

(a) UAV_t **(b)** UAV_l **(c)** UAV_v

Figure 7.22: e_{at}, Time Slot allocation B

Figures 7.23a, 7.23b and 7.23c, show the how the Error Frequencies have distributions similar to the basic scenario but with the e_{at} nearer to 0.

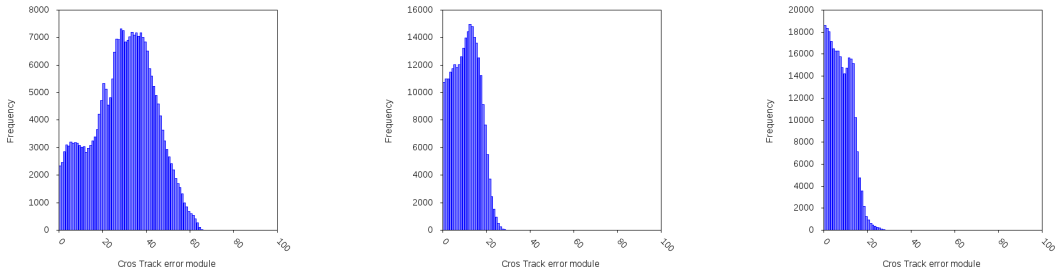

(a) UAV_t **(b)** UAV_l **(c)** UAV_v

Figure 7.23: e_{at} frequencies, Time Slot allocation B

Table 7.13 summarizes the basic statistics of the e_{at} module. UAV_t, UAV_l and UAV_v improves their positioning accuracies with respect the accuracy results of the

Table 7.13: e_{at} Statistics, Time Slot allocation B

	Trajectory		
Statistic	UAV_t	UAV_l	UAV_v
$\overline{e_{at}}$	29.93	10.70	7.93
$\sigma_{e_{at}}$	42.37	8.78	6.20
$CDF_{e_{at}}(95\%)$	103.71	21.48	15.17

Time Bias scenario (see table 7.10) in both $\overline{e_{at}}$ and $\sigma_{e_{at}}$ for the three trajectories. $\sigma_{e_{at}}$ is in line with the accuracy required by the Lincoln Laboratory and the e_{at} of the UAV_t, UAV_l and the UAV_v comply with the required by EUROCONTROL.

Using the Rayleigh CDF of equation C.12 for the Traffic, the required 95 % of accuracy is achieved at a value of 103.71 m, complying with the required by EUROCONTROL for the 3NM separation (330m).

Cross Track Error e_{ct} Figures 7.24b and 7.24c, show the e_{ct} of UAV_t, UAV_l and UAV_v in the tracking, which comply with accuracy performance required by the EUROCONTROL for 3NM separation (table 1.1).

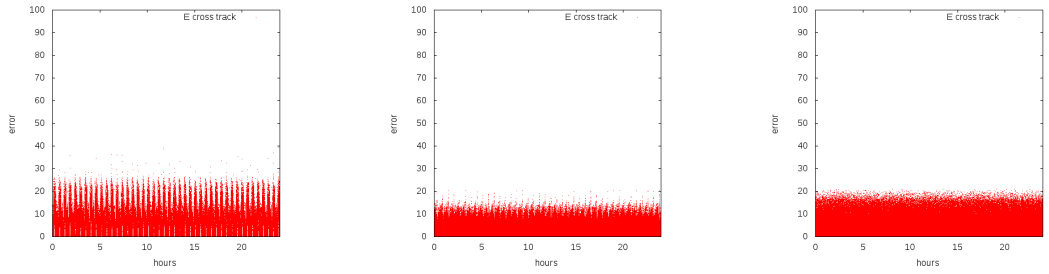

(a) UAV_t **(b)** UAV_l **(c)** UAV_v

Figure 7.24: e_{ct}, Time Slot allocation B

Figures 7.25a, 7.25b and 7.25c, show the e_{ct} frequencies, which have similar patterns that in the basic scenario with the values nearer to 0. This displacement to 0 reflects the improvement in the positioning.

Table 7.14 shows how the UAV_t, UAV_l and UAV_v comply with the Lincoln Laboratory requirement (table 1.2).

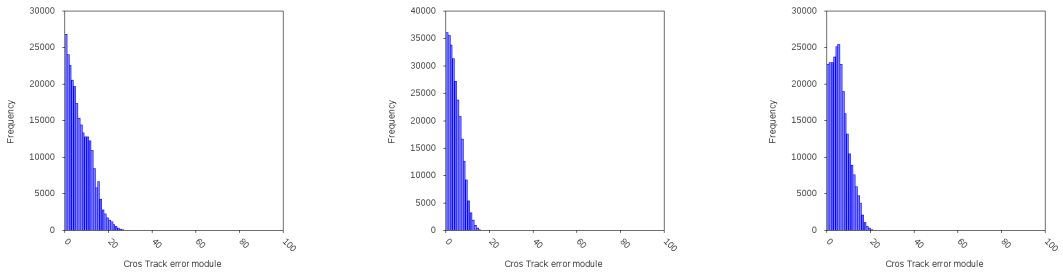

(a) UAV_t **(b)** UAV_l **(c)** UAV_v

Figure 7.25: e_{ct} frequencies, Time Slot allocation B

Table 7.14: e_{ct} Statistics, Time Slot allocation B

	Trajectory		
Statistic	UAV_t	UAV_l	UAV_v
$\overline{e_{ct}}$	7.04	4.29	6.07
$\sigma_{e_{ct}}$	21.25	3.03	4.49
$CDF_{e_{ct}}(95\%)$	52.02	7.41	11.00

For the accuracy requirements of EUROCONTROL in 3NM, UAV_t, UAV_l and UAV_v comply largely.

Comparing the values of $CDF_{e_{ct}}(95\%)$ and $CDF_{e_{at}}(95\%)$ trajectory by trajectory, it could be observed the improvement in the accuracy for the e_{ct}, which in fact is the most critical between e_{at} and e_{ct}. Comparing the values of accuracy of tables 7.11 and 7.14 there are not significant improvements in e_{ct}between Time Bias scenario and Time slot B scenario (which in fact is Time Bias with additional time slots). Nevertheless, considering as a set the e_{at} and e_{ct} there is a significant improvement in the accuracy.

Integrity Figures 7.26a, 7.26b and 7.26c, show the error against the protection level calculated by the Kalman Filter from the noise models.

The integrity values obtained are under the alarm thresholds of 3NM, presenting an aspect similar to the figures 7.21a, 7.21b and 7.21c of the Time Bias scenario.

Table 7.15 shows the compliance with the required separation of the different trajectories. As in table 7.12, all the trajectories comply with the 3NM separation.

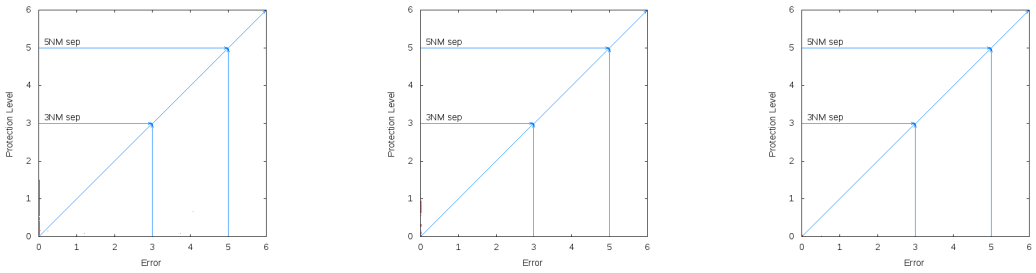

(a) UAV_t **(b)** UAV_l **(c)** UAV_v

Figure 7.26: Integrity Diagrams

Table 7.15: Integrity Alarm Values Compliance

	Trajectory		
Required Separation	UAV_t	UAV_l	UAV_v
5NM	1	1	1
3NM	1	1	1

My happiness consist in appreciate what I have
and do not desire excessively what I do not have.

Lev Nikolaievich Tolstoi 1818 - 1910

8 Discussion

This work presents PoCoLoCo, a methodology to use the high rate of UAS communications as a secondary means for both navigation and surveillance. The feasibility of using the C3 communications, between each air vehicle and its own ground station, as signal of opportunity for navigation and surveillance, has been tested in a reasonably future scenario. In this scenario three different UAS perform a different state or civil mission, with their own flight plan. Assuming flight works are performed concurrently in a same geographic area, most of their signals are visible to the others, allowing multilateration for positioning. The selected scenario is modest for the achieved result: More UAS or/and higher communication rates than the ones proposed will improve accuracy and integrity of the PoCoLoCo. Nevertheless, the results achieved with the selected scenario show enough accuracy and integrity to be used in RNP 1 navigation and in 3NM surveillance. These achievements are obtained using only the radio frequency spectrum that UAS require for their C3. The envisaged UAS communication signals were shared with the rest of the actors to obtain navigation and/or surveillance information, being a clear example of the potential behind the research in CNS integration

The message time of arrival in a TDMA network has been employed to measure the

distances between the receiver and the emitters. After enhancing these measures with information propagated through the network, a fault free solution has been obtained using an extended Kalman filter. Comparing the actual position in the simulation with the positioning solution offered by the EKF, the obtained error has an accuracy better than the 1 NM limit proposed by Eurocontrol for the stringent RNP spaces or the 3NM required by EUROCONTROL in surveillance.

The propagation of the clock bias calculated by each user has shown to be the most effective contribution to the error reduction in the positioning of the rest of users. This propagation becomes critical when referring to integrity values. The reduction of the variance associated to the measures conduces to a smaller protection level that complies with the requirements.

The simulation presented achieves the required values of integrity in RNP 1 in navigation with a reasonable distribution of a reduced number of GS over the territory. This integrity values are improved when additional measures are employed in the calculation, approaching the number and kind of measures to a more realistic scenario.

The positioning analysed for the UAS offers a navigation and surveillance services redundant with the conventional navigation and surveillance systems. The accuracies analysed are obtained from a reduced set of simulated UAS, but are not exclusive for UAS. The rest of users of the airspace could also obtain navigation positioning if they are able to listen the messages of the network i.e: they have access to the network and are synchronized. The rest of users could also be surveyed with the premise of participating actively in the network i.e: exchanging messages through the network with a similar periodicity.

Surveillance has been simulated with a more restricted scenario (pseudorange measured only from the GS) than in Navigation (pseudoranges measured from a mix of GS and UAV), resulting in poorer results. The pseudorange measurement from UAV to UAV in surveillance has been discarded as it increases necessarily the number of messages exchanged through the radio and increases the complexity of the datalink protocols and the positioning.

8.1 Future Works

The obtained results are interesting as they show a performance acceptable for both navigation and surveillance. Nevertheless, this results must be taken with precaution as they are at the initial stages of development.

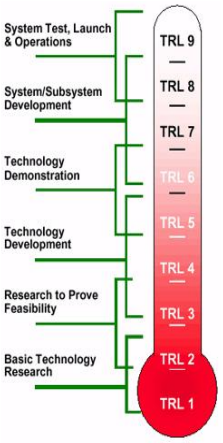

Figure 8.1: Technology Readiness Levels

Taking as reference the figure 8.1, we are proving partially the feasibility of the concept, i.e: TRL2 or TRL3. This concept could still be improved by different ways that should also be verified.

Once this feasibility has been proven, there is still a long way to travel since the TRL2 or TRL3 to the TRL9 which is achieved with the entry into service of the technology.

8.1.1 Technology Development

Future works should focus on more realistic environmental conditions, including simulation of multipath effects as well as the troposphere effect to adapt the known methods to the specificity of the relative navigation in contrast with the GPS. Regarding the estimation methodology, different alternatives to the EKF should be assessed, e.g:the family of Gaussian filters, who shows a better behaviour in front of non-linearities.

An interesting concern is the assessment of the effects on the final positioning that the endogamic reuse of the EKF computed navigation through the network could create.

The effect of employing less accurate positioning means at the rest of users (e.g: trilateration from multiple DME or positioning with DME and VOR) is an interesting point of study as it could be representative of the transition from the current navigation system.

the use of multiple directional antennae could improve the reception offering at the same time a measurement of azimuth in addition to the distance retrieved from the TOA. The azimuth additional information could ameliorate the geometry leading to a significant improvement in the integrity values, specially in scenarios with a small number of users.

Focusing on the evolution of the technological aspects, the localization analysed in this work is possible thanks to the synchronism of the different actors (air vehicles, ground stations...). The way this synchronization is achieved constitutes a really interesting field of research, including the use of CSAC, use of GNSS for synchronism, time protocols on the network... etc

The effect that the correlation accuracy has on the positioning could be important and it depends on the specific frequencies and antennae technologies employed. This effect should be assessed, using the frequencies allocated by the ITU to the control and command of the UAS, once such allocation occurs.

Taking into account the reduced computational requirements (the entire simulation, including data generation of one day and the subsequent navigation for the three UAS, takes less than 5 minutes in a small computer), the employ of the navigation algorithm in real time does not implies performances risks.

8.1.2 Readiness Improvement

Increasing the readiness of the technology since the TRL2 or TRL3, implies that the technology must be developed (TRL3, TRL4 and TRL5)and demonstrated (TRL5 and TRL6). This demonstration implies going beyond the simulations and its use in the real world.

The loquacity of the communications has a side effect in the separation of UAS. In one hand, the flight crew of a UAS is not longer on board, precluding the assumption of the Self Separation, and Collision avoidance(both cooperative and non-cooperative) by the human flight crew.

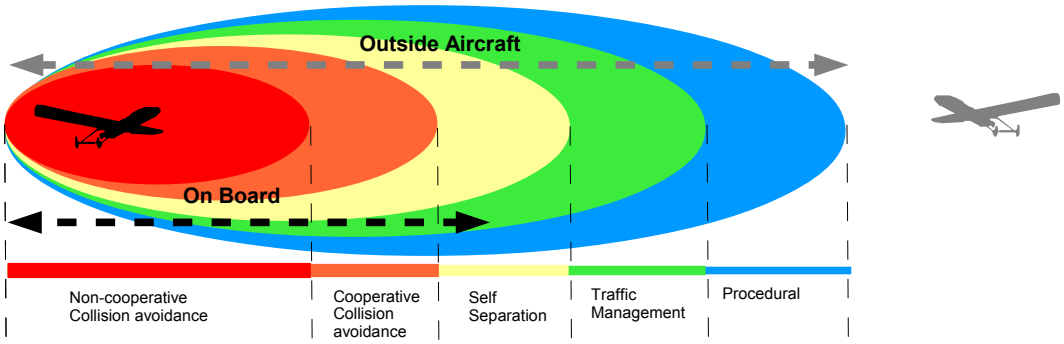

Figure 8.2: Separation and Collision Avoidance Mechanisms in UAS

In the other hand, the loquacity of the communications reduces the time between position updates increasing the quality of the situational awareness available. Reducing the time elapsed between position updates gives the chance to implement some separation and collision avoidance mechanism outside the aircraft, as presented by figure 8.2.

This flexibility could allow new distributions of the aircraft functions; the classical separation between Surveillance (which is performed outside the aircraft by the ANSP) and See & Avoid (which is performed on board by the flight crew) is no longer as rigid as presented in fig 2.12, allowing several distributions of the functionalities. Among the new distributions could be found the use of surveillance data for Sense & Avoid use.

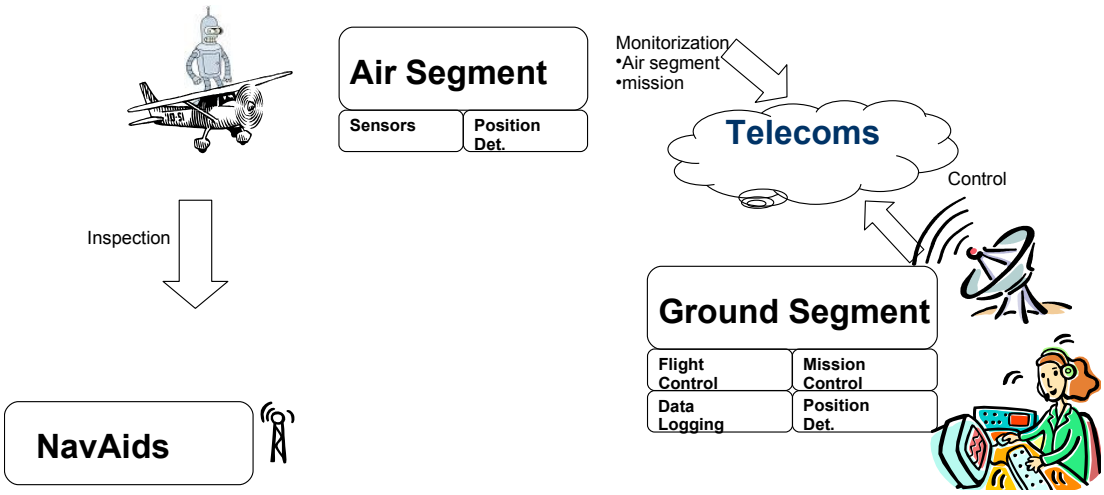

Figure 8.3: PoCo LoCo verification through flight inspection

Increasing the TRL of the concept will require to evolve from the current simulations

to perform actual flight tests. Figure 8.3 summarizes the required architecture required for performing flight inspections of Radio Navigation Aids or Radars using UAS instead of conventional aircraft. The feasibility of such architecture and operations has been already explored by ICARUS research group ((136), (137), (138), (139)) setting the foundations for an applied work in the future.

The localization offered by PoCoLoCo requires the measure of pseudoranges from different known positions. From a point of view of the deployed architecture, this could be achieved by using a monolithic network where all the participants are synchronized or it could also be obtained with pseudorange measures coming from different networks. The monolithic network seems to offers more quality guarantee whilst the option of the different networks seems to offer a bigger flexibility. This architecture differences offers an interesting field of research to adjust the final implementation to the required characteristics not only from the accuracy and integrity perspectives but also from the security point of view.

The scenario employed for the simulation assumes a constant presence of UAS during the 24h of a day. If PoCoLoCo must offer positioning services to the rest of users of the airspace the assumption of the number of UAS operations shall be revisited (even if the number of operations considered has been deliberately kept at a low number). Alternatives as the use of fixed ground infrastructure must be analysed with different levels of confidence on the pseudorange depending on the quality of the actor.

The interaction with the state aircraft must be taken into account. Security concerns could impose some restrictions on the propagation of the aircraft state position. A commercial implementation should deal with different levels of collaboration. The impact of these differences must be assessed at different levels, including the positioning solution as well as the message catalogue.

The relative positions of the GS and the different trajectories affects notably to the positioning accuracy. In a commercial implementation, positioning performance could be guaranteed by ensuring the presence of some actors in a perimetral distribution that benefits from a good geometry.

Appendices

God sometimes geometrizes.

Plato (427 bC - 347 bC)

A Linearization

Kalman filter could be seen as a solver methodology for systems of linear equations. In the case of estimating positions through the trilateration of distances this linearity is not fulfilled. Equation A.1 shows the euclidean distance in 2 dimensions, base of the problem and far from being linear.

$$d_i = \sqrt{x^2 + y^2} \tag{A.1}$$

Obtaining pseudorange measurements from different stations receiving a message from the surveyed aircraft, and applying equation A.1 results a system of equations with 2 variables (x, y) for each pseudorange obtained from ground stations as seen in A.2.

$$\begin{aligned} \rho_a &\simeq \sqrt{(x_a - x_t)^2 + (y_a - y_t)^2} \\ \rho_b &\simeq \sqrt{(x_b - x_t)^2 + (y_b - y_t)^2} \\ &\dots \\ \rho_n &\simeq \sqrt{(x_n - x_t)^2 + (y_n - y_t)^2} \end{aligned} \tag{A.2}$$

Those equations have the problematics of its lack of linearity. The complex resolution of such no linear equations makes preferable the use of linear approximations

that allows the use of simpler resolutions methods. One of the most commons ways for linearisation a function is the approximation to its behaviour around a point with the Taylor's theorem (equation A.3). Note the Multi index notation that simplifies the use of multiple variables in the same formula.

$$f_x = \sum_{|\alpha|=0}^{n} \frac{1}{\alpha!} \frac{\partial^\alpha f(a)}{\partial x^\alpha} (x-a)^\alpha + \sum_{|\alpha|=n+1} R_\alpha(x)(x-a)^\alpha \tag{A.3}$$

In our case, the approximation is kept to the first degree in order (equation A.4) to obtain a system of linear equations:

$$f_x \simeq f_{x_0} + \frac{df_{x_0}}{dx} \Delta x \tag{A.4}$$

the partial derivatives (equation A.4) of the euclidean distance formula A.1 results inA.5:

$$\frac{\partial D}{\partial x} \simeq \frac{1}{2} \left((x-x_a)^2 + (y-y_a)^2 \right)^{\frac{-1}{2}} 2\,(x-x_a) \rightarrow \frac{(x-x_a)}{\sqrt{(x-x_a)^2 + (y-y_a)^2}} \rightarrow \frac{(x-x_a)}{\rho_a} \tag{A.5}$$

and similarly for y A.5:

$$\frac{\partial D}{\partial y} \simeq \frac{(y-y_a)}{\rho_a} \tag{A.6}$$

In Figure A.1 could be observed the transformation performed with Taylor's theorem. The resulting function approaches the original one in a region with some differences (Δx and Δy). Coming back to the 2 dimensions the result of our linearization becomes A.7:

$$\rho_i \simeq \rho_{i_o} + \frac{(x-x_i)}{\rho_{i_o}} \Delta x + \frac{(y-y_i)}{\rho_{i_0}} \Delta y \tag{A.7}$$

where:

- ρ_i is a measurement of the distance obtained from our system.
- ρ_{i_0} is an estimation of the distance.
- $\frac{(x-x_i)}{\rho_{i_0}}$ and $\frac{(y-y_i)}{\rho_{i_0}}$ are components of the unitary vector from station to the track
- Δx and Δy are corrections to the estimated position required to convert them into the real position.

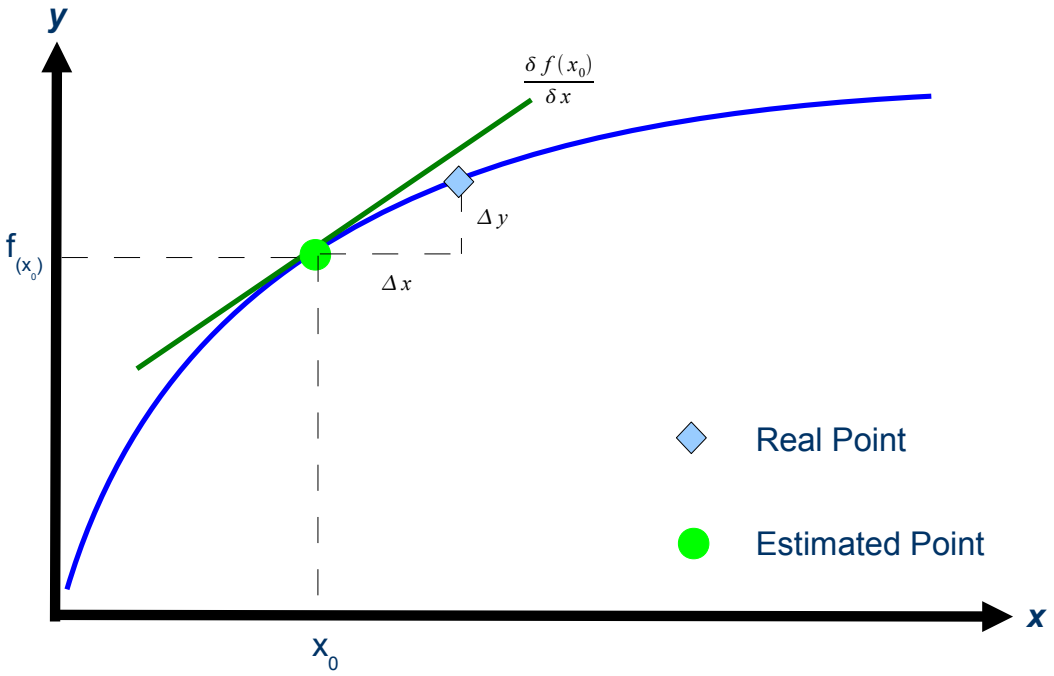

Figure A.1: Linearization scheme

Grouping ρ_i and ρ_{i_0} which are measurement and the estimation of the measurement results A.8:

$$\rho_i - \rho_{i_0} \simeq + \frac{(x - x_i)}{\rho_{i_0}} \Delta x + \frac{(y - y_i)}{\rho_{i_0}} \Delta y \tag{A.8}$$

Assuming this formulation for each pair station-track is obtained an overdimensioned system of linear equations that could be represented in matrix nomenclature A.9:

$$\begin{bmatrix} \rho_1 - \rho_{1_0} \\ \vdots \\ \rho_n - \rho_{n_0} \end{bmatrix} \simeq \begin{bmatrix} \frac{x_0 - x_1}{\rho_{1_0}} & \frac{y_0 - y_1}{\rho_{1_0}} \\ \vdots & \vdots \\ \frac{x_0 - x_n}{\rho_{n_0}} & \frac{y_0 - y_n}{\rho_{n_0}} \end{bmatrix} \begin{bmatrix} \Delta x \\ \Delta y \end{bmatrix} \tag{A.9}$$

$$Y \simeq H X$$

Where:

- Y is the matrix of differences between observed and predicted distances
- H is the geometry matrix who contains the unitary vector of the lines relying the stations with the track (see fig. A.2 for a geometric interpretation).
- X is the matrix containing the differences between estimated positions and real positions.

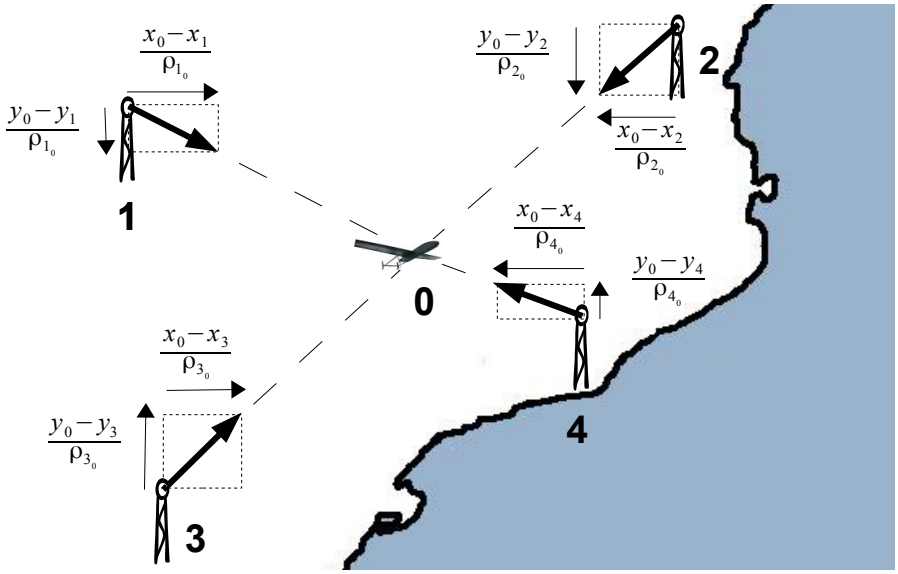

Figure A.2: Matrix H Geometric Interpretation

Which in fact is the opposite to what are we searching a function that provides an estimation of the position of the track using the measurements of the distances as input.

$$\begin{aligned} Y &= H\hat{X} \\ H^T Y &= H^T H\hat{X} \\ \left(H^T H\right)^{-1} H^T Y &= \left(H^T H\right)^{-1} H^T H\hat{X} \\ \left(H^T H\right)^{-1} H^T Y &= I\hat{X} \\ \hat{X} &= \left(H^T H\right)^{-1} H^T Y \end{aligned} \tag{A.10}$$

Equation A.10 allows the track position computation with linear numeric analysis techniques.

God sometimes aritmetizes.

C.G.J.Jacobi, (1804 1851)

B

Extended Kalman Filter

One classical approach for navigation with noisy sources is the use of Kalman filters for estimating the position reducing the error. The Kalman Filter was introduced in (140)

Kalman filter estimates the state of a system controlled in discrete time described equation B.1:

$$X_t = AX_{t-1} + Bu_t + w_{t-1} \tag{B.1}$$

where the current state X_t is obtained through the dynamic equation A from the previous state X_{t-1} plus a control signal u who modifies the state as represented by B and a noise w_{t-1} which is the error of the process. from this state equation it could be observed through an observation equation B.2:

$$Y_t = HX_t + v_t \tag{B.2}$$

where the observation vector Y_t is a function H of the state vector X_t plus a noise v_t from the measurement. Both process and measurement noises are assumed to be independents between them with a normal distribution of its probability B.3.

$$\begin{aligned} p(w) &\simeq N(0, Q) \\ p(v) &\simeq N(0, R) \end{aligned} \tag{B.3}$$

A kalman Filter is organized in two phases:

- Time update or Predict
- measurement update or correct

B.1 Time update or predict

The time update or predict phase uses the filter to provide a noiseless estimation of the state and is also composed by two equations: project the state ahead B.4:

$$\hat{x}_k^- = A\hat{x}_{k-1} + Bu_k \tag{B.4}$$

Where A is the transition Matrix of the difference equation, x the state vector, B is the input matrix and u the input control. Project the error covariance ahead B.5:

$$P_k^- = AP_{k-1}A^T + Q \tag{B.5}$$

Where P is the covariance matrix, A the transition matrix and Q is the covariance matrix of the noise introduced by u_k.

B.2 measurement update or correct

The phase of measurement update uses the data collected to actualize the kalman filter and is composed by 3 different equations: Compute the Kalman GainB.6:

$$K_k = P_k^- H^T \left(HP_k^- H^T + R\right)^{-1} \tag{B.6}$$

Where K is the Kalman filter gain and H is the matrix relating the state and the measurement, R is the covariance matrix of measurements.

Update estimate with measurement Z_k B.7

$$\hat{X}_k = \hat{X}_k^- + K_k \left(Z_k - H\hat{X}_k^-\right) \tag{B.7}$$

Update the error covariance B.8:

$$P_k = \left(I - K_k H\right) P_k^- \tag{B.8}$$

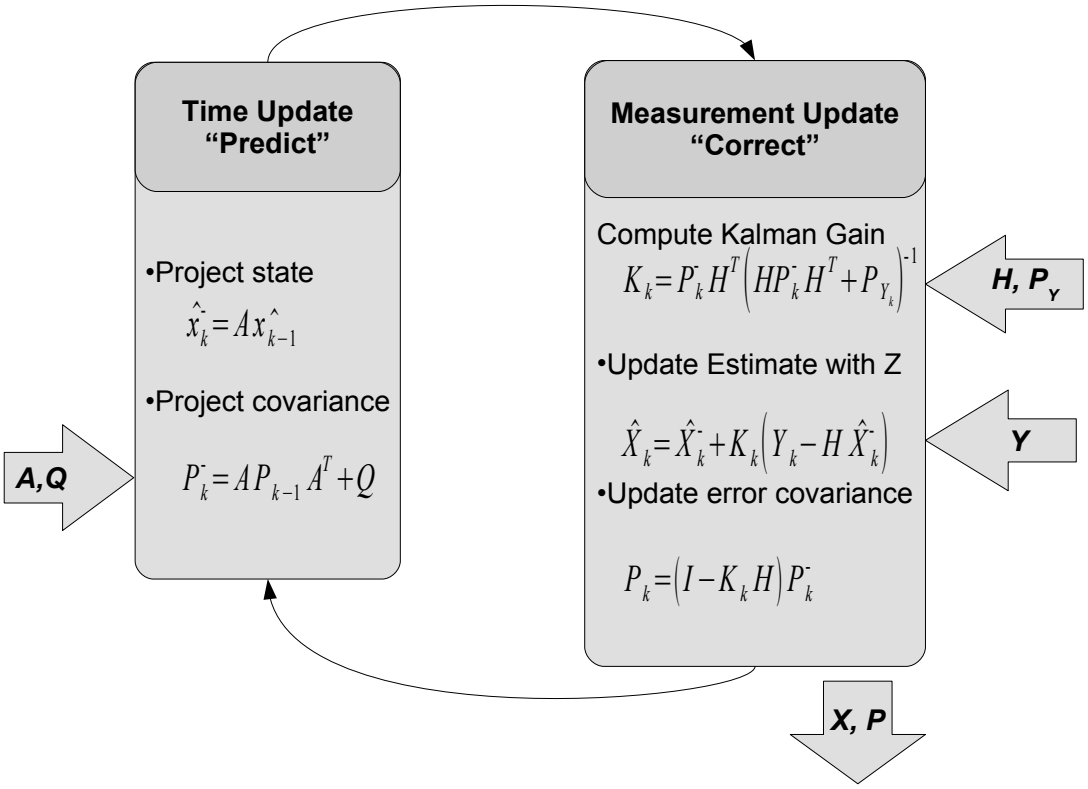

Figure B.1: Kalman Filter Structure

B.3 Kalman filter formulation

Let $Y(k)$, $H(k)$ and $X(k)$ be the vectors and matrix of equation (B.2) at sampling instant k and $\hat{X}(k)$ the best estimator for $X(k)$. A Kalman filtering consists to firstly predict the state vector of the next time sampling. For our application, we choose the following conventional model:

$$\begin{aligned} \hat{X}^-(k) &= A(k-1)\hat{X}(k-1) \\ P^-(k) &= A(k-1)P_{\hat{X}(k-1)}A^T(k-1) + Q(k-1) \end{aligned} \tag{B.9}$$

where the first equation depicts how the prediction of the states ($\hat{X}^-$) is done, by means of a transition matrix (A) which contains some information of the dynamics of the mobile. On the other hand, the second equation models the covariance matrix of this prediction in function of the covariance matrix of the states estimation ($P_{\hat{X}}$) and the process noise (Q). As a second step, an update of the state vector estimation ($\hat{X}$)

is performed by taking into account the previous estimation and a new set of observations (Y) with a measure covariance matrix of (P_Y). The Kalman filter minimises the weighted sum of the squares of the estimation errors, where the weights of each variable are given according to the inverse of the noise variance of the variable (141). Thus, the best estimation of $X(k)$ is given by:

$$\hat{X}(k) = \hat{X}^{-}(k) + K(k)\left[Y(k) - H(k)\hat{X}^{-}(k)\right]^{-1} \tag{B.10}$$

where the so called Kalman gain is written as:

$$K(k) = P^{-}(k)H^{T}(k)[H(k)P^{-}(k)H^{T}(k) + P_{Y(k)}]^{-1} \tag{B.11}$$

Finally, the covariance matrix of the last state vector estimation can be updated as

$$P_{\hat{X}(k)} = [I - K(k)H(k)]P^{-}(k) \tag{B.12}$$

and and the whole process is iteratively repeated by performing a new prediction.

For the sake of simplicity, the time dependency k will be dropped from the notation from now on, in the cases that a confusion is not possible. Figure B.1 summarizes the KF process where the estimation of the state vector and its associated covariance matrix is computed at each iteration of the filter in function of the measurements and the associated updates on the measurement noise and geometry (or measurement) matrix.

Statistics is the first of the inexact sciences.

Edmond de Goncourt(1822 1896)

C Statistical distributions

C.1 χ^2 Distribution

If $Z_1, ..., Z_k$. are independent, standard normal random variables, the sum of their squares,

$$Q = \sum_{i=0}^{k} Z_i^2 \tag{C.1}$$

is distributed according to the chi-squared (χ^2) distribution with k degrees of freedom. This is usually denoted as in eq. C.2, where the parameter k indicates the number of degrees of freedom (i.e: the number of independent variables which squares are being summed).

$$Q \sim \chi_k^2 \tag{C.2}$$

C.1.1 χ^2 Probability Density Function

The Probability Density Function (PDF) of the χ^2 distribution is defined by eq. C.3.

$$f(x;k) = \begin{cases} \frac{1}{2^{k/2}\Gamma(k/2)} x^{k/2-1} e^{-x/2}, & x \geq 0; \\ 0, & otherwise \end{cases} \tag{C.3}$$

where $\Gamma(k/2)$ denotes the Gamma function, which has closed-form values at the half integers

$$\Gamma(n) = \begin{cases} \Gamma(n+1) = n!, & n \in \mathbb{N}; \\ \Gamma\left(\frac{1}{2}n\right) = \sqrt{\pi}\frac{(n-2)!!}{2^{(n-1)/2}}, \end{cases} \tag{C.4}$$

Applying eq. C.4, to some significant numbers representing the must usual degrees of freedom in χ^2, the obtained Γ values are:

- k=1, $\Gamma(\frac{1}{2}) = \sqrt{\pi} \approx 1.7724538509055160273$
- k=2, $\Gamma(1) = 1$
- k=3, $\Gamma(\frac{1}{3}) = \frac{1}{2}\sqrt{\pi} \approx 0.8862269254527580137$
- k=4, $\Gamma(2) = 1$

C.1.2 χ^2 Cumulative Distribution Function

The Cumulative Distribution Function (CDF) of χ^2 is defined as:

$$F(x;k) = \frac{\gamma(k/2, x/2)}{\Gamma(k/2)} = P(k/2, x/2) \tag{C.5}$$

where $\gamma(k,z)$ is the lower incomplete Gamma function and $P(k,z)$ is the regularized Gamma function. For the special case of $k = 2$ the CDF of χ^2 has a simple form:

$$F(x;2) = 1 - e^{-\frac{x}{2}} \tag{C.6}$$

C.2 Rayleigh Distribution

The wide field of application of the χ^2 distribution, motivates the refinement into more specific distributions.

The combination of two variables is specially interesting in navigation as the problem could be formulated adapted to the existing cartography (e.g: Latitude and Longitude or North and East) but some magnitudes shall be observed as a combination of the selected magnitudes (e.g: cross track error or along the track error).

One continuous probability distribution very often observed when the overall magnitude of a vector depends on their 2 dimensions orthogonal components is the Rayleigh distribution.

C.2.1 Rayleigh Probability Density Function

The Probability Density Function (PDF) of the Rayleigh distribution is defined by eq. C.3.

$$f(x;\sigma) = \frac{x}{\sigma^2} e^{-x^2/2\sigma^2} \tag{C.7}$$

C.2.2 Rayleigh Cumulative Distribution Function

The Rayleigh Distribution has a CDF defined by equation C.8.

$$F(x) = 1 - e^{-x^2/2\sigma^2} \tag{C.8}$$

CDF has an intrinsic value in itself as it shows the statistical probability that a measure has as a maximum the value of x. Nevertheless, sometimes we must ensure that the value of the observed magnitude (x) should be under a determinate value with a determinate confidence percentage ($F(x)$) e.g: 95% of the time. Taking the CDF eq.C.8 and isolating x at the right we obtain eq. C.9

$$F(x) - 1 = -e^{-x^2/2\sigma^2} \Rightarrow 1 - F(x) = e^{-x^2/2\sigma^2} \Rightarrow \tag{C.9}$$

applying ln to eq. C.9 and simplifying eq. C.10 is obtained

$$\Rightarrow ln\left(1 - F(x)\right) = ln\left(e^{-x^2/2\sigma^2}\right) \Rightarrow ln\left(1 - F(x)\right) = -x^2/2\sigma^2 \tag{C.10}$$

multiplying eq. C.10 by $-2\sigma^2$ and simplifying results in eq. C.11

$$\Rightarrow ln\left(1 - F(x)\right) 2\sigma^2 = -x^2 \Rightarrow -ln\left(1 - F(x)\right) 2\sigma^2 = x^2 \tag{C.11}$$

making the $\sqrt{eq}$ eq. C.11 by $-2\sigma^2$ and simplifying finally results in eq. C.12

$$\Rightarrow x = \sqrt{-ln\left(1 - F(x)\right) 2\sigma^2} \Rightarrow x = \sqrt{-2ln\left(1 - F(x)\right)}\sigma \tag{C.12}$$

Once isolated the x, the confidence intervals could be calculated. Some interesting confidence intervals (values of $F(x)$) in aviation are:

- Accuracy $F(x) = 0.95$, reached for $x \approx 2,4477\sigma$
- Integrity $F(x) = 1 - 10^{-7}$, reached for $x \approx 5,6777\sigma$
- $F(x) = 1 - 10^{-9}$, reached for $x \approx 6,4379\sigma$

Distrust is the mother of safety.
Aristophanes (446 BC c. 386 BC)

D
Protection Level

To provide a confidence interval that guarantees the accuracy of the error should be taken into account that the error as defined by ICAO is not an aleatory variable but a combination of two (x, y). The combination of two aleatory variable normally distributed results in a Rayleigh distribution whose characteristics could be consulted in section C.2.

Figure D.1 provides a graphical interpretation of the content of Matrix P as retrieved from the Extended Kalman Filter. It provides a measure of the uncertainty in the estimation of the positioning. This estimation is obtained as a combination of the different measures covariances employed by the EKF.

These covariances have been obtaining by estimating the solution of minimum covariance and the covariance itself, reflects a weighted linear combination of the covariances of the measures. This linear combination does not reflects the geometry of the solution and the effect that the measure covariances could have with different geometries.

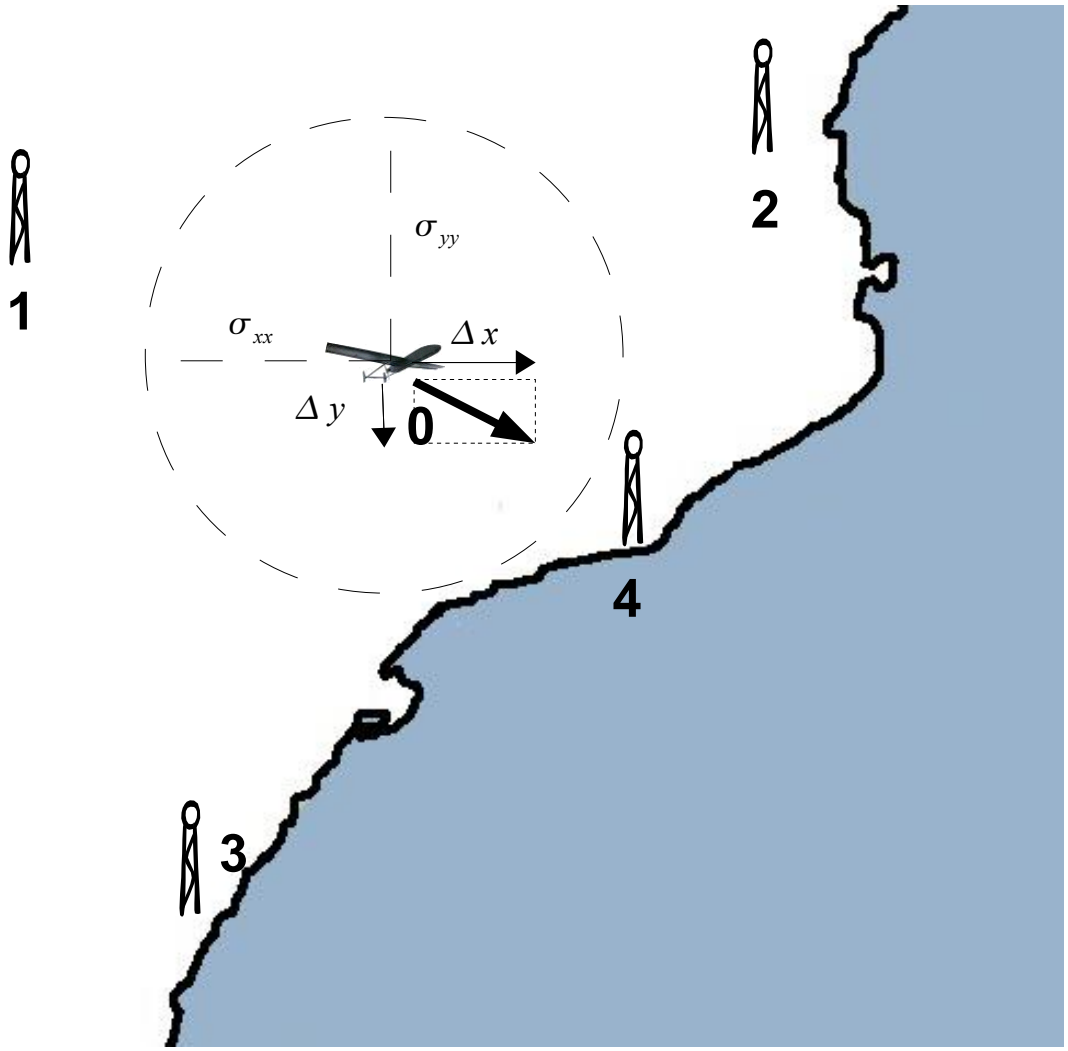

Figure D.1: Covariance Matrix P Geometric Interpretation

D.1 Dilution of Precision

This problem is also present in the GPS positioning where is used the concept of Dilution Of Precision (DOP) for better estimating the confidence that the positioning could give (see (123)). Considering that the different sources of error as independent, then can be root-sum-square to obtain a value for σ. This value is known in GPS as User Equivalent Range Error (UERE). Then the UERE to be applied for each measure of distance from a emitter i is the sum of all the covariances of individual source of

error (see eq. D.1)

$$\sigma_i^2 = \sigma_{clk_i}^2 + \sigma_{clk_r}^2 + \sigma_{v_i}^2 + \sigma_{v_r}^2 \tag{D.1}$$

Once defined the covariance for each measure as the square of the UERE, the calculation of the minimum covariance solution with the Kalman Filter requires a weights matrix as defined as in eq. D.2

$$W = \begin{bmatrix} 1/\sigma_1^2 & 0 & \dots & 0 \\ 0 & 1/\sigma_2^2 & \dots & 0 \\ \vdots & \vdots & \ddots & \vdots \\ 0 & 0 & \dots & 1/\sigma_n^2 \end{bmatrix} \tag{D.2}$$

The Covariances used in Matrix W belongs to the measures, but for estimating how these errors affects to the final positioning shall be employed the law of propagation of error as indicated in eq. D.3.

$$\left(H^T \cdot W \cdot H\right)^{-1} = \begin{bmatrix} d_{east}^2 & d_{en} & d_{eu} & d_{et} \\ d_{en} & d_{north}^2 & d_{nu} & d_{nt} \\ d_{eu} & d_{nu} & d_{up}^2 & d_{ut} \\ d_{et} & d_{nt} & d_{ut} & d_{time}^2 \end{bmatrix} \tag{D.3}$$

$$HDOP = \sqrt{d_{east}^2 + d_{north}^2} \tag{D.4}$$

$$VDOP = \sqrt{d_{up}^2} \tag{D.5}$$

D.1.1 Vertical Dilution of Precision

To take advantage of higher locations for Receiver stations, the optimal solution is to locate them far enough to distribute its uncertainty parallel to the flight, which occurs when the high location is at an infinite distance.

Fig. D.2 shows the geometry of the high elevation locations for receiver stations. For an infinite value of h, the a becomes 0 and the uncertainty of its measure is propagated over the horizontal plane. Diminishing h, the a increases at the same time that the uncertainty component on the vertical axe increases. In the other hand a equals to 0, for an infinite value of d, the vertical uncertainty becomes a wall from the ground to the sky.

Fig. D.3 shows the effect of having Rx stations located at hight, but below the optimal elevation. Being the Receiver station aligned with the altitude of flight, the

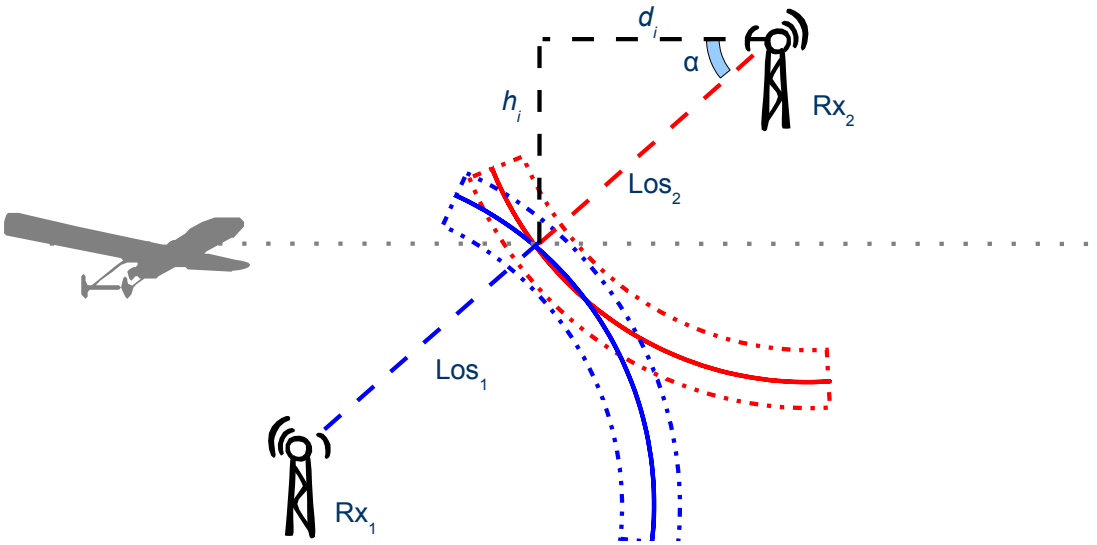

Figure D.2: Optimal High elevations Rx Geometry

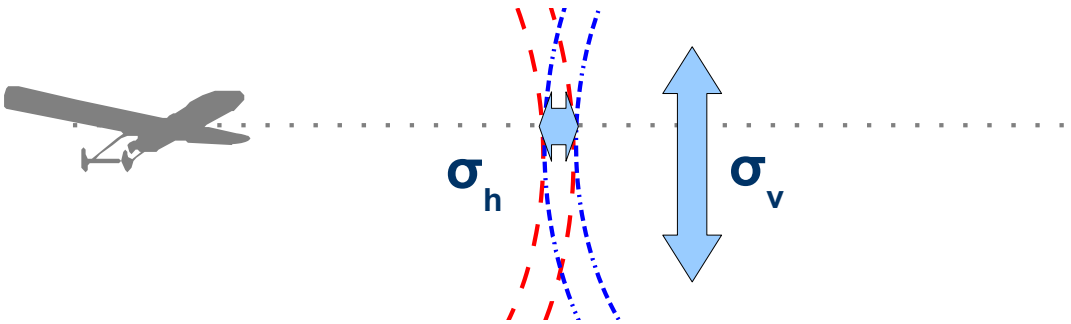

Figure D.3: Uncertainties with Rx at high locations

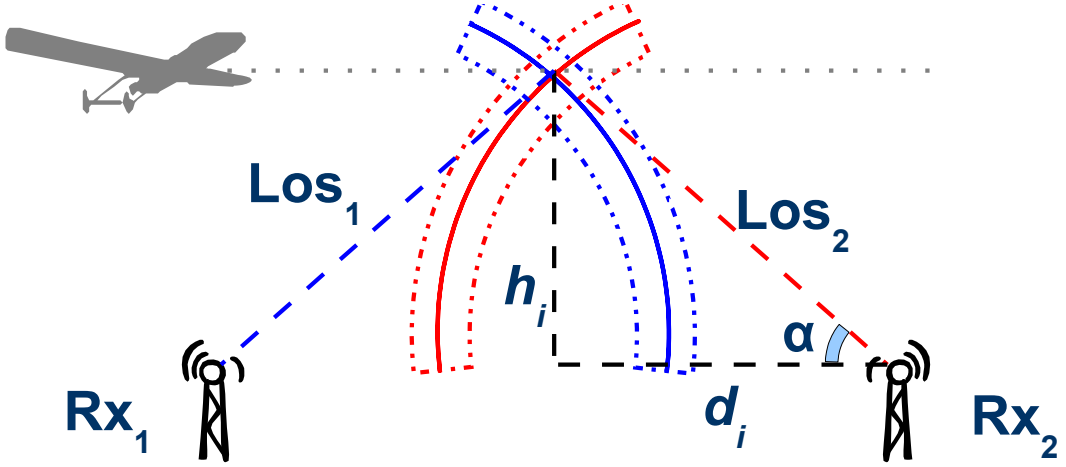

Figure D.4: Elevated Rx reduction of Radius

uncertainties areas becomes more and more vertical increasing the uncertainty in the vertical axe without improving the measurement in the horizontal plane.

The reason behind this displacement on the target altitude is that the system is envisaged for detecting helicopters flying under the approved flight altitude and therefore, the error must be contained at the flight altitude of the offender helicopters.

The proposed geometry condition the location of the Receiver stations. Fig. D.5 shows the geometry of the worst geometry for measuring the z component, just in the middle of two Rx stations.

Approaching any of the Rx Stations produces an uncertainty area more and more horizontal that compensates the uncertainty area produced by the reception of the signal in the farest Rx station that becomes progressively more and more vertical. At this point the Line of Sight of Rx1 and Rx2 must be at an angle of 90. As the height of the intersection between lines of Sight and the trajectories (hi) is known and the angle of the line of Sight with the horizontal plane could be calculated to be 45, the distance between the Rx and the projection of the intersection point over the horizontal plane becomes as indicated in D.6

Fig. D.5 shows the effect over the distance between the vertical projection of the air vehicle and the receiver stations of elevating the receiver station location keeping the alpha value constant. For an alpha value of 45 each additional meter in the elevation of the receiver must be compensated by approaching 1meter the receiver to the intersection

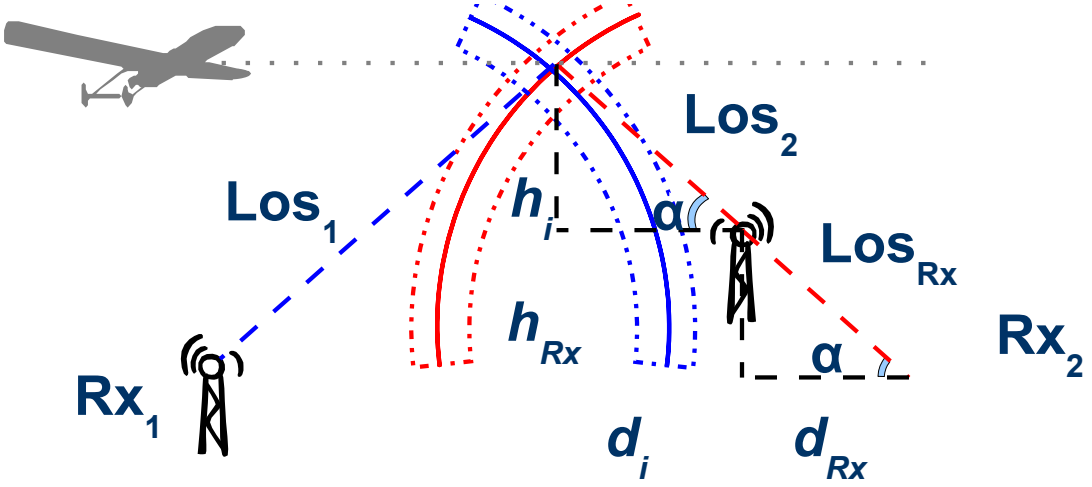

Figure D.5: Optimal Separation of Rx Stations

point.

$$d_i = \frac{h_i}{tan(\alpha)} \tag{D.6}$$

With the formulation of the distance between receiver station and intersection point expressed in Fig. D.5, the separation between receiver stations at MSL correspond with the target flight altitude multiplied by 2 for an alpha value of 45. Accepting alpha values of 30, the reduction of the separation could be limited .

The convenience or not of increasing the number of stations (and its associated cost) to achieve the increment is a client decision, but seems difficult to justify such an increment in the cost for a so small improvement in the accuracy.

D.2 Adequation to ICAOs error definitions

Eq. D.3 gives at the diagonal the covariances at each component (east and north in 2D) and the correlation outside the diagonal. This is interesting when the magnitude observed is expressed in the same reference frame but the ICAO defined navigation errors (see at section E) are defined with a trajectory based frame instead of a geographical frame. To adequate the protection level to the error definitions of ICAO, it is applied the Principal Component Analysis (PCA) to find the direction of maximum variance. After applying PCA to the covariance Matrix defined in eq.D.3, the direction with the

biggest value has a σ defined as in eq.D.7.

$$d_{major} = \sqrt{\frac{d_{east}^2 + d_{north}^2}{2} + \sqrt{\left(\frac{d_{east}^2 - d_{north}^2}{2}\right)^2 + d_{en}^2}} \tag{D.7}$$

Once computed the applicable σ in eq. D.7, the horizontal protection level could be easily computed (see eq. D.8) by multiplying the d_{major} by a constant K to obtain the desired percentage. This constant value K is obtained from the Rayleigh CDF (see eq. C.12) for the different percentages desired:

- $K \approx 2,4477$ for a confidence interval of 95%
- $K \approx 5,6777$ for a confidence interval of $1 - 10^{-7}$.
- $K \approx 6,4379$ for a confidence interval of $1 - 10^{-9}$.

$$HPL = K \cdot d_{major} \tag{D.8}$$

Shall be kept in mind that the HPL calculated in eq.D.8 represents an upper bound for the σ of the positioning error as the considered error depends on the direction of the trajectory (e_{ct} and e_{at}) whilst the estimated HPL depends on the geometry of the different measures employed.

The expected placement of the network users in a very narrow interval of vertical positions in relation with the larger horizontal positions makes unrealistic the calculation of a Vertical Protection Level (VPL) unless for very limited scenarios as landing or Take Off. Consequently, Vertical Dilution of Precision (VDOP) is not further developed in this section.

Everything approaches everything,
with more or less error.

Anonymous

E

ICAO Positioning Errors

Whilst the intuition could drive to consider the euclidean distance as the appropriated method for calculating the error between the actual position of the aircraft and the calculated navigation position of the aircraft, the characteristics of the air traffic drive to a different methodology.

Figure E.1 shows the relation between the ICAO defined trajectory errors and the Euclidean distance. Euclidean Distance ($d_{euclidean}$) weights equally the longitudinal error along the trajectory with the lateral error besides the trajectory and even with the vertical error. Whilst the error along the trajectory (e_{at}) could be assimilated in the real world with delays in the time of arrival or with advancements (not so often as the other case), the lateral error (e_{ct}) could be assimilated with an abandonment of the trajectory and the vertical error could be assimilated to a flight level invasion. In both lateral and vertical errors considerations that could lead to accidents.

This different risk associated to the different errors is reflected in the methodology employed by ICAO in its Performance Based Navigation Manual (47) where the error considered for the lateral error is the minimum distance from the actual point A to the trajectory T.

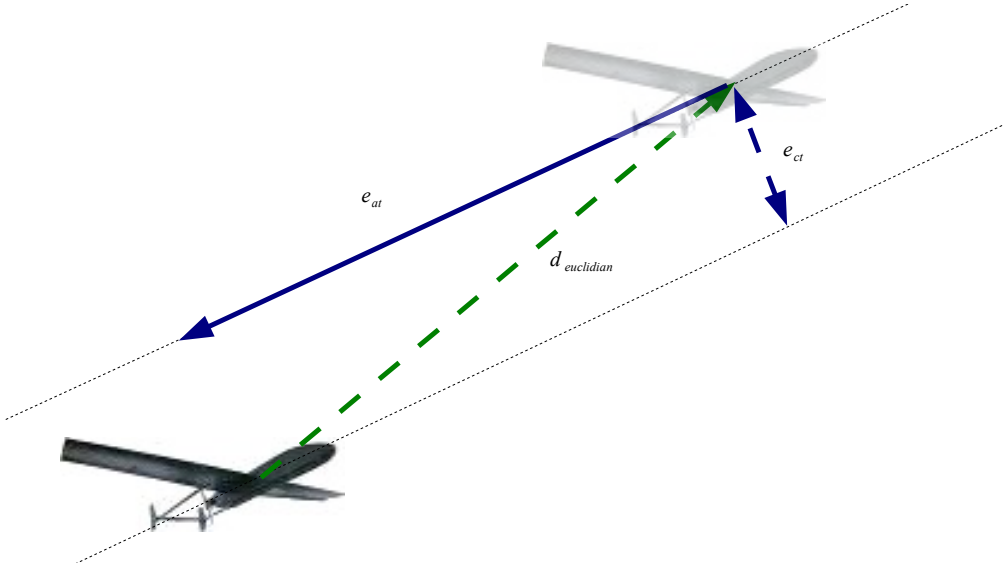

Figure E.1: ICAO defined trajectory errors

E.1 Distance from a Point to a line

For a straight trajectory T expressed as in eq. E.1 the distance from the actual position could be calculated applying eq. E.2.

$$a \cdot x + b \cdot y + c = 0 \tag{E.1}$$

$$d(A,T) = \frac{|a \cdot x + b \cdot y + c|}{\sqrt{a^2 + b^2}} \tag{E.2}$$

With a line expressed with a reduced formulation (see eq.E.3), the equation to be applied for the calculation of the distance between point and the trajectory could be simplified as in eq. E.4.

$$y = a \cdot x + b \tag{E.3}$$

$$d(A,T) = \frac{|a \cdot x_A - y_A + b|}{\sqrt{a^2 + 1}} \tag{E.4}$$

The slope of a stright line could be calculated from two points of the line with the eq. E.5.

$$m = \frac{y_2 - y_1}{x_2 - x_1} \tag{E.5}$$

An alternative method to obtain the slope of the straight line is using the director vector (v_x, v_y) as presented in eq. E.6 instead of two different points. This option is specially interesting for simulations where the flight attitude is available as it could be performed without maintaining a log of the positions.

$$m = \frac{v_y}{v_x} \tag{E.6}$$

Once calculated the slope of the line (with eq. E.5 or eq. E.6), the equation of a line containing a point (x_1, y_1) could be retrieved applying eq. E.7.

$$y - y_1 = m(x - x_1) \tag{E.7}$$

E.2 Vector equations

Another way to formalise the trajectory of the aircraft is employing the vectorial form of the straight line. The equ. E.8 show the Vectorial form of a straight line equation. It is composed by a parameter λ that multiplies a vector $\vec{V}$ that provides the direction of the line and a point P_0 contained in the line.

$$P = \lambda\vec{V} + P_0 \tag{E.8}$$

This vectorial form has the advantage of using directly magnitudes available on the simulation. The attitude of the aircraft could be employed for the vector $\vec{V}$ as well as the position is available for point P_0.

$$\vec{V_1} = \begin{pmatrix} v_{x_1} \\ v_{y_1} \end{pmatrix} \vec{V_2} = \begin{pmatrix} -v_{y_1} \\ v_{x_1} \end{pmatrix} \tag{E.9}$$

A simple method to obtain two orthogonal lines equations is to develop from to orthogonal vectors. Eq. E.9 show a simple method to obtain a orthogonal vector to another in the plane, changing the component and the sign of one of them.

The definition of Cross track error (see eq E.10) by ICAO consider the minimum distance from the simulated point to the trajectory T. This minimum distance between a point and a line is the distance between the estimated point P_e and the intersection point P_i between the trajectory and a orthogonal line that contains the estimated position.

$$e_{ct} = d(P_e, T) = d(P_e, P_i) \tag{E.10}$$

The definition of Along the Track error by ICAO (see eq E.11) is the distance between P_i and the actual position on the trajectory P_a.

$$e_{at} = d(P_a, P_i) \tag{E.11}$$

P_i could be calculated by a system of lineal equations (see eq. E.12)representing the trajectory of the aircraft and a orthogonal line.

$$e_{at} = d(P_a, P_i) \tag{E.12}$$

$$\begin{cases} P_i = \lambda_a \overrightarrow{V_T} + P_a \\ P_i = \lambda_e \overrightarrow{V} + P_e \end{cases} \quad \left\{ \lambda_a \overrightarrow{V_T} + P_a = \lambda_e \overrightarrow{V} + P_e \right. \tag{E.13}$$

$$\left\{ \lambda_a \begin{pmatrix} V_{T_x} \\ V_{T_y} \end{pmatrix} + \begin{pmatrix} P_{a_x} \\ P_{a_y} \end{pmatrix} = \lambda_e \begin{pmatrix} V_x \\ V_y \end{pmatrix} + \begin{pmatrix} P_{e_x} \\ P_{e_y} \end{pmatrix} \right. \tag{E.14}$$

Applying eq. E.9 to eq. E.14 results in eq.E.15

$$\left\{ \lambda_a \begin{pmatrix} V_{T_x} \\ V_{T_y} \end{pmatrix} + \begin{pmatrix} P_{a_x} \\ P_{a_y} \end{pmatrix} = \lambda_e \begin{pmatrix} -V_{T_y} \\ V_{T_x} \end{pmatrix} + \begin{pmatrix} P_{e_x} \\ P_{e_y} \end{pmatrix} \right. \tag{E.15}$$

$$\begin{cases} \lambda_a V_{T_x} + P_{a_x} = \lambda_e - V_{T_y} + P_{e_x} \\ \lambda_a V_{T_y} + P_{a_y} = \lambda_e V_{T_x} + P_{e_y} \end{cases} \quad \begin{cases} \lambda_a V_{T_x} + P_{a_x} = -\lambda_e V_{T_y} + P_{e_x} \\ \lambda_a V_{T_y} + P_{a_y} = \lambda_e V_{T_x} + P_{e_y} \end{cases} \tag{E.16}$$

$$\begin{cases} \frac{V_{T_x}}{V_{T_y}} \left(\lambda_a V_{T_x} + P_{a_x} \right) = \frac{V_{T_x}}{V_{T_y}} \left(-\lambda_e V_{T_y} + P_{e_x} \right) \\ \lambda_a V_{T_y} + P_{a_y} = \lambda_e V_{T_x} + P_{e_y} \end{cases} \tag{E.17}$$

$$\begin{cases} \lambda_a \frac{V_{T_x}^2}{V_{T_y}} + P_{a_x} \frac{V_{T_x}}{V_{T_y}} = -\lambda_e V_{T_x} + P_{e_x} \frac{V_{T_x}}{V_{T_y}} \\ \lambda_a V_{T_y} + P_{a_y} = \lambda_e V_{T_x} + P_{e_y} \end{cases} \tag{E.18}$$

$$\left\{ \lambda_a \frac{V_{T_x}^2}{V_{T_y}} + P_{a_x} \frac{V_{T_x}}{V_{T_y}} + \lambda_a V_{T_y} + P_{a_y} = P_{e_x} \frac{V_{T_x}}{V_{T_y}} + P_{e_y} \right. \tag{E.19}$$

$$\left\{ \lambda_a \frac{V_{T_x}^2}{V_{T_y}} + \lambda_a V_{T_y} = P_{e_x} \frac{V_{T_x}}{V_{T_y}} - P_{a_x} \frac{V_{T_x}}{V_{T_y}} + P_{e_y} - P_{a_y} \right. \tag{E.20}$$

$$\left\{ \lambda_a \left(\frac{V_{T_x}^2}{V_{T_y}} + V_{T_y} \right) = \frac{V_{T_x}}{V_{T_y}} \left(P_{e_x} - P_{a_x} \right) + P_{e_y} - P_{a_y} \right. \tag{E.21}$$

$$\left\{ \lambda_a \frac{V_{T_x}^2 + V_{T_y}^2}{V_{T_y}} = \frac{V_{T_x}}{V_{T_y}} \left(P_{e_x} - P_{a_x} \right) + P_{e_y} - P_{a_y} \right. \tag{E.22}$$

$$\left\{ \lambda_a = \frac{V_{T_y}}{V_{T_x}^2 + V_{T_y}^2} \left(\frac{V_{T_x}}{V_{T_y}} \left(P_{e_x} - P_{a_x} \right) + P_{e_y} - P_{a_y} \right) \right. \tag{E.23}$$

$$\left\{ \lambda_a = \frac{V_{T_x} \left(P_{e_x} - P_{a_x} \right)}{V_{T_x}^2 + V_{T_y}^2} + P_{e_y} \frac{V_{T_y}}{V_{T_x}^2 + V_{T_y}^2} - P_{a_y} \frac{V_{T_y}}{V_{T_x}^2 + V_{T_y}^2} \right. \tag{E.24}$$

$$\left\{ \lambda_a = \frac{V_{T_x} \left(P_{e_x} - P_{a_x} \right)}{V_{T_x}^2 + V_{T_y}^2} + \frac{V_{T_y} \left(P_{e_y} - P_{a_y} \right)}{V_{T_x}^2 + V_{T_y}^2} \right. \tag{E.25}$$

$$\left\{ \lambda_a = \frac{V_{T_x} \left(P_{e_x} - P_{a_x} \right) + V_{T_y} \left(P_{e_y} - P_{a_y} \right)}{V_{T_x}^2 + V_{T_y}^2} \right. \tag{E.26}$$

$$V_{T_x} \approx 0 \left\{ \begin{array}{rcl} P_{a_x} & = & -\lambda_e V_{T_y} + P_{e_x} \\ \lambda_a V_{T_y} + P_{a_y} & = & +P_{e_y} \end{array} \right. \left\{ \begin{array}{rcl} \lambda_e & = & \frac{P_{a_x} - P_{e_x}}{-V_{T_y}} \\ \lambda_a & = & \frac{P_{e_y} - P_{a_y}}{V_{T_y}} \end{array} \right. \tag{E.27}$$

$$V_{T_y} \approx 0 \left\{ \begin{array}{rcl} \lambda_a V_{T_x} + P_{a_x} & = & P_{e_x} \\ P_{a_y} & = & \lambda_e V_{T_x} + P_{e_y} \end{array} \right. \left\{ \begin{array}{rcl} \lambda_a & = & \frac{P_{e_x} - P_{a_x}}{V_{T_x}} \\ \lambda_e & = & \frac{P_{a_y} - P_{e_y}}{V_{T_x}} \end{array} \right. \tag{E.28}$$

It was the best of times,
it was the worst of times.

Charles Dickens, (1812 1870)

Sorry officer,
you mean before in time or in space?

Airbag, Spanish movie (1997)

F

Clock Model

The Range measuring assumed for the relative navigation (see chapter 6) and surveillance (see chapter 7) are based on the synchronization of the clocks of the different users. The different mechanism to achieve this synchronization are not part of this PhD assuming as valid the synchronization values of the literature.

The achievable synchronization has some limits that affect the positioning solution, no matter if it is a surveillance or a navigation performance, the range measurement will have an error as explained in section 4.4.1.1. This measuring error could be increased at the positioning solution by the effect of the DoP as explained in section D.1.

A realistic assessment of the positioning solution requires then the to modelling of the behaviour of the clock onboard the different users. Being the time measuring a complex discipline, the requirements set for a clock model are quite reduced when considering the error in synchronism as the observed magnitude, which is the main magnitude when using the clock for range measuring. Figure F.1 shows the model simulated to achieve realistic values of the synchronism error using a reduced set of parameters:

- Clock Accuracy C_{Ac}

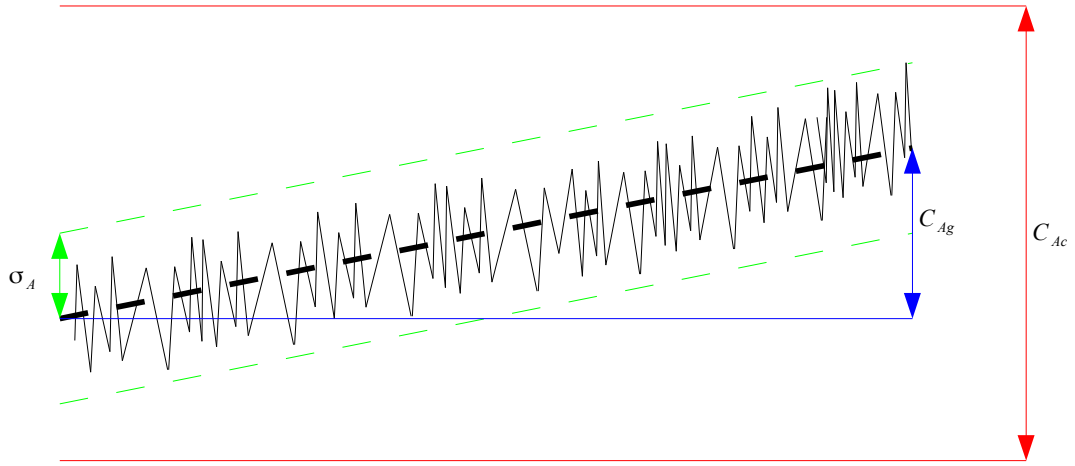

Figure F.1: Simulated Clock Model

- Aging C_{Ag}
- Allan deviation σ_A

The Clock accuracy is assumed as the deviation from the expected value.I.e: the deviation with respect to the common clock, which in the case of the simulations is the GPS clock. This magnitude is offered as the RMS of the values. It is simulated as a gaussian value of 0 mean and RMS Value of 100ns assigned to each clock at the init of the simulation.

The Aging of the clock is the trend to be delayed or advanced. Usually is offered in $ns/24h$, but for the case of high accuracy atomic clocks is often offered as the number of billion years required to be delayed one second. It is simulated as a factor multiplying the current time, the result is added to the Initial accuracy value.

The Allan deviation of the time is a measure of the stability in the time measuring. It represents the deviation between two measures in a time period. It is the square root of the Allan Variance which is also offered as measure of stability. It is simulated as a gaussian value of 0 mean and using the Allan Variance as the Standard deviation.

Then Synchronism error is simulated as expressed by eq F.1:

$$\varepsilon_{synch} = C_{Ac} + C_{Ag} + \sigma_A \tag{F.1}$$

Bibliography

[1] Society of Automotive Engineers. **CERTIFICATION CONSIDERATIONS OR HIGHLY-INTEGRATED OR COMPLEX AIRCRAFT SYSTEMS**. Technical report, 400 Commonwealth Drive, Warrendale, PA 15096-0001, November 1996. ix, 2, 3, 4, 33, 37, 38

[2] **United States Frequency Allocations; the radio spectrum**. Technical report, U.S. Department of Commerce; National Telecommunications and Information Administration; Office of Spectrum Management, October 2003. Available at: http://www.ntia.doc.gov/osmhome/allochrt.pdf. ix, 19

[3] Eduardo Morere Molinero. **Single European Sky: Regulatory Context**, May 2009. 1

[4] **European Aviation Safety Agency - easa.europa.eu**. http://www.easa.europa.eu/ws_prod/index.html. 1, 5

[5] **FAA: Home**. http://www.faa.gov/. 1

[6] Frederic Copigneaux. **EASA and ATM: the way forward**. In *Proceedings of the 2008 International Symposium on Precision Approach and Performance Based Navigation- ISPA 2008*, Bonn, Germany, October 2009. Deutsche Gesellschaft fr Ortung und Navigation. 1

[7] **AMC and GM to Part 21**, October 2003. Available at: http://www.easa.europa.eu/ws_prod/g/doc/Agency_Mesures/Certification_Spec/decision_ED_2003_01_RM.pdf. 1

[8] Mike Russo. **Start with Standards**. In *Proceedings of the 2008 Integrated Communications, Navigation and Surveillance Conference*, Bethesda, MD, USA, May 2008. www.arinc.com. 1

[9] Bill Hershey. **Standardization and Regulation for CNS/ATM Avionics**. In *Proceedings of the 2008 Integrated Communications, Navigation and Surveillance Conference*, Bethesda, MD, USA, May 2008. Available at: http://i-cns.org/media/2008/05/presentations/Session_L_Avionics_Integration_and_Aircraft_Systems/02-Hershey.pdf. 1

[10] David Alexander. **SAE and EUROCAE**. In *The Power Of Standards For New Trajectory Concepts, EUROCAE Annual Symposium*, Dubrovnik, Croatia, May 2009. 1, 2

[11] Donal Ward. **Next Gen Where Are Going and Our Need for Standards**. In *The Power Of Standards For New Trajectory Concepts, EUROCAE Annual Symposium*, Dubrovnik, Croatia, May 2009. 2

[12] Marvin Rausand and Ingrid Bouwer Utne. **Product safety Principles and practices in a life cycle perspective**. *Safety Science*, **47**(7):939 – 947, 2009. 2

[13] EASA. *Certification Specifications for European Technical Standard Orders*, **CS-ETSO amendment 6**. EASA, European Aviation Safety Agency, Ottoplatz, 1 D-50679 Koeln, Germany, October 2010. 2

[14] Society of Automotive Engineers. **GUIDELINES AND METHODS FOR CONDUCTING THE SAFETY ASSESSMENT PROCESS ON CIVIL AIRBORNE SYSTEMS AND EQUIPMENT**. Technical report, 400 Commonwealth Drive, Warrendale, PA 15096-0001, December 1996. 3

[15] Ron van de Leijgraaf. **EUROCAE WG73 SG4 Update on progress SG4: Light UAS in VLOS operation**. In *UAS 2009 Conference Proceedings*, La plaine Saint Denis, Paris, France, June 2009. Blyenburg & Co. 3, 31

[16] Kelly J. Hayhurst, Jeffrey M. Maddalon, Paul S. Miner, George N. Szatkowski, Michael L. Ulrey, Michael P. DeWalt, and Cary R. Spitzer. **Preliminary Considerations for Classifying Hazards of Unmanned Aircraft Systems**. Technical report, NASA, Langley Research Center. Hampton, Virginia (USA), Feb 2007. NASA/TM-2007-214539. 3, 38

[17] **SESAR Release 2013**. Technical report, SESAR Joint Undertaking, Avenue de Cortenbergh 100, B-1000 Brussels, 2013. 5, 10

[18] **European ATM Master Plan**. Technical report, SESAR Joint Undertaking, Avenue de Cortenbergh 100, B-1000 Brussels, October 2012. 5

[19] Office of NextGen. **NextGen Implementation Plan**. Technical report, Federal Aviation Administration, Office of NextGen, 800 Independence Avenue, SW, Washington, DC 20591, June 2013. nextgen@fa.gov. 5, 10

[20] Official Journal of the European Union. **Single European Sky 549/ 2004 The framework Regulation**, March 2004. Available at: http://www.eurocontrol.int/ses/gallery/content/public/docs/pdf/ses/eudocuments/framework_regulation.pdf. 5

[21] Official Journal of the European Union. **Single European Sky 550/ 2004 service provision**, March 2004. Available at: http://www.eurocontrol.int/ses/gallery/content/public/docs/pdf/ses/eudocuments/service_provision.pdf. 5

[22] Official Journal of the European Union. **Single European Sky 551/2004 Airspace regulation**, March 2004. Available at: http://ec.europa.eu/transport/air/single_european_sky/implementing_rules_en.htm. 5

[23] Official Journal of the European Union. **Single European Sky 552/2004 Interoperability**, March 2004. Available at: http://ec.europa.eu/transport/air/single_european_sky/implementing_rules_en.htm. 5

[24] EASA. **Extension of the EASA system to the regulation of Air Traffic Management and Air Navigation Services (ATM/ANS)**, November 2007. 5

[25] Brian Kendal. **The Beginnings of Air Radio Navigation and Communication**. *The Journal of Navigation*, **64**(01):157–167, 2011. 6

BIBLIOGRAPHY

[26] AENA. **Procedimientos operativos para verificacin en vuelo de ayudas del S.N.A.** Technical report, DIVISIN DE INFRAESTRUCTURAS CNS/ATM, June 2008. Procedimientos Operativos para Calibraciones en Vuelo de Ayudas del S.N.A. ; Departamento de Normativa y Evaluacin. 6

[27] **United States Standard Flight Inspection Manual**. Technical report, DEPARTMENTS OF THE ARMY, THE NAVY, AND THE AIR FORCE AND THE FEDERAL AVIATION ADMINISTRATION, FAA: Director of Aviation System Standards, PO Box 20582, Oklahoma City OK 73125, October 2005. 6

[28] L. Nelson Spohnheimer. **ICAO Document 8071 - Manual on Testing of Radio Navigation Aids**. Montreal, 2004. 6

[29] Ian Qvist. **RemoteFlight Inspection of Enroute Facilities**. In *Proceedings of International Flight Inspection Symposium*, Toulouse, 2006. International Committee for Airspace Standards and Calibration (ICASC). 7

[30] Capt. Thomas Wede. **The future of the Flight inspection World A Crystal Ball Look into changes ahead, based on current trends and developments**. In *Proceedings of International Flight Inspection Symposium*, Toulouse, 2006. International Committee for Airspace Standards and Calibration (ICASC). 7

[31] Hubert Zimmermann. **OSI Reference Model - The ISO Model of Architecture for Open Systems Interconnection**. In *IEEE Transactions on Communications*, **28**, pages 425–432, April 1980. Available at: `http://www.comsoc.org/livepubs/50_journals/pdf/RightsManagement_eid=136833.pdf`. 9

[32] International Civil Aviation Organization, editor. *Aeronautical Telecommunications (Annex X*, **Volume II Communication Procedures including those with PANS status**. ICAO, Document Sales Unit, 999 University Street, Montral, Quebec, Canada H3C 5H7, third edition edition, July 2002. 9

[33] International Civil Aviation Organization, editor. *Aeronautical Telecommunications (Annex X*, **Volume III Part I Digital Data Communication Systems; Part II Voice Communication Systems**. ICAO, Document Sales Unit, 999 University Street, Montral, Quebec, Canada H3C 5H7, third edition edition, July 2002. 9

[34] International Civil Aviation Organization, editor. *Aeronautical Telecommunications (Annex X*, **Volume V Aeronautical Radio Frequency Spectrum Utilization**. ICAO, Document Sales Unit, 999 University Street, Montral, Quebec, Canada H3C 5H7, second edition edition, July 2001. 9, 19

[35] Christian Pelmaine, Michael Neale, Dr.-Ing. Norbert Traenapp, Jurgen R. Bittner, and Axel Klaeyle. **UAS Airspace Integration The Communications Challenge**. In *UAS 2008 Conference proceeding*, Paris, France, June 2008. 9

[36] Cristiano Baldoni Govert Ho-Jean-Marc Bara-Gerry O Connell Robert Brown Michael Standar Roger Cato Jim Stenson Olaf Dlugi Alexander Sohn Michael Erb Gerhard Tauss Thorsten Astheimer, David Hilton. **Work Programme for 2008-2013 D6**. Technical report, SESAR Consortium, April 2008. 10

[37] Rhonda Thomas. **FAA ATC Communications Services - System Wide Information Management (SWIM)**, August 2007. 10

[38] Jacky Pouzet. **Future Communication Infrastructure**, May 2009. 10, 19

[39] EUROCONTROL/FAA. **Action Plan 17 Future Communications Study, Final Conclusions and Recommendations Report**. Technical report, EUROCONTROL / FAA, September 2007. 10

[40] B. Kamali. **An overview of VHF civil radio network and the resolution of spectrum depletion**. In *Integrated Communications Navigation and Surveillance Conference (ICNS), 2010*, pages F4–1 –F4–8, Herndon, VA, USA, may 2010. 10

[41] M. Schnell, N. Franzen, and S. Gligorevic. **L-DACS1 laboratory demonstrator development and compatibility measurement set-up**. In *Digital Avionics Systems Conference (DASC), 2010 IEEE/AIAA 29th*, pages 3.E.3–1 –3.E.3–11, Salt Lake City, Utah, USA, oct. 2010. 10

[42] Symmetricom. **XLi time and Frequency System**, November 2009. Available at: `http://www.symmetricom.com/products/gps-solutions/gps-time-frequency-receivers/XLi/`. 11, 76, 86

[43] International Civil Aviation Organization, editor. *Aeronautical Telecommunications (Annex X*, **Volume I Radio Navigation Aids**. ICAO, Document Sales Unit, 999 University Street, Montral, Quebec, Canada H3C 5H7, fifth edition edition, November 1996. 11

[44] Vincenzo Rosario Baraniello and Federico Corraro. **Unconventional Integrated Navigation Systems based on Redundancy of Traditional Navigation Sensors**. In *AIAA Guidance, Navigation and Control Conference*, Toronto, Ontario, Canada, 2010. 12

[45] David A. Domino, David Tuomey, Dr. Anand Mundra, and Arthur Smith. **Air Ground Collaboration through Delegated Separation: Application for Departure and Arrivals**. In *Integrated Communications Navigation and Surveillance Conference (ICNS), 2010*, Herndon, VA, USA, may 2010. 12

[46] ICAO. *Manual on Required Navigation Performance (RNP)*, **Doc 9613-AN/937**. International Civil Aviation Organization, 999 University Street, Montral, Quebec, Canada H3C 5H7, 1999. 12

[47] ICAO. *Performance-based Navigation (PBN) Manual*. International Civil Aviation Organization, 999 University Street, Montral, Quebec, Canada H3C 5H7, third edition edition, 2008. 13, 165

[48] John A. Volpe National Transportation Systems Center. **Vulnerability Assessment of the Transportation infrastructure relying on the global positioning system**. Technical report, 1200 New Jersey Avenue, SE Washington, DC 20590, August 2001. 13, 14

[49] **GNSS Sole Service Feasibility Study**. Technical report, Eurocontrol, Eurocontrol Experimental Centre, May 2003. Available at: `http://www.eurocontrol.int/eec/gallery/content/public/document/eec/report/2003/007_GNSS_Sole_Service_Feasibility_Study.pdf`. 13

[50] ESA. **ESA - Navigation - The present - EGNOS - EGNOS Open Service available: a new era for European navigation begins today**, October 2009. Disponible a: http://www.esa.int/esaNA/SEM2HGF280G_egnos_0.html. 13

[51] ESA. **ESA - Navigation - The present - EGNOS - EGNOS navigation system begins serving Europes aircraft**, March 2011. Disponible a: http://www.esa.int/esaNA/SEM98MUTLKG_egnos_0.html. 13

[52] **Civil-Military CNS/ATM Interoperability Roadmap**, January 2006. 13, 15, 21

[53] Norman Bonnor. **A Brief History of Global Navigation Satellite Systems**. *The Journal of Navigation*, **65**(01):1–14, 2012. 14

[54] International Civil Aviation Organization, editor. *Aeronautical Telecommunications (Annex X*, **Volume IV Surveillance and Collision Avoidance Systems**. ICAO, Document Sales Unit, 999 University Street, Montral, Quebec, Canada H3C 5H7, third edition edition, July 2002. 14

[55] ARINC. **718-4 Mark 3 Air Traffic Control Transponder (ATCRBS/MODE S)**, 1989. 15

[56] RTCA. **RTCA Online Store, Minimum Operational Performance Standards for 1090 MHz Automatic Dependent Surveillance Broadcast (ADS-B)**, June 2006. Disponible a: http://www.rtca.org/onlinecart/product.cfm?id=386. 16

[57] EUROCAE. **ED-102A Electronic Copy - MOPS for 1090 MHz Extended Squitter Automatic Dependent Surveillance - Broadcast (ADS-B) & Traffic Information Services - Broadcast (TIS-B)**, December 2009. 16

[58] Thales. **Development of new primary radar technology**. Technical report, ICAO, aeronautical communications panel, Montreal, Canada, December 2006. 17

[59] W.H.L. Neven, T.J. Quilter, R. Weedon, and R.A. Hogendoorn. **Wide Area Multilateration Report on EATMP TRS 131/04**. Technical report, August 2005. Available at: http://www.eurocontrol.int/surveillance/gallery/content/public/documents/WAM_study_report_1_1.pdf. 17

[60] Roke Manor Research Ltd. **RVSM Monitoring Study Case**. Disponible a: http://www.roke.co.uk/resources/casestudy/039-RVSM.pdf. 17

[61] Michael R. Owen. **Correlation of DME Pulse Trains for Use in Multilateration**. IEEE, May 2007. Available at: http://ieeexplore.ieee.org/stamp/stamp.jsp?tp=&arnumber=4272194&isnumber=4272175. 17

[62] G.S. Harris S.D. Thompson, J.W. Andrews and K.A. Sinclair. **Required Surveillance Performance Accuracy to Support 3-Mile and 5-Mile Separation in the National Airspace System**. Technical Report ATC-323, MIT Lincoln Laboratory, 244 Wood Street Lexington, MA 02420-9108, 2006. 17, 18, 117

[63] John Law Peter Green-Luc Tytgat Bo Redeborn Eric Poitier, Michel Borely. **EUROCONTROL Specification for ATM Surveillance system Performance (Volume 1)**. Technical Report SPEC-0147, EUROCONTROL, EUROCONTROL Headquarters, 96 Rue de la Fusée. B-1130 Brussels, March 2012. 17, 18, 117

[64] Eurocontrol. **ASTERIX Specifications - Documents**, September 2011. Disponible a: http://www.eurocontrol.int/asterix/public/standard_page/documents.html. 18

[65] Francois Cervo. **Military Data Links and ATM**. Glasgow, Scotland, September. 20

[66] Isdefe. **Feasibility Study for civil aviation data link for ADS-B Based on MIDS/LINK 16**. Technical report, Eurocontrol, August 2003. 21

[67] Robert Crow. **An integrated Global CNS system**, May 2005. 21

[68] **Technology Assessment for the Future Aeronautical Communication System**. Technical report, NASA, Reston, Virgina, USA, May 2005. 21

[69] Tricia Gilbert, Glen Dyer, Steve Henriksen, Jason Berger, Jenny Jin, and Tony Boci. **Identification of Technologies for Provision of Future Aeronautical Communications**. Technical report, NASA STI, October 2006. 21

[70] Tricia Gilbert, Jenny Jin, Jason Berger, and Steve Henriksen. **Additional Technologies and Investigations for Provision of Future Aeronautical Communications**. Technical Report CR-2008-214987, NASA, Hendon, Virginia, USA, February 2008. 21

[71] **25 Nations for an Aerospace Breakthrough European Civil Unmanned Air Vehicle Roadmap**, 2005. 24

[72] Federal Aviation Administration. **FAA Modernization and Reform Act of 2012**. Technical report, One Hundred Twelfth Congress of the United States of America, February 2012. 24

[73] European RPAS Steering Group. **Roadmap for the integration of civil Remotely-Piloted Aircraft Systems into the European Aviation System**. Technical report, European RPAS Steering Group, June 2013. 24

[74] Jesus Lopez Pino. **UAS UNMANNED AIRCRAFT SYSTEMS SOBRE SU INTEGRACION EN EL ESPACIO AEREO NO SEGREGADO**. Technical report, Observatorio de UAVs, Robotica y Sistemas Aereos, April 2008. Available at: http://www.portalcultura.mde.es/Galerias/publicaciones/fichero/Monografia_SOPT_1.pdf. 24

[75] **Plan estrategico para el sector aeronautico espanol 2008 2016**. Technical report, Ministerio de Industria, Turismo y Comercio; Centro para el Desarrollo Tecnologico Industrial, July 2007. Available at: http://www.cdti.es/recursos/publicaciones/archivos/43134_257257200791039.pdf. 24

[76] DoD Office of the secretary of Defence. **Unmanned Systems Roadmap 2007-2032**. Technical report, December 2007. 24

BIBLIOGRAPHY

[77] Ian Glenn. **ScanEagle in support of Canadian Forces Operations in Afghanistan**. In *UAS 2009 Conference Proceedings*, La plaine Saint Denis, Paris, France, June 2009. Blyenburg & Co. 24

[78] Dilshan Wasage. **UAS for Counter Insurgency**. In *UAS 2009 Conference Proceedings*, La plaine Saint Denis, Paris, France, June 2009. Blyenburg & Co. 24

[79] Andrea Bartl. **Schiebel Camcopter S-200 Test aboard German Navy Corvettes K130**. In *UAS 2009 Conference Proceedings*, La plaine Saint Denis, Paris, France, June 2009. Blyenburg & Co. 24

[80] **STANAG 4671 un unmanned aerial vehicles systems airworthiness requirements**, March 2007. Available at: http://nsa.nato.int. 24, 25

[81] **STANAG 4670 - Recomended guidance for the training of designated unmanned aerial vehicle Operator (DUO)**, September 2006. Available at: http://nsa.nato.int. 24, 25

[82] Eurocontrol. **EUROCONTROL Specifications for Mil UAVs as OAT Outside Segregated Airspace**, July 2007. Available at: http://www.eurocontrol.int/mil/gallery/content/public/milgallery/documents/UAVspecifications/EUROCONTROLSpecificationsforMilUAVsasOATOutsideSegregatedAirspace(pdf).pdf. 25

[83] Tim Kelly. **A Systematic Approach to Safety Case Management**. In *Proceedings of SAE 2004 World Congress*, Detroit, March 2004. Society for Automotive Engineers. 26

[84] Tim Kelly and Rob Weaver. **The Goal Structuring Notation A Safety Argument Notation**. In *Proceedings of the Dependable Systems and Networks 2004*, Florence, Italy, July 2004. IEEE. 26

[85] FAA. **Interim Operational Approval Guidance, 08-01: Unmanned Aircraft Systems Operations in the U. S. National Airspace System**. Technical report, Federal Aviation Administration, aviation safety unmanned aircraft program office, Mar 2008. Document AIR-160. 26

[86] **Unmanned Aircraft Systems Operations in the U. S. National Airspace System**, March 2008. 27, 28, 40

[87] EASA. **Policy Statement Airworthiness Certification of Unmanned Aircraft Systems (UAS)**. Technical report, European Aviation Safety Agency, Aug 2009. Available at: http://www.easa.eu.int/certification/docs/policy-statements/E.Y013-01_UAS_Policy.pdf. 27, 28, 29

[88] Greg S. Loegering. **The Global Hawk/BAMS Navigation System; an Update to the Odyssey**. *The Journal of Navigation*, **64**(01):15–27, 2011. 27

[89] Reece A. Clothier, Jennifer L. Palmer, Rodney A. Walker, and Neale L. Fulton. **Definition of an airworthiness certification framework for civil unmanned aircraft systems**. *Safety Science*, **49**(6):871 – 885, 2011. 28

[90] Konstantinos Dalamagkidis, Kimon P. Valavanis, and Les A. Piegl. *On integrating unmanned aircraft systems into the national airspace system: issues, challenges, operational restrictions, certification and recommendations*, **26** of *International series on intelligent systems, control, and automation: science and engineering*. Springer-Verlag, 2009. 28, 30, 39

[91] Leslie Cary. **ICAO UAS Study Group**. In *UAS 2009 Conference Proceedings*, La plaine Saint Denis, Paris, France, June 2009. Blyenburg & Co. 28

[92] European Parliament. **Regulation (EC) No 216/2008 of the european parliament and the council of 20 February 2008 on common rules in the field of civil aviation and establishing a European Aviation Safety Agency and repealing Council Directive 91/670/EEC, Regulation (EC) No 1592/2002 and Directive 2004/36/EC**. Technical report, Official Journal of the European Union, Feb 2008. 28

[93] **Policy for Unmanned Aerial Vehicle (UAV) certification**, 2005. Available at: http://www.easa.eu.int/ws_prod/r/doc/NPA/NPA_16_2005.pdf. 28

[94] Yves Morier and David Haddon. **EASA & Civil UAS Airworthiness Policy**. In *UAS 2009 Conference Proceedings*, La plaine Saint Denis, Paris, France, June 2009. Blyenburg & Co. 28

[95] **AMC and GM to Part 21**, December 2010. Available at: http://www.easa.eu.int/agency-measures/acceptable-means-of-compliance-and-guidance-material.php#AMCPart-21. 29

[96] EASA. **Acceptable means of compliance and guidance material to Part 21**. Technical report, European Aviation Safety Agency, Oct 2003. Decision no 2003/1/RM. 29

[97] Transport Canada. **Unmanned Air Vehicle (UAV) Systems Program Design Working Group**. Technical report, Transport Canada Civil Aviation, Mar 2010. Available at: http://www.h-a-c.ca/UAV_Terms_of_Reference_2010.pdf. 29

[98] Gerard Mardine. **EUROCAE WG73 SG1 Activity on UAS Operations**. In *UAS 2009 Conference Proceedings*, La plaine Saint Denis, Paris, France, June 2009. Blyenburg & Co. 30

[99] Michael Allouche. **EUROCAE WG73 SG2 Airworthiness**. In *UAS 2009 Conference Proceedings*, La plaine Saint Denis, Paris, France, June 2009. Blyenburg & Co. 31

[100] Norbert Traenapp. **EUROCAE WG73 SG3 Activity Update on UAS Command and Control, Communications, Spectrum Allocation and Security (C3SS)**. In *UAS 2009 Conference Proceedings*, La plaine Saint Denis, Paris, France, June 2009. Blyenburg & Co. 31

[101] John Walker. **RTCA Special Committee 203 Unmanned Aircraft Systems (UAS) Standards Update**. In *UAS 2009 Conference Proceedings*, La plaine Saint Denis, Paris, France, June 2009. Blyenburg & Co. 31

[102] RTCA. *Operational Services and Environmental Definition (OSED) for Unmanned Aircraft Systems (UAS)*. Radio Technical Commission for Aeronautics, Washington, DC (USA), Jun 2010. Document Do-320. 31

[103] ASTM International. **Standard Specification for Design and Performance of an airborne Sense-and-Avoid System**. Technical report, American Society of Testing & Materials, Feb 2007. Document F2411-07. 31

[104] EASA. **on certification specifications, including airworthiness codes and acceptable means of compliance for very light aeroplanes (CS-VLA)**, November 2003. Available at: http://easa.europa.eu/ws_prod/g/doc/Agency_Mesures/Certification_Spec/decision_ED_2003_18_RM.pdf. 32

[105] **laying down implementing rules for the airworthiness and environmental certification of aircraft and related products, parts and appliances, as well as for the certification of design and production organisations**. Available at: http://eur-lex.europa.eu/LexUriServ/LexUriServ.do?uri=CONSLEG:2003R1702:20091228:EN:PDF. 33

[106] **CIRCULAR OPERATIVA 16 B SOBRE LIMITACIONES DE TIEMPO DE VUELO, MAXIMOS DE ACTIVIDAD AEREA Y PERIODOS MINIMOS DE DESCANSO PARA LAS TRIPULACIONES - Aviacion Civil - Ministerio de Fomento**, July 1995. Available at: http://www.fomento.es/mfom/lang_castellano/direcciones_generales/aviacion_civil/_informacion/normativa/circulares_documen/circulares_operativas/16b-95.htm. 34

[107] Federal Aviation Administration. **Sense and Avoid (SAA) for Unmanned Aircraft Systems (UAS)**. Technical report, Federal Aviation Administration sponsored Sense and Avoid Workshop., Oct 2009. Final Report. 39

[108] Roland E. Weibel and Jr. R. John Hansman. **Safety Considerations for Operation of Unmanned Aerial Vehicles in the National Airspace System**. Technical report, MIT International Center for Air Transportation, Mar 2005. 39, 40

[109] J.K. Kuchar and Lee. C. Yang. **A Review of Conflict Detection and Resolution Modeling Methods**. *IEEE Transactions on Intelligent Transportation Systems*, **1**(4):179–189, Dec 2000. 40

[110] Gary Southcott. **Remotely Piloted Air Systems on Trial and in Operations**. *The Journal of Navigation*, **64**(01):1–14, 2011. 41

[111] J. Barnard. **Small UAV Command, Control and Communication Issues**. In *Communicating with UAV's, 2007 IET Seminar on*, pages 75 –85, Savoy Place, London, UK, dec. 2007. 44, 51, 52

[112] C.T. Howell, A. Jessup, F. Jones, C. Joyce, P. Sugden, H. Verstynen, and J. Mielnik. **The NASA Langley Research Center's Unmanned Aerial System Surrogate research aircraft**. In *Digital Avionics Systems Conference (DASC), 2010 IEEE/AIAA 29th*, pages 5.C.4–1 –5.C.4–14, Salt Lake City, Utah, USA, oct. 2010. 44, 51, 52

[113] EUROCONTROL. **UAS C3 Channel Saturation Study Final Report**. Technical report, EUROCONTROL, 2010. 44, 51, 52

[114] Axel Klayle. **SIGAT Study on military Spectrum requirements for the insertion into the General Air Traffic for the UAS**. In *UAS 2009 Conference Proceedingd*, La plaine Saint Denis, Paris, France, June 2009. Blyenburg & Co. 44

[115] Michael Neale. **UAS Airspace Integration A Control and Communications Perspective**. In *UAS 2009 Conference Proceedings*, La plaine Saint Denis, Paris, France, June 2009. Blyenburg & Co. 44

[116] **MIL-STD 6016, DOD Interface Standards, TADIL J Message Standard**. Technical Report Edition 1.0, Joint Interoperability Engineering Organization, Joint Interoperability Test Command, P.O. Box 12798, Fort Huachuca, AZ 85670-2798, 1997. 52

[117] NWP 6-02.5 AFTTP(I) 3-2.27 FM 6-24.8, MCWP 3-25C. **TADIL J Introduction to tactical digital information link J and quick reference guide**. Technical report, US Army Training and Doctrine Command, Marine Corps Combat Development Command, Navy Warfare Development Command, Air Force Doctrine Center, Fort Monroe, Virginia; Quantico, Virginia; Newport, Rhode Island; Maxwell Air Force Base, Alabama, June 2000. Available at: http://www.adtdl.army.mil. 55

[118] Euromids. **MIDS LVT European production**. Technical report, 1 bis, rue de Paradis, 75010 Paris, France, August 2011. Available at: http://www.euromids.com. 55

[119] Thales UK. **Link 16 Operational Overview**. Technical report, Horizon House, Throop Road, Templecombe, Somerset. BA8 0DH, October 2012. Available at: http://www.thalesgroup.com. 55

[120] Raj Jain and F. Templin. **Requirements, Challenges and Analysis of Alternatives for Wireless Datalinks for Unmanned Aircraft Systems**. In *IEEE Journal on selected areas in communication*, **30**, June 2012. 56

[121] **INTRODUCTION TO TACTICAL DIGITAL INFORMATION LINK J AND QUICK REFERENCE GUIDE**, June 2000. 56

[122] M. Hernandez-Pajares, J.M. Juan Zornoza, and J. Sanz Subirana. *GPS data processing: code and phase Algorithms, Techniques and Recipes.* Univ. Politecnica de Catalunya, Barcelona, Spain, 2005. Available at: http://www.gage.es/TEACHING_MATERIAL/GPS_BOOK/ENGLISH/PDGPS/BOOK_PDGPS_gAGE_NAV_08.pdf. 72, 74

[123] Richard B. Langley. **Dilution of Precision**. *GPS world*, **1**:52–59, May 1999. 91, 158

[124] Bradforf W. Parkinson James J. Spilker Jr. *Global Positioning System: Theory and Applications.* American Institute of Aeronautics and Astronautics, Inc, Stanford University, Stanford, Calidornia, 1996. 91

[125] Marc Ciurana, Francisco Barcelo, and Sebastian Cugno. **Indoor Tracking in WLAN Location with TOA Measurements**. In *MobiWac06*, number ACM 1-59593-488-X/06/0010, pages 121–125, Torremolinos, Malaga, Spain, 2006. 94

BIBLIOGRAPHY

[126] Yaohong Qu and Youmin Zhang. **Cooperative Localization of Low-cost UAV Using Relative Range Measurements in Multi-UAV Flight**. In *AIAA Guidance, Navigation and Control Conference*, Toronto, Ontario, Canada, 2010. 95

[127] Yaohong Qu and Youmin Zhang. **Cooperative localization against GPS signal loss in multiple UAVs flight**. *Journal of Systems Engineering and Electronics*, **22**(1):103 –112, February 2011. 95

[128] Robert Kerczewski and Thomas Kraft. **The Future of Required Total System Performance RTSP**. In *Integrated Communications Navigation and Surveillance Conference (ICNS), 2006*, Herndon, VA, USA, may 2006. 95

[129] Arek Shakarian and Aslaug Haraldsdottir. **Required Total System Performance and Results of a Short Term Conflict Alert Simulation Study**. In *4th US/Europe Air Traffic Management R&D Seminar*, Santa Fe, USA, 2001. 95

[130] Steve Kozco. **Overview of NextGen ICNS Functional Requirements**. In *Integrated Communications Navigation and Surveillance Conference (ICNS), 2010*, Herndon, VA, USA, may 2010. 95

[131] Matthew Blake. **New Vehicles and the Next Generation Airspace System**. In *Integrated Communications Navigation and Surveillance Conference (ICNS), 2010*, Herndon, VA, USA, may 2010. 95

[132] R.L. Stroup, G. Schaffer, J. Whittaker, and K. Niewoehner. **Nextgen Air-Ground integration challenges**. In *Integrated Communications Navigation and Surveillance Conference (ICNS), 2010*, pages G1–1 –G1–9, Herndon, VA, USA, may 2010. 95

[133] Melvyn Rees. **The EUROCONTROL Surveillance Strategy**. In *Proceedings of ESAV 08*, Capri, Italy, September 2008. 116

[134] Thales. **Development of new primary radar technology**. Technical report, Aeronautical Communication Panel (ACP), ICAO, MontReal Canada, 2006. 116

[135] THALES. **Alternative Detection Techniques to Supplement PSR Coverage**. Technical report, Eurocontrol, Feb 2007. Document TR6/SR/PST-041/07. 116

[136] Jorge Ramirez, Cristina Barrado, and Enric Pastor. **NAVAID FLIGHT INSPECTION OPTIMIZATION WITH UAS TECHNOLOGY**. In *Proceedings*, Bonn, Germany, October 2008. 142

[137] Jorge Ramirez, Cristina Barrado, Enric Pastor, and J.C. Garcia. **A proposal for using UAS in radio navigation aids flight inspection**. In *P47th AIAA Aerospace Sciences Meeting Including The New Horizons Forum and Aerospace Exposition*, Orlando, Florida, January 2009. 142

[138] Eduard Santamaria, Marc Perez, Jorge Ramirez, Cristina Barrado, and Enric Pastor. **Mission Formalism for UAS Based Navaid Flight Inspections**. In *9th AIAA Aviation Technology, Integration, and Operations Conference (ATIO)*, Hilton Head, South Carolina, September 2009. 142

[139] C. Barrado, J. Ramirez, M. Perez-Batlle, E. Santamaria, X. Prats, and E. Pastor. **Remote Flight Inspection Using Unmanned Aircraft**. *Journal of Aircraft*, **50**(1):38–46, January 2013. 142

[140] R.E.Kalman. **A new approach to Linear Filtering and Prediction Problems**. In *Transaction of the ASME-Journal of Basic Engineering*, **82**, pages 35–45, Research Institute for Advanced Study, Baltimore, Md, 1960. 149

[141] Greg Welch and Gary Bishop. **An Introduction to the Kalman Filter**. Los Angeles, California, USA, August 2001. 152

Declaration

I herewith declare that I have produced this paper without the prohibited assistance of third parties and without making use of aids other than those specified; notions taken over directly or indirectly from other sources have been identified as such. This paper has not previously been presented in identical or similar form to any other Spanish or foreign examination board.

The thesis work was conducted from 2008 to 2013 under the supervision of Cristina Barrado at Barcelona Tech.

Barcelona,

Jorge Ramirez Alcantara